Two-Phase Coexistence of Colors at Large N

Hiromasa Watanabe

February 2022

Two-Phase Coexistence of Colors at Large N

Hiromasa Watanabe
Doctoral Program in Physics

Submitted to the Graduate School of
Pure and Applied Sciences
in Partial Fulfillment of the Requirements
for the Degree of Doctor of Philosophy in
Science

at the
University of Tsukuba

Contents

1 Introduction

The unification of forces is the big dream for physicists since it means that we finally obtain a "theory of everything." Building the quantum theory of gravity is expected to be a huge step to seek the ultimate theory. One strong candidate is the superstring theory, which consists of tiny bits of the one-dimensional object, *string*, and many kinds of higher-dimensional objects, *branes*, in spacetime. Although string theory has been successful perturbatively, it has not been fully formulated; the nonperturbative definition is still unknown.

Under such circumstances, the properties of branes have been providing us with the progress for constructing string theory nonperturbatively. An example is the concept of duality; string dualities, T-duality, and S-duality, for example, revealed the nontrivial connections of different types of string theory and conjectured the existence of M-theory as a unified description of string theory [1]. Moreover, the *holographic duality* [2, 3] or the *gauge/gravity duality*, more broadly, is conjectured by the two aspects of the branes and connects the sort of Quantum Field Theories (QFT) and theories of gravity. It has been expected that some QFT in the appropriate parameter regions describe the nonperturbative effect of string theory. This conjecture includes the well-known AdS/CFT duality [4–6] and closely relates to the holographic principle and the black hole thermodynamics, especially when considering the finite temperature system. In other words, it suggests how the gauge/gravity duality relates the thermodynamics of gauge theories to one of the black holes; this nontrivial problem has been studied in the literature. This research is also in line with that trend.

The confinement and the thermal phase transition of the gauge theories are intriguing features for the above purpose. The well-studied example of the connection between thermal phase transitions in gauge theories and black holes can be seen in the duality between the thermodynamics of the 4d $\mathcal{N} = 4$ super Yang-Mills theory (SYM) and the type IIB superstring theory on $\mathrm{AdS}_5 \times \mathrm{S}^5$, discussed in section 2. In this case, the confined and deconfined phases on the gauge theory side correspond to the thermal AdS geometry (without black holes) and the "large" black hole geometry in AdS space, respectively. In the canonical ensemble, the first-order phase transition called the Hawking-Page transition [7] separates the above two phases. In addition, a "small" black hole, which is approximately the ten-dimensional Schwarzschild black hole [8, 9], can also appear on the gravity side of the duality in the microcanonical ensemble, depending on the energy scale. Although the counterpart of this physical state had not been well-known in terms of the gauge theory side, an intermediate phenomenon referred to as *partial deconfinement* gives a good picture to it.

Partial deconfinement [10–17] is the coexistence phenomenon in the space of color degrees of freedom. As schematically shown in figure 1, the two sectors, which are referred to as the confined and deconfined sectors, exist simultaneously in color space at some temperatures. It was found on the phase structure of the weakly-coupled Yang-Mills theory on sphere in the large N limit studied in the pioneering papers [18, 9], which are also motivated by understanding the relationship between the thermodynamics in field theory and the black holes in dual gravity. As explained in section 4, the phase structure of these theories is divided by two phase

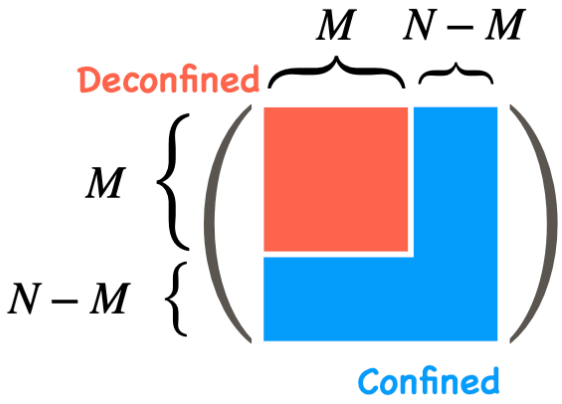

Figure 1: Schematic picture of the gauge and matter field configuration where the partial deconfinement takes place. The $M \times M$-block (red) and the rest (blue) represent the deconfined and confined sectors, respectively.

transitions, the Hagedorn transition and Gross-Witten-Wadia transition [19, 20] that is the peculiar transition at large N. The "phase" partial deconfinement occurs is in between these two phase transitions and characterized by the properties at the transition points. Until the proposal of partial deconfinement, the phase structure had been known well in the community, while no one pointed out the physical interpretation of the intermediate region separated by the two thermal phase transitions from the color degrees of freedom point of view. Partial deconfinement conjectures the change of the number of degrees of freedom contributing to the thermodynamic quantities coming from the kinematical aspects of the large N theories, and hence, the partially-deconfined phase has a potential to describe the negative specific heat in dual gravity in terms of the thermodynamic behaviors in the healthy QFTs.

The organization of this thesis as a comprehensive report of partial deconfinement is as follows; In section 2, the motivation from gravity and the original proposal describing the small black hole state [11,21] is argued. Although above proposal applied to the Higgsing of the D-branes, the mechanism shares the underlying concept with partial deconfinement. In section 3, we explain the generic features and intuitive pictures of partial deconfinement. Here, we give a formal definition of partial deconfinement using the so-called *Polyakov line phase* and its distribution function. Moreover, the 'spontaneous breaking of gauge symmetry' which seems to be an inherent feature of partial deconfinement is partly discussed in this section. Based on the general argument in the previous section, we review the analytic results of the large N theories and employ the concept of the two-phase coexistence of colors to them in section 4. We see in section 5 that the confinement at large N is quit similar to the *Bose-Einstein condensation* (BEC) in the N-body ideal Bose gas system. If looking on the permutation redundancy of the indistinguishable bosons as a kind of gauge symmetry, we can make sense these two apparently different

phenomena in a consistent way. Although the Bose-Einstein condensation is discovered in the non-interacting theory, it has been known that it is effective to examine the superfluidity of ^{4}He which is interacting from the BEC viewpoint. This feature encourages us to expect that the two-phase coexistence in color space can take place even in the case beyond the weak-coupling regime. In section 6, we show the numerical evidences of partial deconfinement in some lower-dimensional bosonic theories as known as *matrix models* from the lattice Monte Carlo simulation. They do not have any spatial dimensions and are superior models for the first step since the occurrence of the confinement/deconfinement transition has nothing to do with the presence of spatial directions. The efficiency in terms of computational cost is another merit to study these models compared to the lattice Monte Carlo simulation of theories with spatial dimensions. The numerical simulations enables us to analyze the configurations of the fields directly and tackle the region where the perturbative approach breaks down. Because of that, we confirm that partial deconfinement occurs in such cases. In section 7, we conclude the thesis and mention the perspectives of the study. There are also some appendices to compensate the contents written in the main text.

2 Deconfinement in dual gravity

The original motivation considering partial deconfinement [11] is to explain how the gauge/gravity duality connects the black hole thermodynamics to the statistical physics of gauge theories, which remains as a nontrivial issue in the literature.

Here, we do not overview the whole story of the gauge/gravity duality due to space limitation and excess of author's ability. See several excellent reviews [8, 22–25] or textbooks [26–29], for example.

The gauge/gravity duality conjectures the equivalence between the some specific theories; the theory of gravitation and the non-gravitating QFT, defined in different spacetimes. A well-known example of this duality is the AdS/CFT correspondence [4–6]. The duality is proposed based on the two different aspects of the system with D-branes, appeared nonperturbatively in string theory. In this correspondence, several coincidences can be confirmed by the numerous studies; the matching of the symmetry, the number of degrees of freedom, and the generating functional of the n-point functions for local operators can be seen using the AdS/CFT dictionary, the corresponding list of the parameters in both theories. Moreover, the phase structure or the Hilbert space in both theories is thought to connect via the duality. In the following, we review the spectrums of type IIB superstring theory on $\mathrm{AdS}_5 \times \mathrm{S}^5$ and the connection to its holographic dual gauge theory, $\mathcal{N} = 4$ super Yang-Mills theory on S^3.

A few comments regarding the gauge/gravity duality are given here. The gauge/gravity duality states more broad relationships. The duality was originally discovered by a concept called *holography* [2, 3] in the context of the black hole thermodynamics [30, 31], suggesting certain gauge theories at strong coupling can express the weakly-coupled gravity. In addition, the equivalences are believed to beyond the AdS and CFT; For instance, the equivalences between the super Yang-Mills theories in other spatial dimensions than three with 16 supercharges and the supergravity are known by the study in reference [32]. It contains the duality regarding the $(0 + 1)$-dimensional super Yang-Mills theory as known as the Banks-Fischler-Shenker-Susskind (BFSS) matrix model [33, 34], which describes the physics of D0-branes. This model is originating from the quantization of supermembrane theory in eleven dimensions [34, 35] and also interesting for the M-theory as a nonperturbative definition of the string theory [1]; it has a potential to describe the M-theory through the string/M-theory correspondence [33, 36]. See an excellent review [37] for the details of the M(atrix) theory. Together with the Berenstein-Maldacena-Nastase matrix model [38] which is a deformation of the BFSS model, it is very important to examine further in order to construct the nonperturbative definition of string theory via the gauge/gravity and string/M-theory dualities.

2.1 Spectrum of IIB superstrings on $\mathrm{AdS}_5 \times \mathrm{S}^5$

In the 't Hooft limit, $g_\mathrm{s} \to 0$ with $\lambda = g_\mathrm{s} N$ fixed and large, so that the supergravity approximation is valid, and when the AdS radius R is much larger than the string length $\ell_\mathrm{s} = \sqrt{\alpha'}$, we can investigate the phase structure of

the type IIB superstring theory on $\mathrm{AdS}_5 \times \mathrm{S}^5$ by the rough estimates. In the following analysis, the parameters in the theory on $\mathrm{AdS}_5 \times \mathrm{S}^5$ is translated into those in the dual $\mathcal{N} = 4$ $\mathrm{SU}(N)$ super Yang-Mills theory on S^3 as

$$m_{\mathrm{s}} \simeq \left(g_{\mathrm{YM}}^2 N\right)^{\frac{1}{4}} R^{-1}, \quad m_{\mathrm{P}} \simeq N^{\frac{1}{4}} R^{-1}, \tag{2.1}$$

where the string mass m_{s} and the ten-dimensional Planck mass m_{P}. Note that the energy scale on the gauge theory side is measured by the units of the S^3 radius in the 't Hooft limit. We will therefore ignore numerical factors in this section and focus on the scaling. In this section, we review the references [8, 27, 9].

2.1.1 Free graviton/string gas

At low energy, the gravitons and their superpartners dominates. We can regard as the stationary wave solutions in the linearized supergravity, and the frequency ω of a stationary mode is quantized in the unit of R. One may seem effectively that the supergravity particles in AdS as confined ones in the box of size R.

$$S(E) \sim (ER)^{9/10}, \tag{2.2}$$

for $E \gg R^{-1}$.

In the dual gauge theory, the Hilbert space contains the products of the chiral primary states and its the superconformal descendants. The product of gauge invariant operators are only influenced by $1/N$-corrections due to the large-N factorization. The energy scale in this phase is now $E \ll N^2$, and hence, the confinement is realized.

2.1.2 Hagedorn string

We have to take excitations of strings into account when the energy E becomes larger and comparable to the string mass m_{s}. Although it is not well-known how to quantize the string theory in AdS, the excitations where $\ell_{\mathrm{s}} \ll R$ can be estimated using the perturbation in power of ℓ_{s}/R.

The string spectrum in ten dimensions shows the Hagedorn behavior

$$S(E) \simeq E\ell_{\mathrm{s}}, \tag{2.3}$$

where

$$E \sim m_{\mathrm{s}}^{10} R^9. \tag{2.4}$$

We can estimate it from the condition that the supergravity particles is compatible to the excited strings.

In the dual gauge theory, each single trace operator is identified with a single string state in this energy scale $\left(g_{\mathrm{YM}}^2 N\right)^{\frac{1}{4}} < E \ll \left(g_{\mathrm{YM}}^2 N\right)^{-\frac{7}{2}} N^2$. The supergravity particles and their stringy excitations correspond to chiral primary states and non-chiral primary ones, respectively.

2.1.3 Small black hole

When the energy becomes further larger, the strings collapse and form a black hole in spacetime. The black hole can be described by the classical solution of supergravity when the string length $\ell_{\rm s}$ is negligibly small relative to the horizon r_+. In addition, the geometry around the black hole can be described approximately by the 10-dimensional Schwarzschild solution if r_+ is much smaller than R. The Bekenstein-Hawking formula states the black hole entropy states that the black hole entropy $S_{\rm BH}$ can be computed by the horizon area A as

$$S_{\rm BH} = \frac{A}{4G_d}, \tag{2.5}$$

where G_d is the Newton constant in d dimensions which relates to the Planck mass in ten dimensions as

$$\ell_{\rm P} = m_{\rm P}^{-1} = \sqrt{G_{10}}, \tag{2.6}$$

on the natural unit. It is the well-known fact that the Hawking temperature T can be read off as

$$T \sim r_+^{-1}, \tag{2.7}$$

by the continuity of the Euclidean metric. Combining above, we can derive

$$S \sim (m_{\rm P} r_+)^8 \propto N^2 T^{-8}, \qquad E \sim m_{\rm P}^8 r_+^7 \propto N^2 T^{-7}, \tag{2.8}$$

and hence,

$$S(E) \sim (E\ell_{\rm P})^{\frac{8}{7}}. \tag{2.9}$$

The above estimate is reliable in the region $\ell_{\rm s} \ll r_+ \ll R$ and hence $m_{\rm P}^8 \ell_{\rm s}^7 \ll E \ll m_{\rm P}^8 R^7$.

2.1.4 Large black hole

When the energy becomes further and further larger, the horizon r_+ grows and becomes comparable to R at somewhere, $E \sim m_{\rm P}^8 R^7$. Beyond there, the ten-dimensional Schwarzschild black hole solution is no longer reliable, and we should move on to the asymptotically AdS_5 solution [7], namely

$$\mathrm{d}s^2 = -f(r,R)\mathrm{d}t^2 + \frac{1}{f(r,R)}\mathrm{d}r^2 + r^2 \mathrm{d}\Omega_3^2, \tag{2.10}$$

and

$$f(r,R) = \frac{r^2}{R^2} + 1 - \frac{r_0^4}{R^2 r^2}, \tag{2.11}$$

where r_0 is the Schwarzschild radius. The horizon is located at r_+ as a solution of $f(r_+,R) = 0$. It leads to the Hawking temperature

$$T = \frac{2r_+^2 + R^2}{2\pi r_+ R^2} \simeq \frac{r_+}{R^2}, \quad (r_+ \ll R) \tag{2.12}$$

The entropy of that AdS Schwarzschild black hole is computed as

$$S \sim \left(\frac{r_+}{l_{\rm P}}\right)^3, \tag{2.13}$$

where $l_{\rm P}$ is the five-dimensional Planck length, connected to $\ell_{\rm P}$ and R

$$l_{\rm P}^3 = \ell_{\rm P}^8 R^{-5}, \tag{2.14}$$

via the matching of the Einstein-Hilbert actions in five and ten dimensions. The energy can be also derived as

$$E \sim \frac{r_+^2}{l_{\rm P}^3}\left(1+\frac{r_+^2}{R^2}\right) \simeq \frac{r_+^4}{l_{\rm P}^3 R^2} \propto T^4. \quad (r_+ \ll R) \tag{2.15}$$

Therefore, the entropy as a function of the energy E is given by

$$S \sim \left(\frac{ER^2}{l_{\rm P}}\right)^{\frac{3}{4}} = \left(\frac{R}{\ell_{\rm P}}\right)^2 (ER)^{\frac{3}{4}}. \tag{2.16}$$

The scaling (2.15) and (2.16) reproduces the expected results at a high energy as known as the Stefan-Boltzmann law in QFTs at finite temperature. In the canonical ensemble, a phase transition called Hawking-Page transition [7] separates the phases with and without the black hole, and this energy region has been interpreted as the deconfined phase in the dual gauge theory.

2.1.5 Short summary and motivation

As will be explained in detail later, the graviton gas phase and the large black hole phase are thermodynamically stable in the canonical ensemble. The Hawking-Page transition decomposed into two phases are translated into the confinement/deconfinement transition on the dual gauge theory side. Although the intermediate phases are metastable phases and unfavored thermodynamically in the canonical ensemble, they are stable physical states in the microcanonical ensemble. The transition between the large and small black hole phases is thought to relate to the Gregory-Laflamme instability [39] [1)]. See also references [43–48] for the detailed analysis of the instability. To determine the gauge theory counterpart of the small black hole phase is an longstanding problem in the context of the AdS/CFT correspondence. Partial deconfinement, the two-phase coexisting phenomenon in the space of the color degrees of freedom is proposed to solve this puzzle.

Moreover, the phase structure of the D0-brane matrix model is expected to be quite similar to the above [32, 49–53]. In the type IIA supergravity in ten dimensions dual to the matrix model, a phase transition between the phase of IIA black zero-brane (or M-theory black string) and the M-theory black hole occurs, where the M-theory circle in eleventh direction starts to become large. The transition from the black string and black hole is

[1)] Precisely speaking, the details of the phase transition is still under discussions. See some attempts on the gravity side, e.g. reference [40, 41] and on the gauge theory side, e.g. reference [42]. The numerical analyses in reference [17] are not sufficiently precise to detect such a fine structure.

related to the Gregory-Laflamme transition. The M-theory black hole is approximately the eleven-dimensional Schwarzschild black hole solution, and hence, its specific heat is expected as negative. The partial deconfinement picture is likely to describe the phase structure of the dual matrix model as well. We will discuss this again in the conclusion of this thesis.

2.2 Gauge theory description of small black hole

Here, let us review the heuristic proposal of the black hole equation of state from the dual 4d $\mathrm{N} = 4$ super Yang-Mills theory on S^3. We mainly review references [11,21], and the similar discussion is also found in reference [12]. Originally, the holographic picture is conjectured and justified via D-brane picture. D-branes can appear in string theory introduced by the boundary condition of open strings. They are massive objects, and hence, distort the background spacetime if we consider a lot of coincident D-branes at a place in spacetime. Such a system at finite temperature can be regarded as the black hole geometry, more precisely, the near extremal black-brane solution of supergravity. Another aspect of this system can be expressed by the Dirac-Born-Infeld theory which gives the low-energy effective theory of D-branes and open strings, and in turn, the (supersymmetric) gauge theory description. Then, the gauge group is chosen by $\mathrm{U}(N)$ or $\mathrm{SU}(N)$ if we consider N coincident D-branes. In super Yang-Mills theory description, as shown in figure 2, the diagonal and off-diagonal elements of the matrix scalar fields encodes the place of D-branes and open string stretching in between, respectively [54]. Therefore, the bound state of D-branes and open strings is the natural counterpart of the black hole in dual gravity. Note that this physical picture can also apply not only to 4d $\mathcal{N} = 4$ super Yang-Mills theory but to the matrix theory [33] or the super Yang-Mills theory on other dimensions as well.

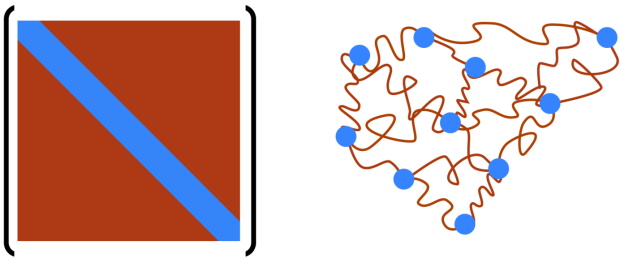

Figure 2: Conceptual picture for elements of the matrix configuration and the bound state of D-branes and open strings. The picture is taken from reference [21].

In the canonical treatment, the transition of the AdS geometry in dual gravity called Hawking-Page transition [7] corresponds to the confinement/deconfinement transition in gauge theory [55]. On the other hand, the small black hole phase is not contained in the above correspondence, and its dual gauge theory description is not well-established. There is one proposal [11] that try to answer the puzzle, which hints the concept of partial

deconfinement. The proposal suggests that the thermal state that the some of N D-branes is bound and the rest is emitted from it is corresponding to the small black hole phase. The change of the number building the D-brane bunch plays the essential role to describe the small black hole phase.

From the scaling of the parameters, the above physical picture is clarified quantitatively in a following manner. As the number of the D-branes in the bound state M changes, the 't Hooft coupling effectively changes as

$$\lambda_{\rm BH} \equiv g_{\rm YM}^2 M = \left(g_{\rm YM}^2 N\right) \cdot \frac{M}{N} = \lambda \cdot \frac{M}{N}, \tag{2.17}$$

where $g_{\rm YM}$ is the four-dimensional Yang-Mills coupling constant. Where $\lambda_M \ll 1$, the $M \times M$-block is weakly-coupled, and hence, the Hagedorn growth occurs.

Using the above picture, the energy of the state can be estimated from the contribution of the small black hole itself and the graviton gas around it, and

$$E_{\rm total} = E_{\rm BH} + E_{\rm gas}. \tag{2.18}$$

where $E_{\rm BH} \sim M^2 = O(N^2)$, $E_{\rm gas} \sim (N - M) = O(N)$. Therefore, in the large N analysis, the effect of the gas is negligible. We assume the whole contribution from the action is written by only the function of the potential term written by six scalar fields X_I $(I = 1, \cdots, 6)$. Then,

$$\frac{1}{g_{\rm YM}^2} {\rm Tr}\, [X_I, X_J]^2 \sim \frac{1}{g_{\rm YM}^2} {\rm Tr}\, \left[X_I^{\rm BH}, X_J^{\rm BH}\right]^2 = \frac{M}{\lambda_{\rm BH}} {\rm Tr}\, \left[X_I^{\rm BH}, X_J^{\rm BH}\right]^2 = M\, {\rm Tr}\, \left[\tilde{X}_I^{\rm BH}, \tilde{X}_J^{\rm BH}\right]^2, \tag{2.19}$$

where $\tilde{X}_I^{\rm BH} = X_I^{\rm BH}/\lambda_{\rm BH}^{1/4}$, and hence, the potential term is independent to the effective coupling constant. Let us identify the temperature T with the possible lowest one in ${\rm SU}(M)$ truncated theory, at which M D-branes build a bound state. Given that, at a fixed temperature T, the eigenvalues of $\tilde{X}_I^{\rm BH}$ is independent on the effective coupling constant $\lambda_{\rm BH}$, it is natural to suppose that, for the eigenvalues of the original fields $X_I^{\rm BH}$, the scaling $X_I^{\rm BH} \sim \lambda_{\rm BH}^{1/4}$ holds. We take the following normalizations

$$\bar{T}(N, g_{\rm YM}^2) \sim 1, \qquad E(N, g_{\rm YM}^2) \sim N^2, \tag{2.20}$$

at the lowest temperature of the large black hole state, so that we can see the scaling easily. The eigenvalues of $X_I^{\rm BH}$ correspond to the radius of the black hole since, as explained, the scalar fields relate to the location of D-branes. The radius will be set at the inverse of the energy scale of the system, and hence, the scaling of the temperature is $T \sim \lambda_{\rm BH}^{-1/4}$. When the normalized temperature decreases as the some D-branes are emitted from the bound state to the bulk, the energy should scale

$$\bar{T}(M, g_{\rm YM}^2) \sim \left(\frac{\lambda_{\rm BH}}{\lambda}\right)^{-1/4} = \left(\frac{M}{N}\right)^{-1/4}, \tag{2.21a}$$

$$E(M, g_{\rm YM}^2) \sim \left(\frac{\lambda_{\rm BH}}{\lambda}\right)^{-1/4} M^2 = N^2 \cdot \left(\frac{M}{N}\right)^{7/4} \sim N^2 \cdot \bar{T}(N_{\rm BH}, g_{\rm YM}^2)^{-7}. \tag{2.21b}$$

Here, we implicitly assumed that the 't Hooft counting is independent on the 't Hooft coupling in the strongly-coupled region. It is a presumable assumption since it is equivalent to that the Newton constant is independent on λ in the dual frame (R_{S^3} and R_{AdS} fixed). Partial deconfinement tells us a way in order the gauge theories to describe the small black hole [11] by introducing a new phase with negative specific heat in the ordinary deconfinement transition in a similar manner to above.

Note that the similar analysis of the ABJM theory [56] reproduce the the correct thermodynamic quantities of eleven-dimensional Schwarzschild solution in supergravity. Note also that similar phases with negative specific heat are expected for other theories [32], for example, the D0-brane quantum mechanics [33, 34]. See the recent report for tackling this problem [57].

In the context of dual gravity description via gauge/gravity duality, intermediate phase has negative specific heat. In more generic gauge theories, there is a variety of the case [10, 13, 14], as we will see in section 3.2.

3 Overview of partial deconfinement

In this section, we show the basic features of partial deconfinement as the coexisting phenomenon of the confined and deconfined sectors in the color space. In particular, we explain them by looking ahead to apply in the deconfinement of the large N $\mathrm{U}(N)$ or $\mathrm{SU}(N)$ gauge theory. As presented in the following sections, the thermal phase that partial deconfinement takes place appears in a more rigid sense, due to the existence of the phase transitions accompanied with the large N limit. Firstly, we discuss a formal definition of partial deconfinement, which is applicable to the broad class of the large-N gauge theory, including theories at strong coupling. We also provide the physical interpretations intuitively partial deconfinement implies in this section, which originates and is somehow related (historically as well) to the string theory picture.

We should emphasize the possibility that the above definition is a temporal one, and the more essential definition might exist. Somehow related to that, since we mainly refer to the intuitions at weak coupling, many of the readers may wonder the application to the theory beyond the weak-coupling regime. To overcome the issues, some key concepts in the field theories have been giving several useful insights; see the correspondence between the confinement at large N and the Bose-Einstein condensation explained in section 5. There, we will give some outlooks concerning the definition of partial deconfinement by focusing on the global symmetries and their spontaneous breakings at finite temperature, recently reported in reference [58].

3.1 Formal definition

For a formal definition, let us introduce the distribution of gauge degrees of freedom, the Polyakov line phases. The Polyakov line, which is the Wilson line towards the temporal direction, is defined by

$$L(t_{\mathrm{i}}, t_{\mathrm{f}}) = \mathcal{P} \exp\left[\mathrm{i}\int_{t_{\mathrm{i}}}^{t_{\mathrm{f}}} \mathrm{d}t A_t\right], \tag{3.1}$$

where $\mathcal{P}$ means path-ordering, and the n-th winding Polyakov loop u_n by

$$u_n = \frac{1}{N}\operatorname{Tr} L(0,\beta)^n = \frac{1}{N}\sum_{j=1}^{N} \mathrm{e}^{\mathrm{i}n\theta_j}. \tag{3.2}$$

This may be understood from that the Polyakov line (3.1) is $N \times N$ unitary matrix [2)], and the its eigenvalues are written as $\mathrm{e}^{\mathrm{i}\theta_1}, \cdots, \mathrm{e}^{\mathrm{i}\theta_N}$. Therefore, we refer the phases $\theta_1, \cdots, \theta_N$ lie between $-\pi$ and $+\pi$ as the Polyakov line phases. Another way to figure it out is the gauge fixing with the static diagonal gauge

$$A_t = \frac{1}{\beta}\operatorname{diag}\left(\mathrm{e}^{\mathrm{i}\theta_1}, \cdots, \mathrm{e}^{\mathrm{i}\theta_N}\right). \tag{3.3}$$

[2)] We implicitly assume the gauge group of the theories is $\mathrm{U}(N)$, instead of $\mathrm{SU}(N)$, since we are interested in the situation at large N in the following argument. If we consider $\mathrm{SU}(N)$ cases at finite N, the constraint $\sum_{j=1}^{N}\theta_j = 0 \bmod 2\pi$ is imposed.

For now, we fix the overall $\mathbb{Z}_N$ rotation ambiguity in the phase of the Polyakov loop by setting $P = u_1 = |u_1|$. Therefore, the Polyakov loops u_n equals to its complex conjugate u_{-n}.

It is convenient to introduce the distribution function of the Polyakov line phases as

$$\rho(\theta) = \frac{1}{N}\sum_{j=1}^{N}\delta(\theta - \theta_j). \tag{3.4}$$

In the large N limit, the number of the Polyakov line phases is taken to be infinite [59]; the dummy variables

$$x_j \equiv \frac{j}{N} - \frac{1}{2} \to x, \tag{3.5}$$

lies continuously between $-\frac{1}{2}$ and $\frac{1}{2}$, in the large N limit. Then the expression of the phases changes to $\theta_j = \theta(x_j) \to \theta(x)$, and the Polyakov loops (3.2) may be

$$u_n \to \int_{-\frac{1}{2}}^{\frac{1}{2}} \mathrm{d}x\ \mathrm{e}^{\mathrm{i}n\theta(x)} = \int_{-\theta_0}^{\theta_0} \mathrm{d}\theta\ \rho(\theta)\mathrm{e}^{\mathrm{i}n\theta}, \tag{3.6}$$

where $0 \le \theta_0 \le \pi$ is determined thermodynamically. Here we perform the variable transformation using the density of the Polyakov line phases $\rho(\theta) = \frac{\mathrm{d}x}{\mathrm{d}\theta}$, and it is nothing but the continuous version of the phase distribution function (3.4). From the properties of the density, the phase distribution is non-negative on the support, and normalized as

$$\int_{-\pi}^{\pi} \mathrm{d}\theta\rho(\theta) = 1. \tag{3.7}$$

By using $\rho(\theta)$, we can distinguish the completely-confined phase, partially-deconfined phase (equivalently, partially-confined phase), and completely-deconfined phase as follows:

The completely-confined phase

The *confined phase*, or for emphasis, *completely-confined* phase refers to an equilibrium state with the uniform phase distribution, $\rho(\theta) = \frac{1}{2\pi}$. See the left panel drawn by blue line in figure 3.

The partially-confined phase / partially-deconfined phase

The *partially-confined* phase, or equivalently, *partially-deconfined* phase refers to an equilibrium state with the nonuniform phase distribution which is positive everywhere, $\rho(\theta) > 0$. The Hagedorn transition separates this phase to the completely-confined phase. See the center panel drawn by orange line in figure 3.

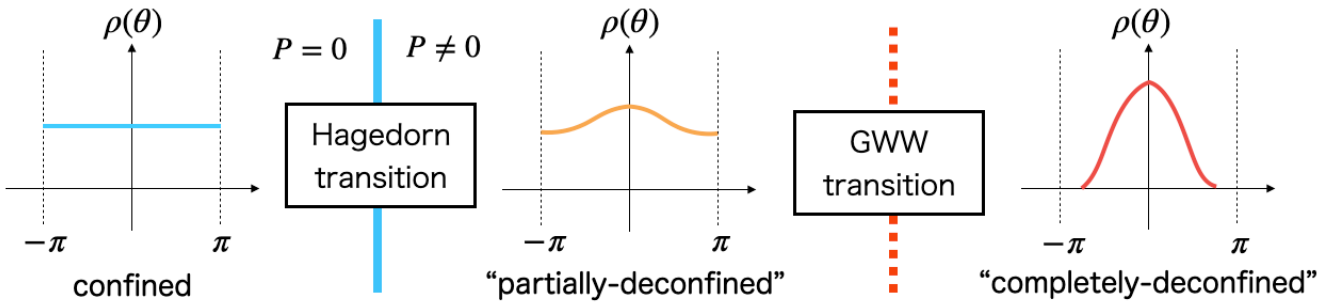

Figure 3: The distributions of the Polyakov line phases. The left, center and right ones show the completely-confined, partially-(de)confined and completely-deconfined phases, respectively. At large N, the phases are separated by two phase transitions, Hagedorn transition and Gross-Witten-Wadia transition. The specific form of the distribution function $\rho(\theta)$ for the partially- and completely-deconfined phases depends on the theory under consideration.

The completely-deconfined phase

The *completely-deconfined* phase refers to an equilibrium state with the nonuniform phase distribution which is non-zero in a finite range. In other words, the eigenvalue distribution is 'gapped.' The undistributed region appears on $|\theta| > \theta_0$. The Gross-Witten-Wadia transition [19, 20] See the right panel drawn by red line in figure 3.

One important point is that the above definition does not refer to the center symmetry. In the context of deconfinement, the Polyakov loop P plays an important role as the order parameter;

$$\begin{array}{ll} P = 0 & \text{(confined phase)} \\ P \neq 0 & \text{(deconfined phase)} \end{array} , \tag{3.8}$$

since the Polyakov loop measures the amount of the free energy to create single static quark. As is well known, the Polyakov loop detects the spontaneous breaking of center symmetry associated with the center of the gauge symmetry. Every elements in the center commutes to the element in gauge group G. For the theories whose gauge group is $G = \mathrm{U}(N)$, the center is $\mathbb{Z}_N$. However, partial deconfinement does not refer the center symmetry but the gauge symmetry itself[3)]. Therefore, it can also be applied to theories without center symmetry, such as the N_{f}-flavor large-N_c QCD or the Gaussian matrix model with N_{f} fundamental scalar fields in the Veneziano limit (the large-N_c limit with N_{f}/N_c fixed).

[3)] In this sense, we propose that partial deconfinement is outside of box of center symmetry, although it relates somehow to that symmetry. Therefore, the terminology of partial deconfinement is somewhat different from the one previously used in the context of center symmetry breaking [60].

Another interesting point is the Gross-Witten-Wadia-like transition other than at large N. The essence of this transition is whether the distribution function becomes 'gapped' or not on the circle. The analogous phenomena may exist in the situation even finite N and different thermodynamic limit is taken. As we will explain further in section 5, we have already found one specific example; the mechanism of the transition agrees naturally with the one of the partially-/completely-deconfined phase transition. We will mention about this topic in the summary.

The actual physical meaning of partial deconfinement is not immediately clear from this formal definition; for example, the physical picture of figure 1. We will try to provide some intuitive explanations below.

3.2 Physical interpretations

In this section, we present several explanations for partial deconfinement focusing on its physical picture. We will keep them abstract and generic here and see the specific examples in detail in the following sections.

3.2.1 Intuitive picture

The thermodynamic aspects of the partially-deconfined phase in the large-N gauge theories can be investigated from the point of view of the microcanonical ensemble [10, 13, 14]. In those theories, the thermodynamics can be analyzed kinematically; What we should do is to count the numbers of degrees of freedom. In the confined phase, thermodynamic quantities such as the energy E and the entropy S are of order N^0 (up to the zero-point energy), however they are of order N^2 in the deconfined phase. There, we are counting *hadrons/glueballs* in the confined phase and *quarks/gluons* in the deconfined phase, to use QCD language. It is the same situation in the canonical ensemble, as will be explained in the opening of section 4.

Then, let us consider a specific value of energy $E = \epsilon N^2$, where ϵ is a small but order N^0 number. That is based on the philosophy of the microcanonical treatment since the energy can be varied as a parameter. However, the energy is too large to realize the confined phase and too small to realize the deconfined phase, following the above criterion of the deconfinement. It cannot be the confined phase, because the energy is too large and it cannot be the deconfined phase, because the energy is too small. The answer is an intermediate phase that the two-phase coexistence takes place with the size $M \sim \sqrt{\epsilon}N$.

In addition to that, the variation of the excited color degrees of freedom may enable healthy QFTs to express the negative specific heat in dual gravity. According to the insight of the ideal gas, the temperature T can be interpreted as the energy per degree of freedom. If the number of color degrees of freedom is fixed and furthermore,independent on the energy, the specific heat which is the T-derivative of the energy must be positive in any case. However, if it has a nontrivial energy dependence, the specific heat also behaves nontrivially and hence can be negative. Note that this picture is matching to the system of the black hole constructed by D-branes and strings [21], as explained in section 2.2.

3.2.2 Phase structures

The significant and essential feature partial deconfinement proposes is that the two phases in the space of color degrees of freedom, the confined and deconfined phases, can coexist. The appearance of the phase structure changes nontrivially depending on the thermodynamics of the theory due to the all-to-all interaction among the color degrees of freedom. Pictorially, we present three possible patterns in figure 4. The blue, orange, and red lines represent the completely-confined phase, partially-deconfined phase (or equivalently, partially-confined phase) and completely-deconfined phase. For each pattern, we state that

- The center panel in figure 4 would be the easiest one to understand. The partially-deconfined phase is realized at a critical temperature $T_1 = T_2 = T_c$. It does not have the hysteresis structure with respect to the temperature T and is on the critical point between the continuous and discrete phase transitions. Many theories such as the large-N Yang-Mills theory on sphere at zero coupling and the Gaussian matrix model we consider both in the main text belongs to this class.

- In the class like the left panel in figure 4, the phase structure has the first-order transition with the hysteresis, and the partially-deconfined phase has a negative specific heat. Such an intermediate phase is not favored as the thermodynamically determined saddle in the canonical ensemble (we used a dotted line to emphasize this feature). Strongly-coupled 4d $\mathcal{N} = 4$ Yang-Mills theory, pure Yang-Mills theory, and the Yang-Mills matrix model discussed numerically in sections 6.4 and 6.5 belong to this class. Depending on the geometry of the ordinary space, instability can set in even in the microcanonical ensemble (see section 3.2.4 for the details).

- The right panel in figure 4 shows the class with non-first-order phase transitions. The partially-deconfined phase is thermodynamically stable both in the microcanonical and canonical ensembles. The large-N_c QCD with N_f-fundamental fields ($\frac{N_c}{N_f}$ fixed), the $O(N)$ free vector model, and the Gaussian matrix model with N_f-fundamental scalar fields belongs to this class.

It is quite instructive to consider a similar but essentially distinct example, water around the temperature of 0 °C and the standard pressure in the thermodynamic limit. Water exhibits a first-order phase transition in the canonical ensemble. Due to the latent heat at the transition temperature, the amount of liquid and solid phases depend on energy E in the microcanonical ensemble. If the energy is appropriately tuned, a mixture of the two phase, namely icy water appears. The situation is resembling the two-phase coexisting phenomenon in the gauge theories at large N.

However, we must notice their differences in the following sense; In the liquid and solid water example, the infinite volume limit works as the thermodynamic limit, while the large N limit is the one in the gauge theories. Recalling the correspondence between the canonical and microcanonical ensembles, it was derived in the situation with large volume. Therefore, the thermodynamics of the large-N gauge theories with finite volume is not the

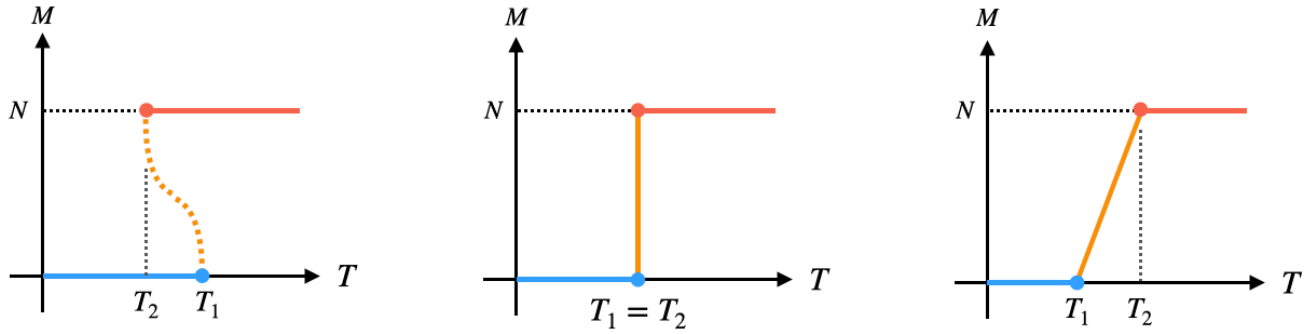

Figure 4: Three basic patterns of T-dependence of M [10]. The blue, orange and red lines are the completely confined, partially-deconfined and completely deconfined phases, respectively. For the $\mathrm{SU}(N)$ theory, the $\mathrm{SU}(M)$ subgroup only deconfines in the intermediate phase, which can be interpreted as the spontaneous symmetry breaking. This figure corresponds to figure 5. [Left] First-order transition with hysteresis. [Middle] First-order transition without hysteresis. [Right] Non-first-order transition.

case, and hence, the microcanonical ensemble is a physically more realistic setup than the canonical ensemble in this case. Moreover, the natures of interaction in both cases are also quite unlike; in the gauge theories, the color degrees of freedom interact nonlocally in the internal space, while the interaction of water molecules is obviously local in the 'ordinary' space. For the case of water, although the metastable phases associated with the first-order phase transition can appear as the supercooled water or superheated ice, they are not stable even in the large volume limit as thermodynamic limit due to the local interaction and small perturbations. The metastable phase in the confinement/deconfinement process can be stabilized in the large N limit as thermodynamic limit due to the nonlocal interaction.

Figure 4 indicates that the gauge symmetry related to the number of colors can be interpreted to be spontaneously broken in the intermediate region. We can understand the feature from the fact that the each point in the orange line can be identified as the Gross-Witten-Wadia-transition point for some sector specified by M in the large N limit. That subsector and its complementary of the full theory describe the each thermodynamics since the number M characterizes the thermodynamics from the excited degrees of freedom, while the rest $N - M$ characterizes the one from the degrees of freedom behave in the ground state. As a result, the symmetry is splitted into two parts accompanied with that. For example, the $\mathrm{SU}(N)$ gauge symmetry can break spontaneously to $\mathrm{SU}(M)_{\mathrm{dec}} \times \mathrm{SU}(N-M)_{\mathrm{con}}$, as a property the saddle points of the effective potential (i.e. the free energy) have. The change of the symmetry must be smooth since the ratio $\frac{M}{N}$ can vary continuously from 0 to 1 at large N. Strictly speaking, it caused by the breaking of the global part of gauge symmetry. In this sense, this concept is compatible with the well-known no-go theorem, the Elitzur's theorem [61]. We will review this feature more concretely using the Gaussian matrix model in the Hamilton formalism 4.3.2. Similar to the Higgs mechanism,

this mechanism provides us with the picture of 'convenient fiction' [62], that is, it is up to those who do the physics whether to preserve or fix the symmetry.

3.2.3 Possible objections

In this section, we list the possible objections regarding the physical pictures implied by partial deconfinement and our replies to them.

1. The confinement/deconfinement transition for the theory at large N can take place even in the theories with finite spatial volume, due to the large N limit as the thermodynamic limit, which is well-known fact [9, 18]. The class of theory contains the lower-dimensional QFTs known as matrix models those do not have any ordinary spatial directions by definition. We show the gauged Gaussian matrix model as a simplest model of the deconfinement in section 4.3. In these cases, the phase separation can happen in the internal 'space' or so-called color space, in which the degrees of freedom interact as all-to-all in general.

2. The confinement/deconfinement transition can also take place even in the theory at zero coupling [18, 9]. Same as the gauged Gaussian matrix model in section 4.3, we can treat the physical degrees of freedom in it just as quantum harmonic oscillators. Due to the nature of quantization, the energy spectrum is discretized, and hence, the degrees of freedom cannot be excited 'mildly.' In this sense, we can reject the objection that all the degree of freedom are excited gradually and not separated into distinct groups with respect to excitation, and the intuition of the two-phase coexistence applies well. This feature is analogous to the case of water around 0 $^\circ$C and the standard pressure; the finite latent heat inhibits such a mild excitation and favors the mixture of the solid and liquid regions.

3. One may wonder that the idea shown in figure 1 does not look gauge invariant. The picture shows the 'typical' configuration of the matrix field in which the two-phase coexistence in the color space takes place. We can handle these configurations if we average with respect to the gauge-equivalent families, which is an ordinary way to estimate the observables in the path integral formalism. This type of configuration can be realized as the master field, which represents the typicality of field configuration in some sense, as will be discussed in section 6.2. Moreover, as we will discuss in section 4.3.2, we can explicitly construct the gauge-singlet states in the Hilbert space in the Hamilton formalism.

4. Associated with the previous objection, one would doubt the necessity of $\mathrm{SU}(M)$-block structure of the deconfined sector of partial deconfinement. In the weak-coupling limit, the field configuration can be expressed by harmonic oscillators. For a field configuration at fixed energy, we can always collect the excited degrees of freedom and form a deconfined block which preserves the sub-symmetry of the full theory, at least in the large-N sense. For the interacting theories, it is nontrivial the they are still in the case due to the additional interaction between the confined and deconfined sectors. Intuitively, it is natural to expect

that the saddle point of the free energy preserves the structure of symmetry. A more precise argument can be seen in the equivalence between color confinement at large N and Bose-Einstein condensation [15], as we will see in section 5.

There is an intriguing toy model referred to as the ant-trail model, which enables us to fill the gap between the picture of D-branes and strings and the phase structure of gauge theory. See appendix B, for the readers who want to know the detail and its fun.

3.2.4 Remarks on negative specific heat

When the specific heat is negative, the partially-deconfined phase sits at the maximum of the effective potential in the canonical ensemble [10], as a solution of the saddle-point condition in the large-N theory. On the other hand, the completely-confined and completely-deconfined phases sit at the minima of the effective potential. See also appendix A for detail. Since the difference of the potential between the minima and maximum is of order N^2, the tunneling between the phases is suppressed at large N. As a result, the local minima is stabilized perfectly, even when it is not the global minimum. This is quite different from the metastable states interacting locally, as explained in section 3.2.2.

If the volume of the ordinary space becomes gigantic, the phase with a negative specific heat is no longer stable. Any small perturbation can cause a decay of the metastable states. It is not necessary to occur if the volume is not large and finite. In the case of matrix models, such an instability cannot exist by definition, because they have no ordinary space. Moreover, 4d $\mathcal{N} = 4$ super Yang-Mills theory on S^3 does not have such an instability [53]. Hence, the partially-deconfined phase in the theory proposed as the dual to the small black hole phase does not have such an instability via the duality [4)] .

[4)] There is a subtlety regarding this point, near the phase transition associated with the localization on the S^5; see section 2.

4 Analytic examples for partial deconfinement

In this section, we review several analytic examples which exhibit the confinement/deconfinement transition and partial deconfinement at large N.

At large N, the free energy also plays the role of the order parameter for the deconfinement in the canonical ensemble since the saddle point approximation becomes exact due to the large N limit. For example, in the large N theories with the adjoint matter fields, the free energy is

$$F \sim \begin{cases} O(N^0) & \text{(in confined phase)} \\ O(N^2) & \text{(in deconfined phase)} \end{cases}. \tag{4.1}$$

This result can be interpreted as the following physical picture [55]; In the confined phase, the condensed objects such as glueballs contribute to thermodynamics. On the other hand, the objects such as the quark-gluon plasma appears in the deconfined phase, and the each color degrees of freedom can contribute. This discussion can be generalized to arbitrary field contents since what we did here is just counting the physical degrees of freedom. In this sense, the confinement/deconfinement transition at large N is tractable kinematically.

4.1 Weakly-coupled Yang-Mills theories on sphere

The features of partial deconfinement have been analytically found in the generic results for the weakly coupled theories, studied in the pioneering papers [9, 18]. These studies pointed out that the confinement/deconfinement transition can exist even in the weak-coupling limit and only due to the gauge-singlet constraint. Here, we briefly review references [9, 18] for the adjoint matter fields and reference [63] for the fundamental matter fields as well. In section 4.3, we will show the same derivation as here in a somehow different way using the $(0+1)$-dimensional bosonic matrix models.

Let us consider the generic setup for free Yang-Mills theory on a compact space (like $\mathrm{R}\times\mathrm{S}^{d-1}$). The restriction to compact space has every modes of the fields massive. First and foremost, we want to know the partition function governing the thermodynamic behavior in the canonical ensemble;

$$Z(\beta) = \sum_{\text{physical states}} \mathrm{e}^{-\beta E_i} = \int \mathrm{d}E\, \Omega(E) \mathrm{e}^{-\beta E}, \tag{4.2}$$

where $\Omega(E)$ is the density of states. We have to keep in mind that there is the Gauss' law constraint and the physical states must be gauge invariant. To compute the partition function, we count the total number of states when we specify the matter contents in some group representation R. Since the above problem is just a combinatorial one, it is convenient to define and use the single-particle partition function for bosons and fermions;

$$z^{\mathrm{R}}_{\mathrm{B}}(\beta) = \sum_{\substack{\text{bosonic} \\ \text{one-particle states} \\ \text{in R}}} \mathrm{e}^{-\beta E}, \qquad z^{\mathrm{R}}_{\mathrm{F}}(\beta) = \sum_{\substack{\text{fermionic} \\ \text{one-particle states} \\ \text{in R}}} \mathrm{e}^{-\beta E}. \tag{4.3}$$

Therefore, the partition function is obtained as the form of group integral by

$$Z(\beta) = \int [\mathrm{d}U] \ \exp\left[\sum_{\mathrm{R}} \sum_{n=1}^{\infty} \frac{1}{n} \left(z_{\mathrm{B}}^{\mathrm{R}}(x^n) + (-1)^{n-1} z_{\mathrm{F}}^{\mathrm{R}}(x^n)\right) \chi_{\mathrm{R}}(U^n)\right], \tag{4.4}$$

where $x \equiv \mathrm{e}^{-\beta} = \mathrm{e}^{-\frac{1}{T}}$. Here, U is the group element and $\chi_{\mathrm{R}}(U)$ is the character for the representation R.

4.1.1 With adjoint matter

For now, let us focus on the $\mathrm{U}(N)$ free Yang-Mills theories on $\mathrm{R} \times \mathrm{S}^{d-1}$ with only adjoint matter fields [18, 9]. This situation includes the zero-coupling limit of 4d $\mathcal{N} = 4$ super Yang-Mills theory on sphere. Since $\chi_{\mathrm{adj}}(U) = \mathrm{tr}(U)\,\mathrm{tr}\left(U^\dagger\right)$ where the trace is in the fundamental representation, the partition function is

$$Z(x) = \int [\mathrm{d}U] \ \exp\left[\sum_{n=1}^{\infty} \frac{1}{n} \left(z_{\mathrm{B}}(x^n) + (-1)^{n-1} z_{\mathrm{F}}(x^n)\right) \mathrm{tr}\, U^n\, \mathrm{tr}\, U^{\dagger\, n}\right], \tag{4.5}$$

which is in the form of a unitary matrix model.

We will see this unitary matrix model can be solved directly. From the rather generic form of the partition function (4.4), we change the variables from U to its eigenvalues $\left\{\mathrm{e}^{\mathrm{i}\theta_j}\right\}$ and the density of the eigenvalues $\rho(\theta)$. Then,

$$Z(x) = \int [\mathrm{d}\theta] \ \exp\left[\sum_{n=1}^{\infty} \frac{1}{n} \left(z_{\mathrm{B}}(x^n) + (-1)^{n-1} z_{\mathrm{F}}(x^n)\right) |u_n|^2\right], \tag{4.6}$$

and

$$u_n = \frac{1}{N} \sum_{j=1}^{N} \mathrm{e}^{\mathrm{i}n\theta_j} = \int_{-\pi}^{\pi} \mathrm{d}\theta \ \ \rho(\theta)\, \mathrm{e}^{\mathrm{i}n\theta}, \tag{4.7}$$

where we use the results at large N because the eigenvalue distribution $\rho(\theta)$ is continuous in the large N limit. The eigenvalues θ_j are nothing but the Polyakov line phases, and the basic properties of the eigenvalue distribution is mentioned in section 3.1. More precisely, we also performed the following replacement of the path integral measure;

$$\int [\mathrm{d}U] \to \prod_i \int_{-\pi}^{\pi} [\mathrm{d}\theta_i] \prod_{i<j} \sin^2\left(\frac{\theta_i - \theta_j}{2}\right). \tag{4.8}$$

As we can see, the factor from the Vandermonde determinant appears. We can further rewrite equation (4.6) to

$$Z(x) = \int [\mathrm{d}\theta_i] \exp\left[-\sum_{i \neq j} V(\theta_i - \theta_j)\right], \tag{4.9}$$

by introducing the pairwise potential

$$\begin{aligned} V(\theta) &= -\ln\left|\sin\frac{\theta}{2}\right| - \sum_{n=1}^{\infty}\frac{1}{n}\left[z_{\mathrm{B}}(x^n) + (-1)^{n-1}z_{\mathrm{F}}(x^n)\right]\cos(n\theta) \\ &= \ln 2 + \sum_{n=1}^{\infty}\frac{1}{n}\left[1 - z_{\mathrm{B}}(x^n) - (-1)^{n-1}z_{\mathrm{F}}(x^n)\right]\cos(n\theta). \end{aligned} \tag{4.10}$$

with the repulsive force from the measure, and the attractive force getting stronger with the temperature.

At low temperatures

At first, let us consider the theory at low temperatures, where the repulsive force in the effective potential (4.10) dominates, and hence, the eigenvalue distribution becomes uniform between $\pm\pi$. In this case, the saddle point approximation is exact due to the large N limit, and the stationary point of the effective potential leads to the uniform distribution of the Polyakov line phases. Combining these facts, the effective action associated with the partition function (4.9) is

$$S[\{u_n\}] = N^2\int \mathrm{d}\theta_1\mathrm{d}\theta_2\,\rho(\theta_1)\rho(\theta_2)V(\theta_1-\theta_2) = \frac{N^2}{2\pi}\sum_{n=1}^{\infty}|u_n|^2V_n(x), \tag{4.11}$$

where we use the Fourier modes u_n, V_n defined in (4.7) and

$$V_n(x) \equiv \int \mathrm{d}\theta\, V(\theta)\cos(n\theta) = \frac{2\pi}{n}\big(1 - z_{\mathrm{B}}(x^n) - (-1)^{n-1}z_{\mathrm{F}}(x^n)\big). \tag{4.12}$$

Here, we implicitly fixed the center symmetry ambiguity such that the phase distribution $\rho(\theta)$ is symmetric around $\theta = 0$ and $V(\theta) = V(-\theta)$. From the fact that the phase distribution becomes uniform at low temperatures, u_n must be zero for all n as long as $V_n > 0$, and equivalently,

$$z_{\mathrm{B}}(x^n) + (-1)^{n-1}z_{\mathrm{F}}(x^n) < 1. \tag{4.13}$$

Note that the free energy is of order N^0 in this phase because of $u_n = 0$.

However, we have to care only $n = 1$ case for the moment because the single partition functions increase monotonically [5] and $0 \le x = \mathrm{e}^{-\beta} < 1$. The uniform distribution is the solution of the stationary condition in the region $T \le T_{\mathrm{H}} = -\frac{1}{\ln x_{\mathrm{H}}}$ where x_{H} satisfies

$$z_{\mathrm{H}} = z_{\mathrm{B}}(x_{\mathrm{H}}) + z_{\mathrm{F}}(x_{\mathrm{H}}) = 1, \qquad \Leftrightarrow \qquad V_1(x_{\mathrm{H}}) = 0. \tag{4.14}$$

This temperature T_{H} is the Hagedorn temperature we mentioned in section 3.1.

[5] For the precise expression of the bosonic and fermionic single-particle partition functions in various dimensions, see appendix B of reference [9].

Near the Hagedorn temperature T_{H}

When the density of states becomes comparable to the Boltzmann weight in the partition function 4.2, namely $\Omega(E) \approx \mathrm{e}^{\beta_{\mathrm{H}} E}$, the partition function diverges [64]. The temperature $T_{\mathrm{H}} = \beta_{\mathrm{H}}^{-1}$ is the Hagedorn temperature we have discussed. In terms of the free energy $\beta F = -\ln Z$, this divergence can be expressed

$$F \sim T_{\mathrm{H}} \ln (T_{\mathrm{H}} - T), \tag{4.15}$$

as the temperature T approaches to the Hagedorn temperature T_{H} from low temperatures. Note that this behavior only means the break down of the effective theory and the some sort of the singularity is need such as the phase transition.

At the Hagedorn temperature $T = T_{\mathrm{H}}$, the coefficient V_1 in equation 4.11 vanishes and the Polyakov loop u_1 can only excite and take nonzero values without changing the value of free energy. In other words, the free energy has a flat direction regarding the value of u_1, and the corresponding saddle-point condition gives

$$\rho(\theta) = \frac{1}{2\pi}(1 + 2u_1 \cos\theta). \tag{4.16}$$

Because of the non-negativity of the distribution function, the Polyakov loop can take any value by $\frac{1}{2}$. Above the point $u_1 = \frac{1}{2}$, the distribution function becomes negative if the same form 4.16 is supposed. In fact, the point can be identified with the transition point where the analytic form of the distribution is altered, the Gross-Witten-Wadia-transition point [19, 20].

Substituting the configuration at $u_1 = \frac{1}{2}$ into the effective action 4.11,

$$S|_{T=T_{\mathrm{H}}} \approx \frac{N^2}{8\pi}(T - T_{\mathrm{H}}) V_1'(x_{\mathrm{H}}), \tag{4.17}$$

and hence, the leading order of the free energy can be derived

$$\frac{F}{N^2} \approx \begin{cases} 0 & (T \to T_{\mathrm{H}-}) \\ -\frac{1}{4}(T - T_{\mathrm{H}}) z'(x_{\mathrm{H}}) \beta_{\mathrm{H}} x_{\mathrm{H}} & (T \to T_{\mathrm{H}+}) \end{cases}. \tag{4.18}$$

This shows the Hagedorn transition, namely a first-order phase transition at T_{H}, which characterizes the deconfinement; the free energy jumps from $O(N^0)$ to $O(N^2)$ before and after the phase transition. Note that this "phase" is not thermodynamically stable in the canonical ensemble, and can be treated as a stable phase in microcanonical ensemble.

At high temperatures

When the temperature gets even higher, the attractive force in the pairwise potential becomes so stronger that the eigenvalues distribute in a finite interval $I = [-\theta_0, \theta_0]$ on the circle. Note that we impose the same

assumption that phase distribution $\rho(\theta)$ is symmetric around $\theta = 0$ and $V(\theta) = V(-\theta)$. The ripping of the distribution at $\theta = \pm\pi$ corresponds to the Gross-Witten-Wadia transition [19, 20].

To determine the distribution function, we rewrite the saddle point condition of the effective action (4.11) as

$$\int_{-\theta_0}^{\theta_0} \mathrm{d}\theta\, \rho(\theta) \cot\frac{\alpha-\theta}{2} = 2\sum_{n=1}^{\infty} a_n u_n \sin(n\alpha), \qquad \alpha \in I, \tag{4.19}$$

where $a_n = z_{\mathrm{B}}(x^n) + (-1)^{n-1} z_{\mathrm{F}}(x^n)$, and solve it with respect to $\rho(\theta)$ and u_n self-consistently for the effective action [6)]

$$S = N\sum_{n=1}^{\infty} \frac{a_n u_n}{n}\left(\operatorname{tr} U^n + \operatorname{tr} U^{\dagger n}\right). \tag{4.20}$$

The method to deal wit it and its exact solution has been known by the study in reference [65] and

$$\rho(\theta) = \frac{1}{\pi}\sum_{n=1}^{\infty} Q_n \cos\left(\left(n-\frac{1}{2}\right)\theta\right)\sqrt{\sin^2\frac{\theta_0}{2} - \sin^2\frac{\theta}{2}}, \tag{4.21}$$

for $\theta \in I$ and $\rho(\theta) = 0$ otherwise. The coefficients Q_n is defined by the Legendre polynomials

$$Q_n \equiv 2\sum_{l=0}^{\infty} a_{n+l} u_{n+l} P_l(\cos\theta_0), \tag{4.22}$$

$$\sum_{l=0}^{\infty} P_l(y) z^l = \left(1 - 2yz + z^2\right)^{-\frac{1}{2}}. \tag{4.23}$$

In the theories we consider, the truncation of the coefficients a_n, such as $a_{n>k} = 0$ for sufficiently large k gives a good approximation and the same qualitative behaviors. When we take $k = 1$, the thermodynamic properties is determined only by u_1 and $Q_n = 0$ for $n > 1$. We obtain the exact solution as

$$\rho(\theta) = \frac{1}{\pi s_0^2}\cos\frac{\theta}{2}\sqrt{s_0^2 - \sin^2\frac{\theta}{2}}, \tag{4.24}$$

and

$$s_0^2 = \sin^2\frac{\theta_0}{2} = 1 - \sqrt{1 - \frac{1}{a_1(T)}}. \tag{4.25}$$

Note that the phase distribution (4.24) is identical to the distribution (4.16) where $\theta_0 = \pi$, namely, at the critical temperature $T = T_{\mathrm{c}}$ and $u_1 = \frac{1}{2}$.

We can also compute the free energy under the truncation $F_{\mathrm{trunc}} \sim O(N^2)$ and

$$\frac{\beta F_{\mathrm{trunc}}}{N^2} = -\frac{1}{N^2}\ln Z_{\mathrm{trunc}} = -\frac{1}{2}\left(\frac{1}{s_0^2} + \ln s_0^2 - 1\right). \tag{4.26}$$

[6)] This effective action is exactly the one solved in references [19, 20].

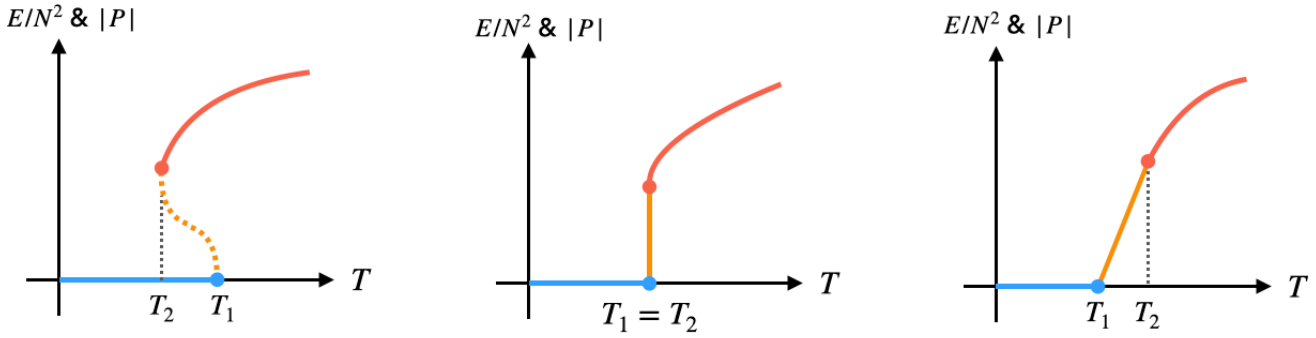

Figure 5: Three basic patterns of T-dependence of the energy E/N^2 and Polyakov loop P [10]. The blue, orange and red lines are the completely confined, partially-deconfined and completely deconfined phases, respectively. This figure corresponds to figure 4. [Left] First-order transition with hysteresis. [Middle] First-order transition without hysteresis. [Right] Non-first-order transition.

Partial deconfinement in terms of $\rho(\theta)$

In conclusion, we obtained the eigenvalue distribution for the free Yang-Mills theories with adjoint matter

$$\rho(\theta) = \begin{cases} \frac{1}{2\pi} & (T \le T_{\rm c}) \\ \frac{1}{2\pi}(1 + 2u_1 \cos\theta) & (T = T_{\rm c} = T_{\rm H}) \\ \frac{1}{\pi s_0^2} \cos\frac{\theta}{2}\sqrt{s_0^2 - \sin^2\frac{\theta}{2}} & (T \ge T_{\rm c}) \end{cases} . \tag{4.27}$$

In this case, the Hagedorn transition is of first order, and the phase structure agrees with the middle panel of figure 1. While the thermodynamic quantities are discontinuous at $T = T_{\rm c}$ in the canonical ensemble, it is not the case in the microcanonical ensemble since the entropy is maximized for each fixed energy. Therefore, it follows that M can be determined by the energy itself. In this case, the Polyakov loop P plays the same role because the free energy is the function of P in the intermediate phase and the energy or entropy comes from the free energy.

At the critical temperature $T = T_{\rm c}$, we can identify

$$u_1 = P = \frac{M}{2N}, \qquad M \le N, \tag{4.28}$$

and

$$\rho(\theta) = \left(1 - \frac{M}{N}\right)\rho_{\rm con}(\theta) + \frac{M}{N}\rho_{\rm dec}(\theta) = \left(1 - \frac{M}{N}\right)\cdot\frac{1}{2\pi} + \frac{M}{N}\cdot\frac{1}{2\pi}(1 + \cos\theta), \tag{4.29}$$

by introducing the distribution functions $\rho_{\rm con}(\theta)$ and $\rho_{\rm dec}(\theta)$ defined at the Hagedorn transition point ($M = 0$) and Gross-Witten-Wadia transition point ($M = N$), respectively. Note that these two phase transitions can be justified in the microcanonical sense not the canonical one. The identification (4.28) is essentially equivalent to the

statement that the Polyakov loop P is an order parameter of partial deconfinement and the size of the deconfined sector can be extracted by P and the minimum of the eigenvalue distribution $\rho(\theta)$.

4.1.2 Comments on finite coupling

The previous analysis is performed in zero-coupling limit. In general, introducing the nonzero coupling changes the phase structure. To incorporate the effect of finite coupling to the effective action, the original study [9] paid attention to the gauge invariance and constraints brought by it. The effective action is determined as a function of $\mathrm{tr}\, U^n$ for any n and must be invariant under gauge transformations. Therefore, the form of effective action only depends on the combinations of the terms such as

$$\mathrm{tr}\, U^{n_1} \cdots \mathrm{tr}\, U^{n_m}\, \mathrm{tr}\, U^{-(n_1+\cdots+n_m)}. \tag{4.30}$$

If considering the perturbation theory for small coupling, the effective action becomes further simplified and

$$S_{\text{eff}} = N^2\Big(m_1^2|u_1|^2 + b|u_1|^4 + O(\lambda^2)\Big), \tag{4.31}$$

where the parameters are determined by the temperature T and the 't Hooft coupling $\lambda = g_{\text{YM}}^2 N$ which is evaluated by at the energy scale, that is, the inverse of the radius of the sphere. Although we omit the higher corrections with respect to the 't Hooft coupling, the generic form is already known [9]. Alternatively, it works to consider the toy model described by the unitary matrices

$$Z(\beta) = \int [\mathrm{d}U]\, \exp\left[-\left((m_1^2-1)|\mathrm{tr}\, U|^2 + \frac{b}{N^2}|\mathrm{tr}\, U|^4 + \cdots\right)\right], \tag{4.32}$$

in order to capture the behaviors of the full theory in weak coupling. The dots at the end represents the higher order corrections in λ. These parameters control the detailed structure of phases. The phase structure of the type shown in the middle panel of figure 5 is the zero coupling case $\lambda = 0, (b = 0)$, as explained in the previous section. When we turn on the finite coupling, the parameter b may become positive or negative. The positive and negative b correspond to the right and left panels of figure 5, respectively[7)]. In other words, this parameter governs the existence of the hysteresis in the intermediate region.

The analysis of the above unitary matrix model of the large N pure Yang-Mills theory on S^3 up to three-loop order shows the negative b [66], and the direct path-integral calculation up to two-loop order provides the consistency check [67]. Besides, the authors of these papers also studied the low-dimensional theories on tori numerically [68].

[7)] See also the figure 4 of reference [9].

4.1.3 With fundamental matter

The argument in section 4.1 is applicable to the theories consists of fields both in the adjoint and fundamental representations. In this case, we take the large N limit with $\frac{N_\mathrm{f}}{N}$ fixed, as known as the *Veneziano limit*. The generalization is discussed for the weak-coupling limit [63, 69, 14] and for the perturbation theory [70].

In addition to define the bosonic and fermionic single-particle partition function in the adjoint representation $z_\mathrm{B}(x), z_\mathrm{F}(x)$, let us define the ones in the fundamental representation $\mathcal{Z}_\mathrm{B}(x), \mathcal{Z}_\mathrm{F}(x)$. Then, the generic form of the partition function of the $\mathrm{U}(N)$ unitary matrix model is

$$\begin{aligned} Z(x) = \int [\mathrm{d}U] \exp \Bigg[&\sum_{n=1}^{\infty} \frac{1}{n} \big\{ \mathcal{Z}_\mathrm{B}(x^n) + (-1)^{n-1} \mathcal{Z}_\mathrm{F}(x^n) \big\} \Big(\operatorname{tr} U^n + \operatorname{tr} U^{\dagger n} \Big) \\ &+ \sum_{n=1}^{\infty} \frac{1}{n} \big\{ z_\mathrm{B}(x^n) + (-1)^{n-1} z_\mathrm{F}(x^n) \big\} \operatorname{tr} U^n \operatorname{tr} U^{\dagger n} \Bigg]. \end{aligned} \tag{4.33}$$

The first term appeared additionally is the contribution of the field contents in the fundamental representation because of the group character $\chi_\mathrm{fund}(U) = \operatorname{tr}(U) + \operatorname{tr}\big(U^\dagger\big)$. The replacement of the integral measure with respect to the eigenvalues of gauge field provides the pairwise potentials

$$V_\mathrm{A}(\theta) = \ln 2 + \sum_{n=1}^{\infty} \frac{1}{n} \big\{ 1 - z_\mathrm{B}(x^n) - (-1)^{n-1} z_\mathrm{F}(x^n) \big\} \cos n\theta, \tag{4.34a}$$

$$V_\mathrm{F}(\theta) = -\sum_{n=1}^{\infty} \frac{2}{n} \big\{ \mathcal{Z}_\mathrm{B}(x^n) + (-1)^{n-1} \mathcal{Z}_\mathrm{F}(x^n) \big\} \cos n\theta, \tag{4.34b}$$

and

$$Z = \int [\mathrm{d}\theta_i] \exp \left[- \left\{ \sum_{j \neq i} V_\mathrm{A}(\theta_i - \theta_j) + \sum_i V_\mathrm{F}(\theta_i) \right\} \right]. \tag{4.35}$$

At low temperature

We can perform the same computation as the case with the adjoint matters. Suppose eigenvalue distribution is symmetric around $\theta = 0$, and hence, $V_\mathrm{A}(\theta) = V_\mathrm{A}(-\theta)$ and $V_\mathrm{F}(\theta) = V_\mathrm{F}(-\theta)$.

$$\begin{aligned} S[\{u_n\}] =& \sum_{n=1}^{\infty} \frac{N^2}{n} \int \mathrm{d}\alpha \, \mathrm{d}\beta \, \rho(\theta_1) \rho(\theta_2) \big[1 - z_\mathrm{B}(x^n) - (-1)^{n-1} z_\mathrm{F}(x^n) \big] \cos n(\theta_1 - \theta_2) \\ &- \sum_{n=1}^{\infty} \frac{2NN_\mathrm{f}}{n} \int \mathrm{d}\theta \, \rho(\theta) \big[\mathcal{Z}_\mathrm{B}(x^n) + (-1)^{n-1} \mathcal{Z}_\mathrm{F}(x^n) \big] \cos n\theta \\ =& \frac{N^2}{\pi} \sum_{n=1}^{\infty} \left[V_n^\mathrm{A}(x) |u_n|^2 + \frac{2N_\mathrm{f}}{N} V_n^\mathrm{F}(x) u_n \right], \end{aligned} \tag{4.36}$$

where $V_n^{\mathrm{A}}, V_n^{\mathrm{F}}$ are the Fourier modes in the adjoint and fundamental representations, respectively, defined as

$$V_n^{\mathrm{A}}(x) = \frac{\pi}{n}\big[1 - z_{\mathrm{B}}(x^n) - (-1)^{n-1} z_{\mathrm{F}}(x^n)\big], \tag{4.37a}$$

$$V_n^{\mathrm{F}}(x) = -\frac{\pi}{n}\big[\mathcal{Z}_{\mathrm{B}}(x^n) + (-1)^{n-1}\mathcal{Z}_{\mathrm{F}}(x^n)\big]. \tag{4.37b}$$

Therefore, the stationary condition of equation (4.36) gives

$$u_n = -\frac{N_{\mathrm{f}}}{N}\left(\frac{V_n^{\mathrm{F}}}{V_n^{\mathrm{A}}}\right). \tag{4.38}$$

As mentioned in the adjoint matter case, only we have to consider is the $n = 1$ case, and hence,

$$V_1^{\mathrm{F}}(x) < 0, \tag{4.39}$$

is always kept, and $V_1^{\mathrm{A}}(x)$ is positive when $z_{\mathrm{B}}(x) + z_{\mathrm{F}}(x) < 1$. As a result, the lowest mode u_1 becomes nonzero unless zero temperature or the ratio $\frac{N_{\mathrm{f}}}{N}$ is zero, which returns the theory only with adjoint matters. Although we can formally define the Hagedorn temperature T_{H} as the solution of

$$[z_{\mathrm{B}}(x_{\mathrm{H}}) + z_{\mathrm{F}}(x_{\mathrm{H}})] = 1, \tag{4.40}$$

where u_1 is excited and becomes nonzero, this condition is never satisfied in the stationary condition above zero temperature. Instead,

$$[z_{\mathrm{B}}(x) + z_{\mathrm{F}}(x)] + \frac{N_{\mathrm{f}}}{N}[\mathcal{Z}_{\mathrm{B}}(x) + \mathcal{Z}_{\mathrm{F}}(x)] \leq 1. \tag{4.41}$$

It is worthwhile to mention lastly that the free energy of the above stationary point is

$$\beta F = -\frac{{N_{\mathrm{f}}}^2}{\pi}\sum_n \frac{\left(V_n^{\mathrm{F}}\right)^2}{V_n^{\mathrm{A}}} \propto {N_{\mathrm{f}}}^2, \tag{4.42}$$

which differs from the result for the low-temperature phase of the theories with adjoint matters, $f \sim O(N^0)$. This scaling implies that the color singlet objects such as the mesons and glueballs dominates to thermodynamics. However, this phase is not the completely-confined phase according to the Polyakov loop as the order parameter, and seems rather partially-confined phase. We will justify this physical picture in terms of the distribution of the Polyakov line phases.

Around Gross-Witten-Wadia temperature T_{GWW}

We treat the phase distribution $\rho(\theta)$ and its Fourier modes u_n independently and solve with respect to them self-consistently under the stationary condition [65] for the following effective action

$$S = N\sum_{n=1}^{\infty}\frac{c_n}{2n}\Big(\operatorname{tr} U^n + \operatorname{tr} U^{\dagger n}\Big), \tag{4.43}$$

where

$$c_n(x) = 2\left(a_n(x)u_n + \frac{N_{\rm f}}{N}b_n(x)\right), \tag{4.44a}$$

$$a_n(x) = z_{\rm B}(x^n) + (-1)^{n-1}z_{\rm F}(x^n), \tag{4.44b}$$

$$b_n(x) = \mathcal{Z}_{\rm B}(x^n) + (-1)^{n-1}\mathcal{Z}_{\rm F}(x^n), \tag{4.44c}$$

which is in the same manner as for the adjoint matter.

At low temperatures below the Gross-Witten-Wadia temperature $T = T_{\rm GWW}$, the phase distribution is non-uniform and nonzero everywhere on the circle;

$$\rho(\theta) = \frac{1}{2\pi}\left[1 + 2\sum_{n=1}^{\infty} u_n \cos(n\theta)\right], \tag{4.45}$$

where

$$u_n = \frac{N_{\rm f}}{N}\frac{b_n}{1-a_n} = -\frac{N_{\rm f}}{N}\left(\frac{V_n^{\rm F}}{V_n^{\rm A}}\right). \tag{4.46}$$

which is the same expression as equation (4.38). We can compute the free energy in terms of the coefficients in (4.44) and

$$\frac{\beta F}{N^2} = -{N_{\rm f}}^2\sum_{n=1}^{\infty}\frac{b_n^2}{1-a_n}, \tag{4.47}$$

which is identical to one derived from (4.42).

When temperature glows and becomes higher than the Gross-Witten-Wadia temperature, the region where $\rho(\theta) = 0$ for $|\theta| > \theta_0$ on the circle appears. The Gross-Witten-Wadia temperature separates the low- and high-temperature phases at the point $\theta_0 = \pi$. The solution of the stationary condition in this phase is given by

$$\rho(\theta) = \frac{1}{\pi}\sum_{n=1}^{\infty} Q_n \cos\left(\left(n-\frac{1}{2}\right)\theta\right)\sqrt{s_0^2 - \sin^2\frac{\theta}{2}}. \tag{4.48}$$

The difference from the adjoint case appears the definition of the coefficients

$$Q_n \equiv \sum_{l=0}^{\infty} c_{n+l}P_l(\cos\theta_0), \tag{4.49}$$

where $P_l(y)$ is the Legendre polynomial, and the coefficients c_n is defined in (4.44).

The truncation of the coefficients a_n, b_n may work as a good approximation and afford the qualitatively similar behaviors. If we assume $a_n = b_n = 0$ for $n \leq 2$, for simplicity, the phase distribution this simplified model can be obtained

$$\rho(\theta) = \frac{1}{\pi s_0^2}\cos\frac{\theta}{2}\sqrt{s_0^2 - \sin^2\frac{\theta}{2}}, \tag{4.50}$$

which is identical to the expression of adjoint case (4.24), and

$$s_0^2 = \sin^2\frac{\theta_0}{2} = \left[2\left(a_1 u_1 + \frac{N_{\rm f}}{N} b_1\right)\right]^{-1} = \frac{1}{Q_1}. \tag{4.51}$$

In the truncated model, from (4.26) and the replacement $a_n \to \frac{1}{2}c_n$, we can compute the free energy which is of order N^2

$$\frac{\beta F_{\rm trunc}}{N^2} = -\frac{1}{2}\left(\frac{1}{s_0^2} + \ln s_0^2 - 1\right) - \frac{N_{\rm f}}{N} b_1 u_1 = -\frac{1}{s_0^2} - \frac{1}{2}\ln s_0^2 + \frac{7}{4} - s_0^2 + \frac{s_0^4}{2} - (1-a_1)\left(1 - s_0^2 + \frac{s_0^4}{4}\right). \tag{4.52}$$

The minimum of the phase transition vanishes at the Gross-Witten-Wadia temperature $T_{\rm GWW}$, where $\theta_0 = \pi$ and $s_0^2 = 1$. The expressions of the phase distribution $\rho(\theta)$ and free energy connects smoothly at $T = T_{\rm GWW}$. We can compare them, at least, in the truncated model. For the phase distributions, they are a match with

$$\rho_{\rm GWW}(\theta) = \frac{1}{2\pi}(1 + \cos\theta). \tag{4.53}$$

From equation (4.47), the free energy in the low-temperature phase is

$$-\left.\frac{\beta F}{N^2}\right|_{n=1} = {N_{\rm f}}^2 \frac{b_1^2}{1-a_1} = \frac{1}{4}(1-a_1) = \frac{N_{\rm f}}{2N} b_1, \tag{4.54}$$

and the one in the high-temperature phase is, from equation (4.52)

$$-\left.\frac{\beta F_{\rm trunc}}{N^2}\right|_{s_0^2=1} = \frac{1}{4}(1-a_1) = \frac{N_{\rm f}}{2N} b_1, \tag{4.55}$$

which shows the agreement of the expressions of the free energy at $T = T_{\rm GWW}$. Note that one can see that the order of this phase transition is third and the similarity to the original transition [19, 20].

Partial deconfinement

Using the nature of the large N theory, we can prove that the partially-deconfined phase exists in the low-temperature phase, as discussed in references [14, 71]. Let us consider the generic form of the free energy for the $\mathrm{U}(N)$ gauge theories consisting of the adjoint and fundamental fields;

$$\beta F = \sum_{n=1}^{\infty} \left\{ N^2 a_n(x) |u_n|^2 + N N_{\rm f} b_n(x)(u_n + u_n^*) \right\}. \tag{4.56}$$

The coefficients $a_n(x), b_n(x)$ relate to the bosonic and fermionic single-particle partition functions and are determined by the field contents in the adjoint and fundamental representations, respectively. Below the Gross-Witten-Wadia temperature, equation (4.47) describes the saddle-point solution, and hence, we can estimate the

thermodynamical quantities from it. For the later use, we derivative the free energy by β and calculate the energy E

$$E = \frac{\partial(\beta F)}{\partial \beta} = \sum_{n=1}^{\infty} \left\{ N^2 \frac{\partial a_n}{\partial \beta} |u_n|^2 + N N_{\rm f} \frac{\partial b_n}{\partial \beta} (u_n + u_n^*) \right\}. \tag{4.57}$$

At zero temperature $T = 0$, the variable x also becomes zero. In some specific model such as the weakly-coupled large N_c QCD with $N_{\rm f}$ fermions ($N_{\rm f}/N_c$ fixed) discussed in references [69,14] or the Gaussian matrix model with $N_{\rm f}$ fundamental scalars that will be discussed in section 4.3.3, one can identify that the Hagedorn temperature formally exists at zero temperature$T_{\rm H} = 0$. The phase structure for this generic model is shown schematically in the figure 6, which is quite similar to the phase structure in the right panel of figure 5.

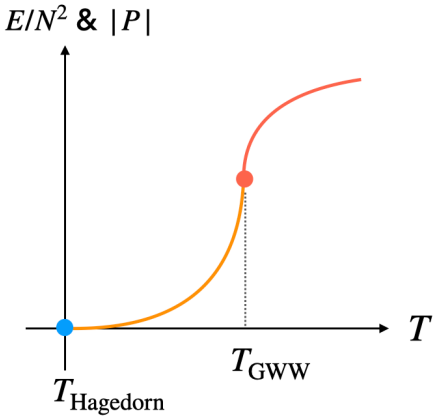

Figure 6: Phase structure for the large N theory with the adjoint and fundamental matters. The ordinary confinement/deconfinement transition at which the Polyakov loop jumps to nonzero value exists at zero temperature $T = 0$ (blue dot). At a rather higher temperature, there is the Gross-Witten-Wadia temperature of full theory $T_{\rm GWW}(N)$ (red dot). The phase structure resembles the one shown in the right panel of figure 5. We can interpret that the low-temperature phase (orange line) separated by these phase transition points is nothing but the partially-deconfined phase.

Let us further define the free energy of the $\mathrm{SU}(M)$ subsector

$$\beta \tilde{F} = \sum_{n=1}^{\infty} \left\{ N^2 a_n(x) |\tilde{u}_n|^2 + N N_{\rm f} b_n(x) (\tilde{u}_n + \tilde{u}_n^*) \right\}, \tag{4.58}$$

and corresponding energy

$$\tilde{E} = \frac{\partial(\beta \tilde{F})}{\partial \beta} = \sum_{n=1}^{\infty} \left\{ N^2 \frac{\partial a_n}{\partial \beta} |\tilde{u}_n|^2 + N N_{\rm f} \frac{\partial b_n}{\partial \beta} (\tilde{u}_n + \tilde{u}_n^*) \right\}. \tag{4.59}$$

Above, we utilized the fact that we can always collect the excited quanta in the $\mathrm{SU}(N)$ subsector since considering free theory. The Polyakov loops in the subsector is defined as

$$\tilde{u}_n = \frac{1}{M}\sum_{j=1}^{M} \mathrm{e}^{\mathrm{i}n\theta_j}, \tag{4.60}$$

and satisfy the following relation

$$u_n = \frac{1}{N}\left(\sum_{j=1}^{M} + \sum_{j=M+1}^{N}\right)\mathrm{e}^{\mathrm{i}n\theta_j} = \frac{M}{N}\tilde{u}_n + 0. \tag{4.61}$$

At $T = T_{\mathrm{GWW}}(M, N_{\mathrm{f}})$ the $\mathrm{SU}(M)$ sector reaches the Gross-Witten-Wadia transition point. The Polyakov line phases not contained in the $\mathrm{SU}(M)$ subsector form the uniform distribution since they are not excited thermodynamically, and hence,

$$\min\tilde{\rho}(\theta) = 0 \quad \leftrightarrow \quad \min\rho(\theta) = \frac{1}{2\pi}\left(1 - \frac{M}{N}\right), \tag{4.62}$$

and from this expression we can read the value M off. We will see the actual phase distribution for the theory with fundamental matters in section 4.3.3, which is essentially same analysis with above one, and the demonstration strongly supports the presence of the phase partial deconfinement takes place.

Moreover, partial deconfinement can be seen in terms of the thermodynamic quantities. For example, the energy E and entropy S are

$$E = E_{\mathrm{GWW}}(M, N_{\mathrm{f}}), \qquad S = S_{\mathrm{GWW}}(M, N_{\mathrm{f}}), \tag{4.63}$$

because the contribution of the Polyakov loops u_n from other than the $\mathrm{SU}(M)$ subsector always vanishes up to zero-point offset.

These observations imply that partial deconfinement takes place in the color sector and separate into the confined and deconfined sectors, while it does not seem to happen in the flavor sector and perform any separation. Intuitively speaking, the behavior of partial deconfinement for the fundamental matters happens like in figure 7, in contrast to figure 1 for the adjoint fields case. Another evidence not to happen the two-phase coexistence for the flavor sector may be the consensus with the Vafa-Witten theorem [72] which restricts the spontaneous breaking of the vector-like continuous symmetry. As discussed in reference [14], there is a possibility of the flavor symmetry breaking, namely, the loophole of the Vafa-Witten theorem. The theorem assumes the positivity of the fermion determinant in the Euclidean path integral. If we introduce the nonzero baryon chemical potential $\mu_{\mathrm{B}} \neq 0$, the fermion determinant can be complex, and hence, the assumption is no longer valid.

4.2 $\mathrm{O}(N)$ vector model

Up here, we have seen the case of the free Yang-Mills theories with adjoint fields. In this section, let us take a look at the three-dimensional free theory of N-component N_{f}-flavor vector of scalar fields on S^2 with the radius

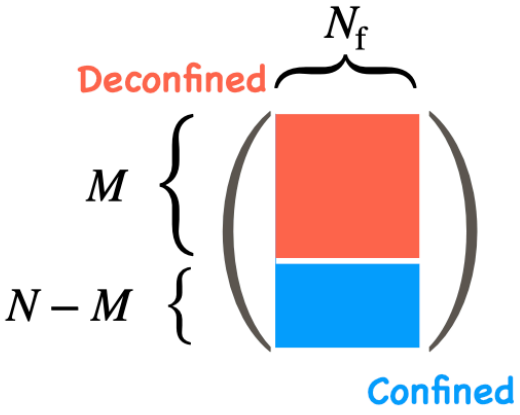

Figure 7: Schematic picture of the matter field configuration in the fundamental representation where the partial deconfinement takes place. The $M \times N_{\rm f}$ -block (red) and the rest (blue) represent the deconfined and confined sectors, respectively.

R which also takes place the confinement/deconfinement transition due to the gauge-singlet condition [73] and partial deconfinement below the GWW temperature $T_{\rm GWW}(N)$ [13]. In the large N limit with $\frac{N_{\rm f}}{N}$ fixed, the deconfinement transition is characterized by the growth of thermodynamic quantity such as the entropy S from N^0 to N^2 in a double scaling limit with respect to the radius R and N.

This model originates from the coupling of $\vec{\phi}(x)$ with the $\mathrm{O}(N)$ gauge field in the Chern-Simons action and its infinite-level limit, for example. The motivation to study this type of model comes from the gauge/gravity duality, particularly the connection between the thermodynamic behavior in QFT and black holes in the bulk. Specifically, the duality between this model and the higher spin gravity as known as Vasiliev gravity [74–76] has conjectured [77] and been studied in the literature (see references [78–81], and textbook [82] *in Japanese*, for example). This model is also interesting to compare the (de)confinement at large N to the N-particle quantum mechanics of the indistinguishable ideal Bose gas that exhibits the Bose-Einstein condensation at low temperatures explained in section 5.

The model consists of N-component vector of scalars

$$\vec{\phi}(x) = (\phi_1(x), \cdots, \phi_N(x)), \tag{4.64}$$

which transforms in the $\mathrm{O}(N)$ fundamental representation. In order for simplicity to consider the occurrence of partial deconfinement, the number of flavor $N_{\rm f}$ is set to be one. Note that we now consider the theory on $\mathrm{S}^2_R \times \mathrm{S}^1_\beta$, and hence, $d = 3$. The generalization to the generic dimension d and flavors $N_{\rm f} > 1$ is straightforward.

We can start from the following partition function described by the Polyakov line phases θ_i;

$$Z(\beta) = \frac{1}{N!}\int \prod_i \mathrm{d}\theta_i \exp\left[\sum_{i<j} 2\ln\left|\sin\frac{\theta_i-\theta_j}{2}\right| + 2N_{\mathrm{f}}\sum_{n=1}^{\infty}\frac{1}{n}z_{\mathrm{S}}(x^n)\sum_i \cos(n\theta_i)\right], \tag{4.65}$$

where

$$z_{\mathrm{S}}(x) = x^{\frac{d}{2}-1}\frac{1+x}{(1-x)^{d-1}}. \tag{4.66}$$

This expression is analogous to equation (4.5) for the weakly-coupled Yang-Mills theories explained the previous sections.

To solve this model, we can apply the method essentially same as the previous sections. Skipping the detail, we figure out that the Polyakov loop is zero at zero temperature and nonzero at finite temperature, and the Gross-Witten-Wadia transition occurs at

$$T_{\mathrm{GWW}}(N) = \frac{\sqrt{3}}{\pi R}\sqrt{N}. \tag{4.67}$$

Therefore the phase structure looks similar to figure 6. Below the $T_{\mathrm{GWW}}(N)$, we can confirm that the two-phase coexistence in terms of color degrees of freedom takes place. If we define the parameter b as

$$b \equiv \frac{TR}{\sqrt{N}} \sim N^0, \tag{4.68}$$

the distribution of the Polyakov line phases is obtained, from stationary condition, by

$$\rho(\theta) = \frac{1}{2\pi} + \frac{2b^2}{\pi}f(\theta), \tag{4.69}$$

where

$$f(\theta) = \sum_{n=1}^{\infty}\frac{\cos(n\theta)}{n^2} = \frac{\pi^2}{12} + \frac{(|\theta|-\pi)^2}{4}. \tag{4.70}$$

The GWW-transition point is where the minimum of the phase distribution goes to zero, namely $\min\rho(\theta) = 0$, and hence, $b = b_{\mathrm{GWW}} = \frac{\sqrt{3}}{\pi}$. Using this parameter,

$$\rho(\theta; b_{\mathrm{GWW}}) = \frac{3}{2\pi^2}(|\theta|-\pi)^2, \tag{4.71}$$

which becomes zero at $\theta = \pm\pi$, as we can see. As a result, the phase distribution can be written as the combination of the distribution function defined at $T = 0$ and $T = T_{\mathrm{GWW}}(N)$;

$$\rho(\theta; T) = \left(1 - \frac{b^2}{b_{\mathrm{GWW}}^2}\right)\rho_{\mathrm{con}}(\theta) + \frac{b^2}{b_{\mathrm{GWW}}^2}\cdot\rho(\theta; b_{\mathrm{GWW}}). \tag{4.72}$$

The ratio of the mixture with the confined and deconfined sector is

$$\frac{M}{N} = \frac{b^2}{b_{\mathrm{GWW}}^2}, \quad \Leftrightarrow \quad TR = b\sqrt{N} = b_{\mathrm{GWW}}\sqrt{M}, \tag{4.73}$$

In the above relation, we can regard the temperature T as the critical temperature in O(M) theory, namely,

$$T_{\mathrm{GWW}}(M)R = b_{\mathrm{GWW}}\sqrt{M}. \tag{4.74}$$

In conclusion,

$$\rho(\theta; T = T_{\mathrm{GWW}}(M)) = \left(1 - \frac{M}{N}\right) \cdot \frac{1}{2\pi} + \frac{M}{N} \cdot \rho_{\mathrm{GWW}}(\theta; M), \tag{4.75}$$

which is in the same form as the obtained in the previous example.

At high temperature, $b \gg 1$ but still of order N^0, the attractive force in the effective action for the Polyakov line phases θ becomes extremely strong, and their distribution becomes sharpen. In the case, the free energy is

$$\beta F = 4\zeta(5){N_{\mathrm{f}}}^2 T^5, \tag{4.76}$$

From that, we can also calculate the energy and entropy scaling at $1 \ll T = T_{\mathrm{GWW}}(M) \leq T_{\mathrm{GWW}}(N)$, and

$$E = AT^5 = E_{\mathrm{GWW}}(M) \sim M^{\frac{5}{2}}, \qquad S = \frac{5}{4}AT^4 = S_{\mathrm{GWW}}(M) \sim M^2, \tag{4.77}$$

where $A = 16\zeta(5)$. Certainly, the phase transition occurs where the entropy increases to of order N^2. However, notice that the energy scaling with M is different for the free vector fields from the previous examples with the matrix degrees of freedom.

Above discussion is based on the path integral formalism. We can derive this thermodynamics in the Hamilton formalism as well. We will discuss that by utilizing the Gaussian matrix model in the next section, which can be applied to this model.

4.3 Gauged Gaussian matrix model

Previous examples are the theory defined on sphere and have some spatial directions. However, as we can see in this section, even the toy models not containing the spatial dimensions can exhibit the confinement/deconfinement transition at finite temperature. That surprising model we look at here is the $(0 + 1)$-dimensional matrix quantum mechanics called gauged Gaussian matrix model or just Gaussian matrix model. The gauged Gaussian matrix model is an analytically solvable toy model for the deconfinement and had been studied in terms of partial deconfinement analytically [13, 12] numerically [17, 71]. The discussion studying the deconfinement at large N is essentially parallel to the previous examples. Since the model is simpler and easier to calculate than the above examples, we added some materials to analyse the model in appendix C.

4.3.1 $N_{\mathrm{f}} = 0$ case

For starter, let us consider the original model of the gauged Gaussian matrix model consisting of only the matrix fields. The action of the model is

$$S = N\sum_{I=1}^{D}\int_0^\beta \mathrm{d}t\,\mathrm{Tr}\left\{\frac{1}{2}(D_t X_I)^2 + \frac{1}{2}X_I^2\right\}, \tag{4.78}$$

where X_I is $N \times N$ hermitian matrices. The index I runs 1 to D. The covariant derivative is defined as $D_t X_I = \partial_t X_I - \mathrm{i}g\,[A_t, X_I]$ with the temporal gauge field A_t. The circumference towards the temporal direction is identified with the inverse temperature $\beta = \frac{1}{T}$.

To perform the functional integral and obtain the partition function, we choose the static diagonal gauge

$$A_t = \frac{1}{\beta}\,\mathrm{diag}\,(\theta_1, \cdots, \theta_N), \tag{4.79}$$

and fix the gauge redundancy. The Polyakov line phases θ_i are independent on t and $\theta_i \in (-\pi, \pi]$. The form of the free energy[8] is given by

$$\beta F = -\ln Z(\beta) = \frac{\beta N^2 D}{2} + N^2 \sum_{n=1}^{\infty} \frac{1 - Dx^n}{n} |u_n|^2, \tag{4.80}$$

where $x = \mathrm{e}^{-\beta}$, same as before. For detailed calculations, see appendix C.

Same as the previous free theories with adjoint matters, this model exhibits the confinement/deconfinement transition which is of first order at $T = T_{\mathrm{c}} = \frac{1}{\ln D}$ in the canonical ensemble (the middle panel of figure 4 and 5). At low temperatures, the coefficients of u_n are all positive, and hence, the saddle point condition requires $u_n = 0$ for any n. At $T = T_{\mathrm{c}}$, the coefficient for $n = 1$ becomes zero while the rest keeps positive values. Therefore, only the Polyakov loop $P = u_1$ can take any value between 0 and $\frac{1}{2}$ as the saddle point solution. The deconfinement transition accompanies two different phase transitions, the Hagedorn transition at $P = 0$ and the Gross-Witten-Wadia transition at $P = \frac{1}{2}$. The intermediate phase appears where $0 \le P \le \frac{1}{2}$ separated by these transitions. Note that we again fix the ambiguity of center symmetry in the Polyakov line phase by the condition $P = |P|$.

Using a similar analysis to one of the free Yang-Mills theories, the distribution of the Polyakov line phases $\rho^{(\mathrm{P})}(\theta)$ is obtained by

$$\rho^{(\mathrm{P})}(\theta)\Big|_{T=T_{\mathrm{c}}} = \frac{1}{2\pi}\,(1 + 2P\cos\theta)\,, \tag{4.81}$$

in which we emphasize that it represents distribution for the Polyakov line phases.

We can compute the energy and entropy as functions of the Polyakov loop[9] ,

$$E|_{T=T_{\mathrm{c}}} \equiv \frac{N}{\beta}\int \mathrm{d}t \sum_I \mathrm{Tr} X_I^2\Big|_{T=T_{\mathrm{c}}} = \frac{D}{2}N^2 + N^2P^2 \tag{4.82}$$

$$S|_{T=T_{\mathrm{c}}} = \ln D \cdot N^2 P^2. \tag{4.83}$$

As we can see, the energy E and entropy S glows from N^0 to N^2 up to the zero-point energy $\frac{d}{2}N^2$ in conjunction with the growth of P from 0 to $\frac{1}{2}$. Keep in mind that the free energy $F = E - TS$ is

$$F|_{T=T_{\mathrm{c}}} = \frac{D}{2}N^2, \tag{4.84}$$

[8] More precisely, the value of the effective potential at the stationary point $\frac{\partial V_{\mathrm{eff}}}{\partial u_n} = 0$.

[9] There is a subtlety to compute these quantities at the critical temperature. Introducing a "source term" and removing at the end of calculation enables us to avoid it. See appendix A.1 of reference [13].

and does not depend on P. Therefore, every value of the Polyakov loop equally contributes to the canonical partition function.

Partial deconfinement

As mentioned, the partially-deconfined phase appears at $T = T_{\rm c}$ as an intermediate phase divided by the two distinct phase transitions. In this section, we restrict the argument at the critical temperature. There, the size of the deconfined sector M can change from $M = 0$ to $M = N$. Again, the value can be read off from the physical quantities or the offset of the phase distribution. In the case of the Gaussian matrix model as well, we can identify the Polyakov loop as

$$P = \frac{M}{2N}. \tag{4.85}$$

It leads that the distribution of the Polyakov line phases (4.81) can be expressed by

$$\rho^{(\mathrm{P})}(\theta) = \frac{1}{2\pi}\left(1 + \frac{M}{N}\cos\theta\right) = \left(1 - \frac{M}{N}\right)\cdot\frac{1}{2\pi} + \frac{M}{N}\cdot\frac{1+\cos\theta}{2\pi}, \tag{4.86}$$

and therefore

$$\rho^{(\mathrm{P})}_{\rm con}(\theta) = \frac{1}{2\pi}, \tag{4.87}$$

and

$$\rho^{(\mathrm{P})}_{\rm dec}(\theta) = \frac{1}{2\pi}(1+\cos\theta). \tag{4.88}$$

For the energy E and entropy S in equations (4.82), (4.83), we can rewrite the expressions to

$$E = \frac{D}{2}N^2 + \frac{M^2}{4} = \frac{D}{2}(N^2 - M^2) + \left(\frac{D}{2} + \frac{1}{4}\right)M^2, \tag{4.89}$$

and

$$S = \frac{\ln D}{4}M^2 = 0\cdot(N^2 - M^2) + \frac{\ln D}{4}M^2. \tag{4.90}$$

In this way, we can separate two different contributions coming from the confined and deconfined sectors in terms of the color degrees of freedom. We show the equations such that the first term is interpreted as the contribution from the ground state, while the second one is the value of each observable for an $\mathrm{SU}(M)$ truncated theory at the Gross-Witten-Wadia-transition point where only M degrees of freedom can be excited. The two-phase coexistence as schematically shown in figure 1 explains this M-dependence.

We give a comment to avoid the later confusion; when we carry out the numerical simulation at large but finite N, we utilize the equation (4.85) to determine the size of deconfined sector M by $2NP \in [M - \frac{1}{2}, M + \frac{1}{2}]$.

4.3.2 The Hamilton formalism

We can parallelly study the thermodynamics of the partially-deconfined phase for the Gaussian matrix model at large N in the Hamilton formalism [13]. In this approach, we can understand the spontaneous breaking of gauge symmetry more clearly.

The Hamiltonian of this model is given by

$$\hat{H} = \frac{1}{2}\sum_{I} \mathrm{Tr}\left(\hat{P}_I^2 + \hat{X}_I^2\right) = \frac{1}{2}\sum_{I,\alpha} \mathrm{Tr}\left(\hat{P}_{I\alpha}^2 + \hat{X}_{I\alpha}^2\right), \tag{4.91}$$

where

$$\hat{P}_{jk} = \sum_{\alpha=1}^{N^2-1} \hat{P}_\alpha \tau_{jk}^\alpha, \qquad \hat{X}_{jk} = \sum_{\alpha=1}^{N^2-1} \hat{X}_\alpha \tau_{jk}^\alpha, \tag{4.92}$$

with $\mathrm{SU}(N)$ generators τ^α. Here, the commutation relation $\left[\hat{X}_{I\alpha}, \hat{P}_{J\beta}\right] = \mathrm{i}\delta_{IJ}\delta_{\alpha\beta}$ is satisfied. The creation and annihilation operators are defined by these operators as

$$\hat{A}_I^\dagger = \frac{1}{\sqrt{2}}\left(\hat{X}_I - \mathrm{i}\hat{P}_I\right), \qquad \hat{A}_I = \frac{1}{\sqrt{2}}\left(\hat{X}_I + \mathrm{i}\hat{P}_I\right), \tag{4.93}$$

which is the analogue of the harmonic oscillators in the ordinary quantum mechanics. The arbitrary physical states can be obtained as a gauge singlet, and

$$\mathrm{Tr}\left(\hat{A}_I^\dagger \hat{A}_J^\dagger \hat{A}_K^\dagger \cdots\right)|0\rangle = \sum_{i,j,k,l\cdots=1}^{N} \left(\hat{A}_{I,ij}^\dagger \hat{A}_{J,jk}^\dagger \hat{A}_{K,kl}^\dagger \cdots\right)|0\rangle, \tag{4.94}$$

where the Fock vacuum $|0\rangle$ which satisfies $\hat{A}_I|0\rangle = 0$.

Let us also consider the truncated operator $\hat{A}_I^{\dagger\prime}$ which is reduced from $\hat{A}_I^\dagger$ to the $\mathrm{SU}(M)$-subsector. Applying that operator, the states which are $\mathrm{SU}(M)$-invariant but not $\mathrm{SU}(N)$-invariant can be constructed

$$\mathrm{Tr}\left(\hat{A}_I^{\dagger\prime} \hat{A}_J^{\dagger\prime} \hat{A}_K^{\dagger\prime} \cdots\right)|0\rangle = \sum_{i,j,k,l\cdots=1}^{M} \left(\hat{A}_{I,ij}^\dagger \hat{A}_{J,jk}^\dagger \hat{A}_{K,kl}^\dagger \cdots\right)|0\rangle, \tag{4.95}$$

where the indices in the sum run from 1 to M, not N. Obviously, this type of the state is not the invariant under some $\mathrm{SU}(N)$ transformations. Combining such states and constructing the energy eigenstate $|E;\mathrm{SU}(M)\rangle$ with the energy (4.89) determined by M, we can explain the entropy in equation (4.90), and see the consistency with the distribution of the Polyakov line phases (4.86) in the path integral formalism.

When one would like to discuss in an $\mathrm{SU}(N)$-invariant way, we can construct the $\mathrm{SU}(N)$-invariant states $|E\rangle_{\mathrm{inv}}$ by the linear combination of all possible embeddings of $\mathrm{SU}(M)$ into $\mathrm{SU}(N)$. Namely, we can perform the $\mathrm{SU}(N)$ symmetrization using the $|E;\mathrm{SU}(M)\rangle$;

$$|E\rangle_{\mathrm{inv}} \equiv \frac{1}{\sqrt{\mathcal{N}}}\int_{\mathrm{SU}(N)} \mathrm{d}U\, \mathcal{U}(|E;\mathrm{SU}(M)\rangle), \tag{4.96}$$

where $\mathcal{U}$ represents the gauge transformations and $\mathcal{N}$ is the normalization factor related to the volume of the $\mathrm{SU}(N)$ group. The integral is taken over all $\mathrm{SU}(N)$ gauge transformations. This type of the eigenstates also explains the entropy and the phase distributions above in a consistent manner.

A notable feature is that one cannot distinguish the $\mathrm{SU}(N)$-symmetrized, gauge-invariant state $|E\rangle_{\mathrm{inv}}$ from the state with a particular embedding of the $\mathrm{SU}(M)$, $|E;\mathrm{SU}(M)\rangle$ in the situation we have considered at large N. It can be interpreted as the occurrence of the spontaneous breaking of gauge symmetry. Let us consider a state with a particular embedding $|\mathrm{SU}(M)\rangle_1$ and its gauge transformed state $|\mathrm{SU}(M)\rangle_2$ by some unitary transformation[10] Let $\hat{O}$ be a gauge-invariant operator which is a polynomial of $O(N^0)$ matrices. Here, we introduce the 'short' gauge-invariant operators $\hat{O}$ as a polynomial of $O(N^0)$ matrices. The 'short' operators are suitable to investigate these states with energy of order N^2 since they do not change the energy and hence the thermodynamics in the system drastically. Then, we can derive

$$ {}_2\langle \mathrm{SU}(M)|\hat{O}|\mathrm{SU}(M)\rangle_1 = 0, \tag{4.97}$$

since one has to act $O(N^2)$ creation and annihilation operators in order to bridge between $|\mathrm{SU}(M)\rangle_1$ and $|\mathrm{SU}(M)\rangle_2$. This has an essentially same meaning as the super-selection rule; distinct embeddings of $\mathrm{SU}(M)$ to $\mathrm{SU}(N)$ are separated into distinct super-selection sectors. It can work even when the embeddings are very close in the large N limit. Suppose that V is a generator of $\mathrm{SU}(N)/\mathrm{SU}(M)$ with a small but of order N^0 norm $\sqrt{\mathrm{Tr}(VV^\dagger)}$. When we obtain $|\mathrm{SU}(M)\rangle_2$ by the transformation $\mathrm{e}^{\mathrm{i}V}$, the relation (4.97) is satisfied in the large N limit with fixed $\frac{M}{N}$ [11]. In conclusion, the same expectation value is obtained for $\hat{O}$ which is independent of whether to use a specific embedding or a super-position of whole embedding.

4.3.3 $N_{\mathrm{f}} > 0$ case

We can easily consider the deconfinement for the bosonic matrix model, including not only the adjoint scalars but also the fundamental scalars. Adding such a type of matter fields changes the phase structure significantly. The phase structure is rather similar to the case of the vector model explained in sections 4.1.3 and 4.2. In this section, let us study the Gaussian matrix model with N_{f}-fundamental scalar fields ϕ_A. They are N-component complex fields, and the index A runs 1 to N_{f}. The action of the matrix model is

$$ S = N\int_0^\beta \mathrm{d}t\left[\mathrm{Tr}\left\{\frac{1}{2}(D_t X_I)^2 + \frac{1}{2}X_I^2\right\} + \left|\tilde{D}_t\phi_A\right|^2 + |\phi_A|^2\right], \tag{4.98}$$

[10] For example, let $|\mathrm{SU}(M)\rangle_1$ be a state representing only the upper-left $M\times M$ block is excited and hence deconfined, while $|\mathrm{SU}(M)\rangle_2$ be one representing only the lower-right $M\times M$ block is done.

[11] Imagine a situation that the upper-left $M\times M$ block is deconfined in $|\mathrm{SU}(M)\rangle_1$, and $|\mathrm{SU}(M)\rangle_2$ is the one that the M-th and $M+1$-th rows and columns are exchanged. Although they seems almost identical, they are actually not since the length of the operator $\hat{O}$ has to be of order N^1 to bridge between $|\mathrm{SU}(M)\rangle_1$ and $|\mathrm{SU}(M)\rangle_2$.

where the covariant derivative for the fundamental scalar fields is defined as $\tilde{D}_t = \partial_t - \mathrm{i}A_t$. Of course, we can consider the model with independent masses and coupling constants for the scalar fields. Here, we take those parameters as the identical ones for simplicity.

One can compute the partition function of this model analytically by performing the functional integral. The free energy, the equivalent quantity to the partition function as the function of the Polyakov loops u_n can be obtained by

$$\beta F = \frac{\beta N^2}{2}\left(D + \frac{2N_{\mathrm{f}}}{N}\right) + N^2 \sum_{n=1}^{\infty}\left[a_n(x)\,|u_n|^2 + \frac{N_{\mathrm{f}}}{N} b_n(x)\,(u_n + u_n^*)\right], \tag{4.99}$$

where

$$a_n(x) = \frac{1}{n}(1 - Dx^n), \qquad b_n(x) = -\frac{x^n}{n}. \tag{4.100}$$

Again, we use the notation $x = \mathrm{e}^{-\beta}$. For the detailed computation, see also appendix C. The saddle-point condition implies that, at low temperatures,

$$u_n = -\frac{N_{\mathrm{f}}}{N}\cdot\frac{b_n}{a_n} = \frac{N_{\mathrm{f}}}{N}\frac{x^n}{1 - Dx^n}, \tag{4.101}$$

and the phase structure of this model is like figure 6. At zero temperature, all u_n become zero and the completely-confined phase is realized. In this sense, we can regard zero temperature as the 'Hagedorn' temperature. The distribution of the Polyakov line phase at the low temperature phase, namely below the Gross-Witten-Wadia-transition point $T_{\mathrm{GWW}}(N)$ is

$$\rho^{(\mathrm{P})}(\theta; T) = \frac{1}{2\pi}\left(1 + 2\sum_{n=1}^{\infty} u_n \cos(n\theta)\right), \tag{4.102}$$

which is identical with equation (4.45). Substituting the solution of the saddle-point condition, the free energy at the low temperature phase is given by

$$\beta F = \frac{\beta N^2}{2}\left(D + \frac{2N_{\mathrm{f}}}{N}\right) - {N_{\mathrm{f}}}^2 \sum_{n=1}^{\infty}\frac{x^{2n}}{1 - Dx^n}. \tag{4.103}$$

It scales $O({N_{\mathrm{f}}}^2)$ up to the offset, which indicates the mesonic degrees of freedom are dominant in this phase.

Partial deconfinement

The partially-deconfined phase appears as a thermodynamically stable phase in the range of the temperatures between the 'Hagedorn' temperature $T_{\mathrm{H}} = 0$ and the Gross-Witten-Wadia temperature $T_{\mathrm{GWW}}(N)$. The properties of partial deconfinement can be seen in terms of the distribution of the Polyakov line phases. The two-phase separation implies that the phase distribution behaves

$$\rho^{(\mathrm{P})}(\theta; T) = \left(1 - \frac{M}{N}\right)\rho^{(\mathrm{P})}_{\mathrm{con}}(\theta) + \frac{M}{N}\rho^{(\mathrm{P})}_{\mathrm{dec}}(\theta; M). \tag{4.104}$$

The distribution function $\rho^{(\mathrm{P})}_{\mathrm{dec}}(\theta; M)$ is defined on the Gross-Witten-Wadia point of $\mathrm{SU}(M)$ theory described by $\tilde{u}_n = \frac{N}{M} u_n$. Remembering the dependence of the deconfined degrees of freedom M to the temperature explained in section 3.2.2, the size M relates to the temperature of the distribution of whole theory $\rho^{(\mathrm{P})}(\theta; T)$, $T = T_{\mathrm{GWW}}(M)$. In section 4.1.3, we discussed the separation of the phase distribution somehow abstractly. Here, we demonstrate the separation specifically using the forms of u_n at the saddle point (4.101). The figure 8 shows the two phase distributions; one using the expression in the low-temperature phase (4.102), and the other combining the uniform distribution $\rho^{(\mathrm{P})}_{\mathrm{con}} = \frac{1}{2\pi}$ and the expression defined at the Gross-Witten-Wadia transition point for truncated $\mathrm{SU}(M)$ theory

$$\rho^{(\mathrm{P})}_{\mathrm{dec}}(\theta; M) \equiv \tilde{\rho}^{(\mathrm{P})}(\theta; T_{\mathrm{GWW}}(M)) = \frac{1}{2\pi}\left(1 + 2\sum_{n}^{\infty} \tilde{u}_n \cos(n\theta)\right), \tag{4.105}$$

which satisfies (4.62). In the former expression as well, the size of the deconfined sector M is evaluated by the minimum of the phase distribution. As we can see, these two different distributions shows a remarkable agreement. We emphasize that the temperature T is directly connected to the size of the deconfined sector M for the theory with this type of phase structure, even in the canonical ensemble; every temperature is the Gross-Witten-Wadia temperature of the some subsector in the full theory, and the rank of the gauge group for the subsector M is determined by the minimum of the distribution of the Polyakov line phases $\rho^{(\mathrm{P})}(\theta)$. This is justified at large N and M.

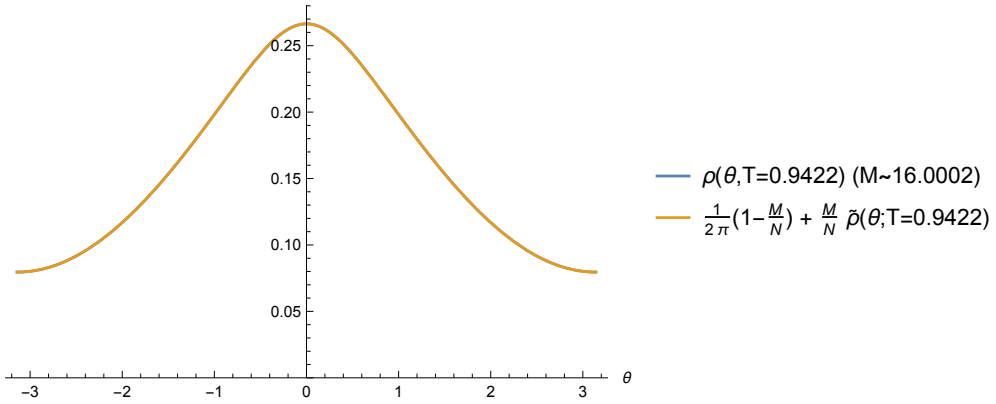

Figure 8: The plots of the phase distribution using two different expressions. One is using the original expression (4.45) (blue line) and the other is using the ansatz of partial deconfinement, the combination of the contributions defined at the Hagedorn and Gross-Witten-Wadia transition points with an appropriate weight (orange line). The difference between these two lines is too small to distinguish.

Moreover, we can understand the two-phase coexistence from the fact that the energy contributions from the

deconfined sector dominates. The energy below the Gross-Witten-Wadia temperature is given by the configuration at the saddle-point as

$$E = \frac{\partial(\beta F)}{\partial \beta} = \frac{N^2}{2}\left(D + \frac{2N_{\rm f}}{N}\right) + N^2 \sum_{n=1}^{\infty}\left[\frac{\partial a_n(T)}{\partial \beta}\left|u_n\right|^2 + \frac{N_{\rm f}}{N}\cdot\frac{\partial b_n(T)}{\partial \beta}\left(u_n + u_n^*\right)\right]. \tag{4.106}$$

The first term is the zero-point energy, and the second term expresses the contribution of excitations. One can specify the energy contributions from the adjoint and fundamental scalar fields in a following manner;

$$E^{(\mathrm{X})} = \frac{D}{2}N^2 + DN^2\sum_n x^n|u_n|^2 = \frac{D}{2}N^2 + DM^2\sum_n x^n|\tilde{u}_n|^2, \tag{4.107}$$

$$E^{(\phi)} = NN_{\rm f} + NN_{\rm f}\sum_n x^n(u_n + u_n^*) = NN_{\rm f} + MN_{\rm f}\sum_n x^n(\tilde{u}_n + \tilde{u}_n^*), \tag{4.108}$$

connecting the expressions of the $\mathrm{U}(N)$ full theory to those of the $\mathrm{SU}(M)$ subsector. We can follow the discussion in the previous sections and state that the thermodynamic quantities such as the energy is controlled by the size of the deconfined sector M.

5 BEC-Confinement correspondence

A remarkable connection between color confinement in large-N gauge theories and Bose-Einstein condensation (BEC) [83] plays a crucial role to establish the insight of partial deconfinement [15]. As mentioned in section 4, the gauge-singlet constraint is the key of the confinement/deconfinement transition, not the strength of interaction in the large-N gauge theories. It is the well-known fact that the spin statistics of bosons associated with the particle permutations is the essence of the Bose-Einstein condensation, and the condensations occurs even in the non-interacting theory. In the following, we confirm this kind of redundancy provides with the common mechanism to both sides. Moreover, we saw that the size of the deconfined sector M can be read off from the distribution of the Polyakov line phases;

$$\min \rho^{(\mathrm{P})}(\theta) = \frac{1}{2\pi}\left(1 - \frac{M}{N}\right), \tag{5.1}$$

which is quite analogous to the number of the particles in BEC as we will mention in the following. In this section, we review the correspondence based on reference [15].

5.1 Comparison with ideal boson gas

At first, we consider the system with N ideal boson gas in R^d. The Hamiltonian is described by d-component harmonic oscillators $\vec{x}_1, \cdots, \vec{x}_N$, and

$$H = \sum_{c=1}^{N}\left(\frac{\vec{p}_c^{\,2}}{2m} + \frac{m\omega^2}{2}\vec{x}_c^{\,2}\right). \tag{5.2}$$

There is the S_N-permutation symmetry associated with Bose-Einstein statistics. Although it is unfamiliar for many people, we can treat this system as the S_N-gauged quantum mechanics of N-component vectors. To compare the following analysis with particularly the one of $\mathrm{O}(N)$ vector model on S^d [12] under the translation $(\vec{x}_1, \cdots, \vec{x}_N) \Leftrightarrow (\phi_1, \cdots, \phi_N)$ helps our understanding to this correspondence.

In the Hamilton formalism, the Fock states

$$|\vec{n}_1, \vec{n}_2, \cdots, \vec{n}_N\rangle \equiv \prod_{i=1}^{d} \frac{\hat{a}_{i1}^{\dagger n_{i1}}}{\sqrt{n_{i1}!}} \frac{\hat{a}_{i2}^{\dagger n_{i2}}}{\sqrt{n_{i2}!}} \cdots \frac{\hat{a}_{iN}^{\dagger n_{iN}}}{\sqrt{n_{iN}!}}|0\rangle, \tag{5.3}$$

can span the extended Hilbert space containing non-gauge-invariant states, using d-dimensional integer-valued vectors $\vec{n}$. The gauge-singlet states are defined as the S_N-permutation-invariant states. Using the standard Fock state, the states expressing the particle condensation are given by

$$\hat{P}\left|\vec{n_1}, \cdots, \vec{n}_M, \vec{0}, \cdots, \vec{0}\right\rangle, \tag{5.4}$$

[12] Notice that we take $d = 3$ in section 4.2 for convenience, and the generalization to higher d is straightforward.

where

$$\hat{P} = \frac{1}{N!} \sum_{g \in \mathrm{S}_N} \hat{g}, \tag{5.5}$$

is the projection operator and $\hat{g}$ is a unitary operator acting on the Hilbert space, which corresponds to the group element $g \in \mathrm{S}_N$. The states before this projection is unsymmetrized state and nothing but the counterpart of $|E; \mathrm{O}(M)\rangle$ for the vector model, analogous to $|E; \mathrm{SU}(M)\rangle$ for the Gaussian matrix model explained in section 4.3.2.

In the grand canonical ensemble with the chemical potential μ (≤ 0), the number of excited particles can be derived as

$$M = \int_0^\infty \mathrm{d}\varepsilon \left. \frac{c_d\, \varepsilon^{d-1}}{\mathrm{e}^{\beta(\varepsilon-\mu)-1}} \right|_{\mu=0} = \frac{T^d \zeta(d)}{\omega^d}, \tag{5.6}$$

where $c_d = (\Gamma(d) \cdot \omega^d)^{-1}$, and Bose-Einstein condensation is formed when $M = M(\mu = 0) < N$. This relation determines the critical temperature T_c where $M = N$, and hence

$$T_\mathrm{c} = \left(\frac{N}{\zeta(d)} \right)^{\frac{1}{d}} \omega, \tag{5.7}$$

and

$$\frac{M}{N} = \left(\frac{T}{T_\mathrm{c}} \right)^d. \tag{5.8}$$

These results are remarkably resembling the relations (4.67) and (4.73) in $\mathrm{O}(N)$ vector model, while d is chosen to 3 there.

As will be omitted details in this thesis, the thermodynamic quantities such as the energy and entropy below that critical temperature can be obtained by

$$E(T = T_\mathrm{c}(M)) = E_\mathrm{c}(M), \qquad S(T = T_\mathrm{c}(M)) = S_\mathrm{c}(M), \tag{5.9}$$

as analogues of equation (4.77). Certainly, their contribution is coming only from excitation. While the Bose-Einstein condensation was first found in the non-interacting theory, it can appear even at strong coupling, for example, the superfluid helium [84]. It led to a two-component fluid theory made by particles in the ground and excited states and capture the thermodynamic properties of the system. We can find that this two-component description and partial deconfinement are laid on the common mechanism, as will see in the next section.

5.2 Common mechanism with partial deconfinement

For the system with N ideal boson gas, the partition function incorporating the redundancy of permutation is obtained [85] by

$$Z = \sum_{g \in G} \mathrm{Tr} \left(\hat{g} \mathrm{e}^{-\beta \hat{H}} \right), \tag{5.10}$$

where $G = \mathrm{S}_N$. The trace is performed over $|\vec{n}_1, \vec{n}_2, \cdots, \vec{n}_N\rangle$ in equation (5.3). Again, $\hat{g}$ is a unitary operator corresponding to the group element $g \in G$. The insertion of $\hat{g}$ works as the projection to the gauge-invariant Hilbert space, after the summation over the gauge group G;

$$\begin{aligned} Z &= \sum_{g\in G} \sum_{\vec{n}_1,\cdots,\vec{n}_N} \langle \vec{n}_1, \cdots, \vec{n}_N | \hat{g} \mathrm{e}^{-\beta \hat{H}} | \vec{n}_1, \cdots, \vec{n}_N \rangle \\ &= \sum_{\vec{n}_1,\cdots,\vec{n}_N} \mathrm{e}^{-\beta\left(E_{\vec{n}_1}+\cdots+E_{\vec{n}_N}\right)} \sum_{g\in \mathrm{S}_N} \langle \vec{n}_1, \cdots, \vec{n}_N | \hat{g} | \vec{n}_1, \cdots, \vec{n}_N \rangle \\ &= \sum_{\vec{n}_1,\cdots,\vec{n}_N} \mathrm{e}^{-\beta\left(E_{\vec{n}_1}+\cdots+E_{\vec{n}_N}\right)} \sum_{g\in \mathrm{S}_N} \langle \vec{n}_1, \cdots, \vec{n}_N | \vec{n}_{g(1)}, \cdots, \vec{n}_{g(N)} \rangle. \end{aligned} \tag{5.11}$$

For the ground state $|\vec{0}, \vec{0}, \cdots, \vec{0}\rangle$, every element $g \in G$ contributes equally, which leads to an enhancement by a factor $N!$. On the other hand, for generic excited states, only $g = \mathbf{1}$ contributes to partition function since all N particles are in different states. In other words, the generic states are suppressed by a factor $N!$ compared to the ground state, which causes the condensation.

The above formulation enables us to handle the gauge-singlet condition explicitly. Similarly, we could apply it to different gauge groups such as $\mathrm{SU}(N)$ and more generic field contents. Actually, the partition function for the large-N gauge theory (4.4), for instance, is one counterpart of that. We have seen that the operator $\hat{g}$ implements the gauge transformation in the Hilbert space corresponding to a group element $g \in G$. For the $\mathrm{U}(N)$ or $\mathrm{SU}(N)$ theory, this element g can be interpreted as the Polyakov loop (3.2), as a role of mediator reflecting the Gauss' law constraint. In the examples shown in section 4, we can see this makes sense.

In order to determine the distribution function of the Polyakov line phase, we look at permutation matrices that keep the typical state in the thermodynamics unchanged. When the Bose-Einstein condensation is realized, long cyclic permutations exchanging the particles in the condensation dominate [85], and the off-diagonal long-range order (ODLRO) appears [86]; Let $\hat{\rho}$ be the density matrix of the N-particle system, $\hat{\rho}_1$ be the one-particle density matrix in which the rest $N-1$ particles are traced out. Using its spectral decomposition with normalized states, it is also written by

$$\hat{\rho}_1 = n_{\max} |\Psi\rangle\langle\Psi| + \sum_i n_i |\Psi_i\rangle\langle\Psi_i|, \tag{5.12}$$

where $n_{\max}$ is the biggest eigenvalue and $|\Psi\rangle$ represents its eigenstate. The Bose-Einstein condensation appears when $n_{\max}$ is of order N. In the previous example for non-interacting bosons, the eigenstate $|\Psi\rangle$ is the one-particle ground state, and $n_{\max} = N - M$, which gives the number of particles in the ground state. In terms of the Polyakov line and its phases, long cyclic permutations affect to the constant offset of the phase distribution $\rho^{(\mathrm{P})}(\theta)$. Remembering the constant offset becomes nonzero when the Bose-Einstein condensation is realized, this is the analogue of the Gross-Witten-Wadia transition associated with deconfinement for gauge theories. This is the reason why the constant distribution of the Polyakov line phases is a good indicator of confinement. Note

that, even if the phase distribution is not uniform, we can extract the constant offset from non-uniform part;

$$\rho^{(\mathrm{P})}(\theta) = C + \tilde{\rho}^{(\mathrm{P})}(\theta), \tag{5.13}$$

where $C \geq 0$ is the minimum of $\rho^{(\mathrm{P})}(\theta)$ and $\tilde{\rho}^{(\mathrm{P})}(\theta)$ is a non-constant distribution whose minimum is zero. This C is related to M as

$$C = \frac{1}{2\pi}\left(1 - \frac{M}{N}\right). \tag{5.14}$$

Therefore, we can pick a particular ordering of θ_i such that $\theta_1, \cdots, \theta_M$ give the nonuniform part $\tilde{\rho}(\theta)$, and $\theta_{M+1}, \cdots, \theta_N$ give the constant part C. It leads to the separation of the degrees of freedom to the confined and deconfined sectors. When we consider some matrix fields, the phase separation shown in figure 1 can be seen.

We emphasize again that the Bose-Einstein condensation can occur at strong coupling such as the superfluid helium [84] proposed by F. London. The situation is similar to various quantum field theories at weak and strong coupling (see e.g. [66, 87]), and hence, it is plausible to motivate that partial deconfinement can be valid even beyond weak coupling.

Another comment is about the counterpart of the Gross-Witten-Wadia transition for the theory other thermodynamic limit than the large N limit is taken. Although the Gross-Witten-Wadia (GWW) transition is no longer the precise phase transition at the finite N, the GWW-transition point corresponds to the point where the global symmetry restores [58]. In the reference [58], the authors study the specific examples with the global symmetry that is broken and preserved in the confined and deconfined phase in the traditional meaning, and in the partially-deconfined phase, the symmetry is spontaneously broken. The result may suggest to define partial deconfinement in terms of the global symmetry breaking[13)], although further detailed studies are needed to confirm the identification between that definition and the original one.

[13)] See also the independent but somehow relating works [88, 89] to present the intermediate phase associated with the symmetry breaking and the two-phase separation.

6 Numerical analysis

In this section, we show the numerical results of the lattice Monte Carlo simulations for the bosonic matrix models [16, 17, 71].

Until now, we mainly studied the properties of partial deconfinement in the weakly-coupled theories focusing on the saddle-point configurations of the Polyakov loops u_n. In the studies [16, 17], we can confirm that partial deconfinement can take place even beyond the weak coupling regime though the nonperturbative analysis by the lattice Monte Carlo simulations. Moreover, the two-phase separation as shown in figure 1 can be seen specifically in the matter field configurations. More details about the simulation will be explained in appendices D, E, and F.

6.1 Simulation schemes

In our Monte Carlo simulation, we employ the several schemes for optimization or demonstration explicitly studying the partially-deconfined phase. Let us summarize on the list for the simulations in each model;

- For the Gaussian matrix model without the fundamental scalar fields ($N_{\mathrm{f}} = 0$) explained in section 6.3, we performed the naive Monte Carlo simulation since the simulation cost is so low that we do not have to introduce any modification.
- For the Gaussian matrix model with the fundamental scalar fields ($N_{\mathrm{f}} > 0$) explained in section E.3, we performed the constrained simulation.
- For the Yang-Mills matrix model, we performed both the "efficient" simulation in section 6.4 and the constrained simulation in section 6.5. We compare the obtained results with the one in reference [16] and see its consistency.

6.1.1 "Efficient" simulation

The size of the deconfined sector M can change from 0 to N in $\mathrm{U}(N)$ or $\mathrm{SU}(N)$ theories. Therefore, we need a long time to generate the Monte Carlo configurations with the specific value of M in order to evaluate the quantities at fixed M. We can take a more efficient approach by adding a source term

$$\Delta S = \begin{cases} \frac{\gamma}{2}\left(|P| - p_1\right)^2 & \left(|P| < p_1\right) \\ \frac{\gamma}{2}\left(|P| - p_2\right)^2 & \left(|P| > p_2\right) \end{cases} \tag{6.1}$$

to the action in order to restrict the Polyakov loop $P = \frac{1}{N}\sum_{j=1}^{N} \mathrm{e}^{\mathrm{i}\theta_j}$. If we take the parameter γ sufficiently large, this method enables us to collect the configurations in the region between p_1 and p_2, that is, M at some fixed values effectively. Note that this method leaves the configurations at $p_1 < |P| < p_2$ undeformed.

6.1.2 Constrained simulation

We further introduce a new approach to study the properties of partial deconfinement in detail. Although this deformation may look similar to one explained in the previous section, there is a huge difference in the physical sense.

Let us define the Polyakov loops in each sector, as

$$P_M = \frac{1}{M}\sum_{j=1}^{M} \mathrm{e}^{\mathrm{i}\theta_j}, \quad P_{N-M} = \frac{1}{N-M}\sum_{j=M+1}^{N} \mathrm{e}^{\mathrm{i}\theta_j}. \tag{6.2}$$

We introduce the source term

$$\Delta S = \begin{cases} \frac{\gamma}{2}\left(|P_M| - \left(\bar{P}+\delta\right)\right)^2 & \left(|P_M| > \bar{P}+\delta\right) \\ \frac{\gamma}{2}\left(|P_M| - \left(\bar{P}-\delta\right)\right)^2 & \left(|P_M| < \bar{P}-\delta\right) \\ \frac{\gamma}{2}\left(|P_{N-M}| - \delta\right)^2 & \left(|P_{N-M}| > \delta\right) \end{cases} \tag{6.3}$$

to the action. The value $|P_M|$ and $|P_{N-M}|$ can be constrained to be around $\bar{P}$ and 0, respectively, with a width δ if we take the parameter γ sufficiently large. We used $\gamma \sim 10^5$ and $\delta = 0.002$ in our simulations.

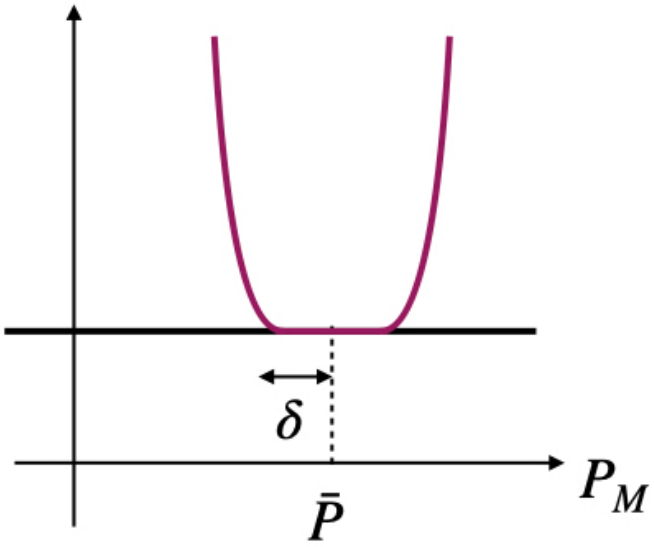

Figure 9: The intuitive picture of the role of the source term in the constrained simulation. With this term, we can generate the Monte Carlo configurations of which the observable takes the value as we aimed.

If our scenario regarding partial deconfinement is correct, this constraint should fix the S_N permutation symmetry and make the upper-left $\mathrm{SU}(M)$ block deconfined while keeping the rest confined, as in figure 1. In

other words, we can realize a 'gauge fixing' in figure 1 for the configurations generated in the path integral formalism. In the large N limit where the size M can be also treated as $O(N)$, this deformation does not change the thermodynamics of the $\mathrm{SU}(M)$-partially-deconfined phase. As we will mention later, we will confirm that, in our numerical simulation, this deformation works just for optimization and does not affect the original physics up to numerical errors.

6.2 Typicality and master field

At large N, the path integral can be evaluated by a "typical" configuration at the saddle point up to a gauge transformation. The configuration is the so-called *master field* which is a solution of the saddle point equation It was named by Coleman in his textbook [90], and the existence of such a typical field configuration in large-N gauge theories was discussed by Witten [91]. For the review of the master field, see also references [92, 93]. In reference [94], we can find a few comments of the master field for the deconfinement in 4d pure Yang-Mills theory at $N = \infty$, in the literature of lattice Monte Carlo simulations.

Following the paper [17], the master fields $\left\{\Phi^{(\mathrm{master})}\right\}$ are referred to as a configuration in the Euclidean path integral of the theory with fields $\{\Phi\}$ at large N. They provide the accurate expectation values for properly normalized observables to leading order in the expansion with respect to $1/N$;

$$\langle f(\{\Phi\})\rangle = f(\{\Phi^{(\mathrm{master})}\}) \qquad (\text{at large } N), \tag{6.4}$$

where $f(\cdot)$ represents a properly normalized gauge invariant following the 't Hooft scaling. Note that the invariant does not affect the dominant configuration in the path integral, similarly to the operator $\hat{O}$ mentioned in section 4.3.2. The strategy is to find out the features of the master field describing the partially-deconfined phase firstly though the lattice Monte Carlo simulations in the solvable model such as the Gaussian matrix model. After that, we figure out the features in nontrivial theories such as the Yang-Mills matrix model. We should notice that the (lattice) configurations in the path integral do not simply connect to the quantum states in the Hamiltonian formalism, except that the expectation values of gauge-invariant observables coincide. We can make sense that since the configurations have to be averaged to compute the expectation values with the Boltzmann weight, unlike the wave functions. Of course, the master field cannot also be identified directly with the wave function corresponding to the state in the Hilbert space.

The lattice Monte Carlo simulations utilize the importance sampling, and hence, the sample-by-sample fluctuations of the properly normalized quantities [14] are suppressed as N is taken to be large. In the strict large N limit, the configuration generated in lattice simulations coincide with the master field, of course if we could perform such simulations. In fact, we can only do for large but finite N values in actual simulations. Therefore, we regard the lattice configurations obtained by the Markov Chain Monte Carlo algorithm at sufficiently large N

[14] For example, E/N^2 is such a quantity, which is of order N^0 in the large N limit.

as master fields. In other words, we study the configurations of the models when the finite N fluctuations of the observables evaluated by them can be negligible in the numerical analysis.

It generates the canonical ensemble in the standard lattice Monte Carlo simulations, and one may wonder the stability of the intermediate phase for the models with the first-order transition. To clarify the subtlety, we move on to the microcanonical picture and rely on the relationship to the master field. Since the thermal phase is defined at each energy, it is reasonable to assume that the microcanonical ensemble at each fixed energy E can be represented by one master field, and expect that each saddle point has a corresponding master field. In the case of the first-order phase transition without hysteresis, such as the Gaussian matrix model with the phase structure as shown in the middle panel of figures 4 and 5, each value of the Polyakov loop between 0 and one at the Gross-Witten-Wadia-transition point, or equivalently, each M between 0 and N minimizes the free energy at $T = T_{\rm c}$. Hence, we have to treat all values of M severally. We expect that a single master field exists for each M, and we identify them with the dominant configurations for a given pair (T, M). Note that the situation is much simpler when we consider the model with the continuous phase transition since the canonical ensemble matches to the microcanonical ensemble. For the overview of the microcanonical ensemble and canonical ensemble, see appendix A.

As mentioned in the beginning of this section, the master field has an ambiguity of gauge redundancy. We perform the lattice Monte Carlo simulations under a gauge fixing to eliminate the redundancy. The gauge degrees of freedom are no longer dynamical in the lower-dimensional models we consider now. We choose the static diagonal gauge, which reduce the gauge symmetry up to S_N permutations. Under the gauge, the gauge field takes the form

$$A_t = \frac{1}{\beta}\,\mathrm{diag}\,(\theta_1, \cdots, \theta_N), \tag{6.5}$$

where $\theta_1, \cdots, \theta_N$ are independent of time t, and θ_i takes a value between $\pm\pi$. Again, the Polyakov loop P is expressed as $P = \frac{1}{N}\sum_{j=1}^{N} \mathrm{e}^{\mathrm{i}\theta_j}$ by definition. In the partially-deconfined phase at the critical temperature $T = T_{\rm c}$, the Polyakov line phases can be divided into two groups; without loss of generality, we can pick up M of them $(\theta_1, \cdots, \theta_M)$, and $N - M$ of them $(\theta_{(N-M)}, \cdots, \theta_N)$ such that they distribute with $\frac{1+\cos\theta}{2\pi}$ and $\frac{1}{2\pi}$, respectively. These groups represents nothing but the confined and deconfined sectors, respectively. This operation fixes the residual S_N permutation symmetry to $\mathrm{S}_M \times \mathrm{S}_{N-M}$, which means that the exchanges performed inside these distinct groups are indistinguishable. In fact, such a separation is not unique due to the residual symmetry under the inter-group exchanges of θ's with the same value. The permutation acting on two groups does not modify the form of the phase distribution. Strictly speaking, the Faddeev-Popov term

$$S_{\rm FP} = -\sum_{i<j} \ln\left|\sin^2\left(\frac{\theta_i - \theta_j}{2}\right)\right|, \tag{6.6}$$

introduced by the gauge fixing inhibits the coincidence of θ at finite N. However, it is a desired feature in the large N limit that neighboring θ's approach infinitesimally close and the distribution function can be regarded

as continuous. Our numerical results show a consistency with the separation, including the consequence of this ambiguity [15]. For an explicit example, see section 6.3.2, especially after equation (6.22).

In the following section, we show the relationship of the master field and partial deconfinement in lattice configurations of the Gaussian matrix model, and the Yang-Mills matrix model.

6.3 Case : Gaussian matrix model

For starter, we study the simplest case, the Gaussian matrix model (without fundamental scalar fields, $N_{\rm f} = 0$) to establish the analysis method for partial deconfinement. At first, we discuss the model with the hermitian matrix fields X_I and without fundamental scalars ($N_{\rm f} = 0$). See some preliminary results for the model with fundamental scalars in appendix E.3. We generate field configurations by the lattice Monte Carlo simulation without any constraints mentioned in section 6.1.

6.3.1 Distributions of scalar degrees of freedom

As a straightforward characterization of the master field, we define the distribution for the scalar fields. Namely, analogous to the gauge field and the distribution of the Polyakov line phases, we study the distribution of the independent degrees of the freedom with respect to the adjoint scalar fields

$$\sqrt{N}X_{I,jj}(t), \quad \sqrt{2N}\mathrm{Re}X_{I,jk}(t), \quad \sqrt{2N}\mathrm{Im}X_{I,jk}(t), \quad (j<k), \tag{6.7}$$

those are the diagonal and off-diagonal elements of all the scalar hermitian matrices. In this thesis, we denote them as a random variable 'x' and its distribution as $\rho^{(\mathrm{X})}(x)$ in comparison with $\rho^{(\mathrm{P})}(\theta)$. We make sense the two-phase coexistence at the critical temperature $T = T_{\rm c}$, if we can specify the contributions to the distribution function from the confine and deconfined sectors, denoting them by $\rho^{(\mathrm{X})}_{\rm con}(x)$ and $\rho^{(\mathrm{X})}_{\rm dec}(x)$, respectively. According to the faith of partial deconfinement, we set an ansatz

$$\rho^{(\mathrm{X})}(x;M) = \left[1-\left(\frac{M}{N}\right)^2\right]\cdot\rho^{(\mathrm{X})}_{\rm con}(x) + \left(\frac{M}{N}\right)^2\cdot\rho^{(\mathrm{X})}_{\rm dec}(x). \tag{6.8}$$

Here, the number of the scalar degrees of freedom in the deconfined sector M is related to the observables, especially the Polyakov loop P by equation (4.85). The ansatz is proposed by the picture of partial deconfinement that the confined and deconfined sectors coexist in the space of color degrees of freedom. Hence, to confirm above relation will become a strong evidence for partial deconfinement since it is highly nontrivial if we do not expect that.

For the numerical analysis later, let us summarize the analytic properties of the distribution function of scalars $\rho^{(\mathrm{X})}(x)$. As explained, it is convenient to move on to the 'gauge-fixed' picture, in which the S_N symmetry with respect to θ_j is reduced to $\mathrm{S}_M \times \mathrm{S}_{N-M}$.

[15] Practically, when we permute θ_i and θ_j, we also exchange the i-th and j-th rows and columns of the scalar fields.

At first, the Polyakov line phases θ_j and these scalar degrees of freedom x are correlating; Notice that the part of the action describing the scalar can be written as

$$\begin{aligned} & N\int_0^\beta dt \sum_I \sum_{j,k} \frac{1}{2}\left(\left|\partial_t X_{Ijk} - \frac{i(\theta_j-\theta_k)}{\beta} X_{Ijk}\right|^2 + |X_{Ijk}|^2\right) \\ & = N\int_0^\beta dt \sum_I \sum_{j,k} \frac{1}{2}\left\{|\partial_t(\mathrm{Re}X_{Ijk})|^2 + \left(1+\frac{(\theta_j-\theta_k)^2}{\beta^2}\right)|\mathrm{Re}X_{Ijk}|^2 \right. \\ & \qquad \left. + |\partial_t(\mathrm{Im}X_{Ijk})|^2 + \left(1+\frac{(\theta_j-\theta_k)^2}{\beta^2}\right)|\mathrm{Im}X_{Ijk}|^2\right\}. \end{aligned} \tag{6.9}$$

Looking at this expression, the distribution of $\sqrt{2N}\mathrm{Re}X_{I,jk}(t)$ and $\sqrt{2N}\mathrm{Im}X_{I,jk}(t)$ depends only on $\theta_j - \theta_k$. At the critical temperature $T = T_\mathrm{c}$ where partial deconfinement takes place and considering the $\mathrm{SU}(M)$-partially-deconfined phase, the separation of θ_i's into two groups $\theta_1, \cdots, \theta_M$ and $\theta_{M+1}, \cdots, \theta_N$ can be done. If we average the phases over $j = M+1, \cdots, N$ or $k = M+1, \cdots, N$, the distribution of $\theta_j - \theta_k$ is uniform, behaved as in the completely-confined phase. Associated with that, the distribution of x behaves as in the completely-confined phase. On the other hand, if we take the average over $j, k = 1, \cdots, M$, $\theta_j - \theta_k$ is no longer uniform, and hence, the distribution of x is deformed from one in the confined sector.

Using the distribution function $\rho^{(\mathrm{X})}(x)$, we can compute the expectation value of the energy in a different way; the energy expectation value E in the path integral formalism defined by equation (4.89) can be directly rewritten to

$$E = \left\langle \frac{N}{\beta}\int_0^\beta \mathrm{d}t\, \mathrm{Tr}\, X_I^2 \right\rangle = DN^2 \int \mathrm{d}x\, x^2 \rho^{(\mathrm{X})}(x), \tag{6.10}$$

in terms of the second moment or so-called variance of $\rho^{(\mathrm{X})}(x)$. Furthermore, using the distributions in confined and deconfined sector,

$$DN^2 \int \mathrm{d}x\, x^2 \rho^{(\mathrm{X})}(x) = D(N^2-M^2)\int \mathrm{d}x\, x^2 \rho^{(\mathrm{X})}_{\mathrm{con}}(x) + DM^2 \int \mathrm{d}x\, x^2 \rho^{(\mathrm{X})}_{\mathrm{dec}}(x), \tag{6.11}$$

where

$$DM^2 \int \mathrm{d}x\, x^2 \rho^{(\mathrm{X})}_{\mathrm{dec}}(x) = \left\langle \frac{N}{\beta}\int_0^\beta \mathrm{d}t \sum_{1\le j,k\le M} |X_{I,jk}|^2 \right\rangle \tag{6.12}$$

corresponds to the deconfined sector and

$$D(N^2-M^2) \int \mathrm{d}x\, x^2 \rho^{(\mathrm{X})}_{\mathrm{con}}(x) = \left\langle \frac{N}{\beta}\int_0^\beta \mathrm{d}t \sum_{j\ge M+1 \text{ or } k\ge M+1} |X_{I,jk}|^2 \right\rangle \tag{6.13}$$

corresponds to the confined sector. Note that this separation is not unique as well as the distribution function of the Polyakov line phases due to the residual symmetry. Namely, the $\mathrm{S}_M \times \mathrm{S}_{N-M}$ permutations do not change the phase distributions $\rho^{(\mathrm{P})}_{\mathrm{con}}(\theta)$ and $\rho^{(\mathrm{P})}_{\mathrm{dec}}(\theta)$, and in turn, keep $\rho^{(\mathrm{X})}_{\mathrm{con}}(x)$ and $\rho^{(\mathrm{X})}_{\mathrm{dec}}(x)$ unchanged.

From the result in equation (4.89), we can compute the variance analytically as

$$\int \mathrm{d}x\; x^2 \rho^{(\mathrm{X})}_{\mathrm{con}}(x) = \frac{1}{2} \tag{6.14}$$

and

$$\int \mathrm{d}x\; x^2 \rho^{(\mathrm{X})}_{\mathrm{dec}}(x) = \frac{1}{2} + \frac{1}{4D}. \tag{6.15}$$

The inclement comes from the deconfinement of the upper-left $M \times M$-block in figure 1. Because of our specific choice of separation into two groups, the upper-left $M \times M$-block can be identified with the completely-deconfined phase of the $\mathrm{SU}(M)$ theory. As a result, we build a way to describe partial deconfinement in terms of the independent scalar degrees of freedom x, and hence, the actual separation in terms of the matter fields of the theory.

Although, the variances from the distribution functions in the confined and deconfined are tractable in an analytic manner, the exact forms of the distributions are not known. Therefore, we employ the numerical analysis to figure out the problem. Generating many samples of x and plot their histogram enables us to determine the distributions in equation (6.8) from lattice configurations at fixed N and M[16]. For fixing M, we refer to the value of the Polyakov loop, that is, $M = 2NP$. So far, we tend to assume a specific configuration, the upper-left $M \times M$ sector to be deconfining like in figure 1. In fact, the very same distributions $\rho^{(\mathrm{X})}_{\mathrm{dec}}(x)$ and $\rho^{(\mathrm{X})}_{\mathrm{con}}(x)$ are obtained as long as the static diagonal gauge is used since they average over the specific form of configuration and its gauge equivalents. To determine $\rho^{(\mathrm{X})}_{\mathrm{con}}(x)$ and $\rho^{(\mathrm{X})}_{\mathrm{dec}}(x)$ numerically, we solve the relation (6.8) by combining with different values of M. As an example, for $r_a = (M/N)^2$, $r_b = (M'/N)^2$, we can get

$$r_b\, \rho^{(\mathrm{X})}(x; M) - r_a\, \rho^{(\mathrm{X})}(x; M') = (r_b - r_a)\rho^{(\mathrm{X})}_{\mathrm{con}}(x), \tag{6.16}$$

and

$$(1 - r_b)\rho^{(\mathrm{X})}(x; M) - (1 - r_a)\rho^{(\mathrm{X})}(x; M') = (r_a - r_b)\rho^{(\mathrm{X})}_{\mathrm{dec}}(x). \tag{6.17}$$

The lattice configurations, at fixed $D = 2$, N and L at the critical temperature $T = T_{\mathrm{c}}$, are used in the basis for $\rho^{(\mathrm{X})}(x)$. From that, we can construct $\rho^{(\mathrm{X})}_{\mathrm{con}}(x)$ and $\rho^{(\mathrm{X})}_{\mathrm{dec}}(x)$ solving equations (6.16) and (6.17) for a couple of pairs of M and M'. There, the values of the variance are available to check a consistency for the above logic.

In figure 10, we can see that the distributions obtained by several M match each other, which supports the existence of $\rho^{(\mathrm{X})}_{\mathrm{con}}(x)$ and $\rho^{(\mathrm{X})}_{\mathrm{dec}}(x)$ and its consistency. In that analysis, the finite lattice size effects can be seen to be small; figure 11 shows that using 4 sites towards the time direction is already enough in this case, implying a nice convergence in the continuum extrapolation. The variances in the confined and deconfined sectors estimated numerically agree with the ones at large N, equations (6.14) and (6.15), within the statistical errors and this indicates that the numerical analysis is robust. For the numerical data, see table 1 in appendix D.

[16] For example, it is possible to collect $DLN^2 = 49152$ data samples from a single configuration with $D = 2$, $N = 32$, $L = 24$, where L is the number of lattice points to the temporal direction.

What we should mention for future reference is that the form $\rho^{(\mathrm{X})}_{\mathrm{con}}(x)$ and $\rho^{(\mathrm{X})}_{\mathrm{dec}}(x)$ do not agree with the Gaussian distribution with the above variances at the critical temperature $T = T_{\mathrm{c}}$. This result reminds us that the lattice field configurations are not direct connected to the wave function as explained in the previous section. At a sufficiently low temperature $\rho^{(\mathrm{X})}_{\mathrm{con}}(x)$ approaches to the Gaussian distribution, as shown in figure 12. In the completely confined phase, the distribution in the confined sector $\rho^{(\mathrm{X})}_{\mathrm{con}}(x)$ must be equivalent to the original one $\rho^{(\mathrm{X})}(x)$, and hence, it is affected by the thermal corrections.

6.3.2 Correlation between scalar and gauge degrees of freedom

Another way to detect the coexisting of the confined and deconfined sectors is to focus on the correlation between the matrix scalar fields X_I and the Polyakov line phases θ_i as the gauge degrees of freedom. Let us consider the vector-like quantity K_i defined by

$$K_i \equiv \sum_{I,j} \frac{1}{\beta} \int \mathrm{d}t |X_{I,ij}|^2. \tag{6.18}$$

For the Gaussian matrix model at large N, the distribution of $|X_{I,ij}|^2$, that is, $\rho^{(\mathrm{X})}(x)$ depends on $\theta_i - \theta_j$. At each value of $\frac{M}{N}$, a one-to-one correspondence between θ_i and K_i would exist, given by the components which are labeled by the same index i. The correspondence originally comes from the Gauss' law constraint. Practically, at least, it is obvious that there are data of the scalar and gauge components sharing the color index i.

For the Gaussian matrix model, this quantity relates to the expression of the energy (4.89) by $E = N \sum_{i=1}^{N} K_i$. In the completely-confined phase below the critical temperature $T < T_{\mathrm{c}}$ where $M = 0$,

$$\langle K_i \rangle_{\mathrm{con}} \equiv \frac{1}{N} \sum_{i=1}^{N} K_i|_{M=0} = \frac{E|_{M=0}}{N^2} = \frac{D}{2}, \tag{6.19}$$

since the all degrees of freedom in the configuration stay in the ground state. We can regard that contribution as one in the confined sector at $T = T_{\mathrm{c}}$ (the blue area in figure 1).

For the contribution from the deconfined sector, $\langle K_i \rangle_{\mathrm{dec}}$, let us consider the physic at the point the Gross-Witten-Wadia transition of the full theory occurs. At the point in $\mathrm{SU}(N)$ theory, where all elements are excited thermally (the red area in figure 1), namely at the point $T = T_{\mathrm{c}}$ and $M = N$,

$$\langle K_i \rangle_{\mathrm{GWW},N} \equiv \frac{1}{N} \sum_{i=1}^{N} K_i|_{\mathrm{GWW},N} = \frac{E|_{\mathrm{GWW},N}}{N^2} = \frac{D}{2} + \frac{1}{4}. \tag{6.20}$$

When we fix the S_N permutation symmetry and choose a separation $\theta_1, \cdots, \theta_M$ and $\theta_{M+1}, \cdots, \theta_N$ such that they distribute as $\frac{1+\cos\theta}{2\pi}$ and $\frac{1}{2\pi}$, respectively, each θ_i should belong to the confined or deconfined sector. If θ_i is in the deconfined sector,

$$\langle K_i \rangle_{\mathrm{dec}} = \left(1 - \frac{M}{N}\right) \langle K_i \rangle_{\mathrm{con}} + \frac{M}{N} \langle K_i \rangle_{\mathrm{GWW},M} = \frac{D}{2} + \frac{M}{4N}, \tag{6.21}$$

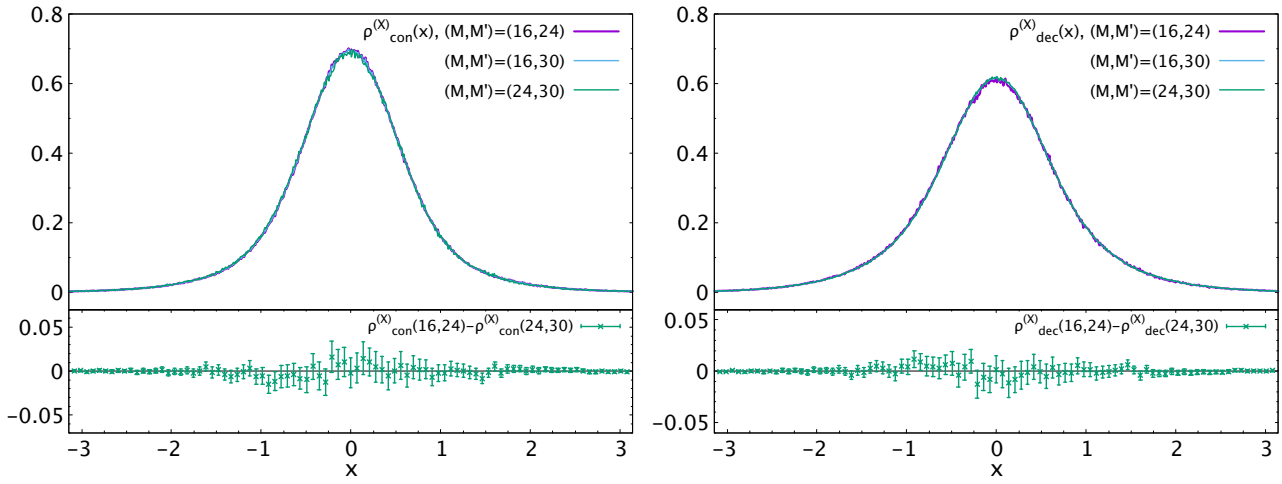

(a) $\rho^{(\mathrm{X})}_{\mathrm{con}}(x)$

(b) $\rho^{(\mathrm{X})}_{\mathrm{dec}}(x)$

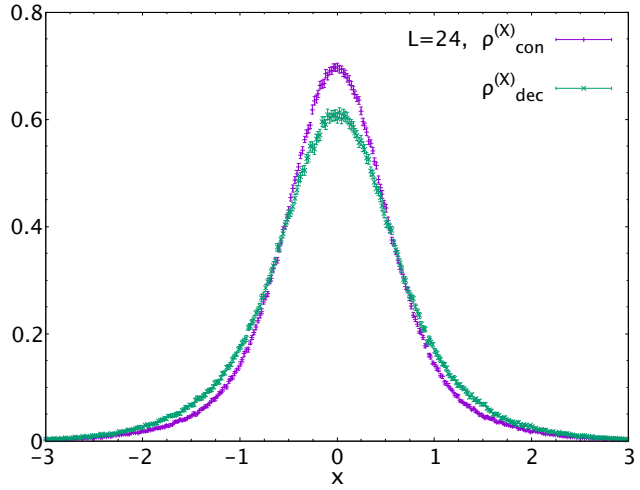

(c) $(M, M') = (16, 24)$

Figure 10: The distribution functions $\rho^{(\mathrm{X})}_{\mathrm{con}}(x)$ and $\rho^{(\mathrm{X})}_{\mathrm{dec}}(x)$ from the Gaussian Matrix model, $D = 2$, $N = 32$, $L = 24$, at the critical temperature $T = T_{\mathrm{c}} = \frac{1}{\ln 2}$. We can see the matching of forms for the different combinations of M and M'. These plots are taken from reference [17].

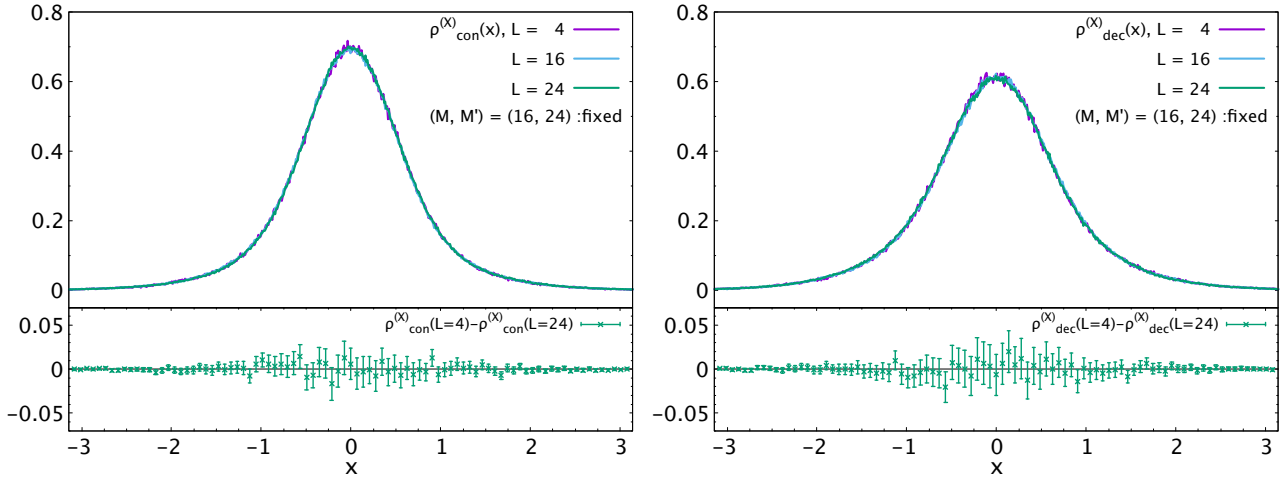

(a) $\rho^{(\mathrm{X})}_{\mathrm{con}}(x)$ (b) $\rho^{(\mathrm{X})}_{\mathrm{dec}}(x)$

Figure 11: The comparison with $\rho^{(\mathrm{X})}_{\mathrm{con}}(x)$ and $\rho^{(\mathrm{X})}_{\mathrm{dec}}(x)$ from the Gaussian Matrix model, $D = 2$, $N = 32$, and $L = 4, 16, 24$, at the critical temperature $T = T_{\mathrm{c}} = \frac{1}{\ln 2}$. We can see that the finite lattice size effect is small. These plots are taken from reference [17].

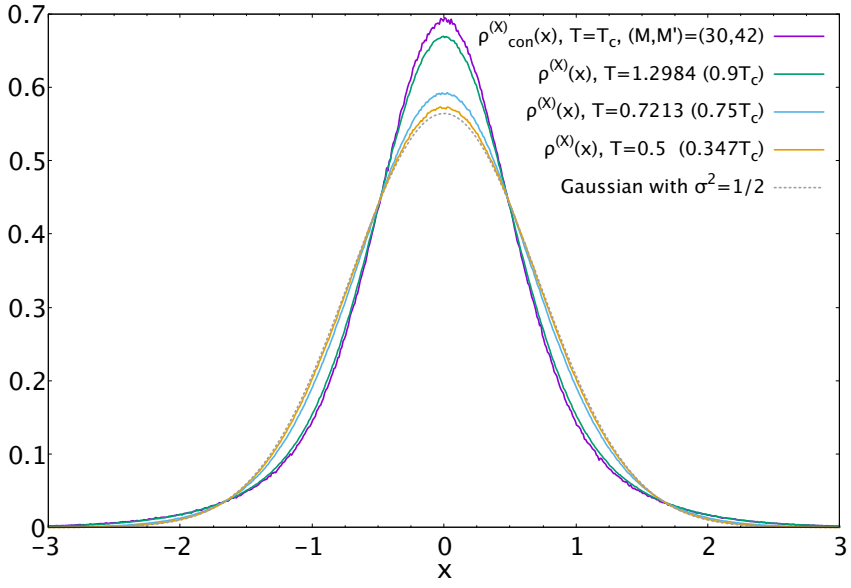

Figure 12: The distributions $\rho^{(\mathrm{X})}(x)$ from the Gaussian matrix model, at low temperatures, $D = 2, N = 48$, $L = 16$. We can see that the distribution approaches to the Gaussian distribution as the temperature goes down. These plots are taken from reference [17].

since $N-M$ and M components in $|X_{ij}|^2$ belongs in the confined and deconfined sectors, respectively. Similarly, we expect $\langle K_i \rangle_{\rm con} = \frac{D}{2}$ if θ_i is in the confined sector. Therefore, the expectation value averaging them over becomes

$$\langle K_i \rangle_{\rm p.d.} = \left(1 - \frac{M}{N}\right) \langle K_i \rangle_{\rm con} + \frac{M}{N} \langle K_i \rangle_{\rm dec} = \frac{D}{2} + \frac{1}{4}\left(\frac{M}{N}\right)^2 . \tag{6.22}$$

In the left side of figure 13, we show the two-dimensional histograms of (θ_i, K_i) for $D = 2$, $N = 48$, $L = 16$, at the critical temperature $T = T_{\rm c}$, and at each M separately [17]. The two-dimensional histograms imply only one peak at each θ (represented by warm color cells). Furthermore, a relation

$$K_i = 1 + \frac{M}{2N} \cos\theta_i \tag{6.23}$$

can be seen with good accuracy from the observation of the binned histograms shown in the right panel of figure 13. The binned histograms are drawn by averaging over the samples K_i corresponding to a θ_i bin of size $\Delta\theta = 0.02$. We expect that the fluctuation at each fixed θ_i comes from the finite-N effect and it is suppressed as N becomes large. By using the distribution of θ_i in the confined and deconfined sectors (4.87) and (4.88), we obtain equations (6.19) and (6.21), and hence, also equation (6.22); by substituting (6.23), the above expectation value can be understood in terms of the expectation value estimated by the distribution function of the Polyakov line phase as well. Explicitly,

$$\langle K_i \rangle_{\square} = \int {\rm d}\theta \; K_i \, \rho^{(\rm P)}_{\square}(\theta), \tag{6.24}$$

where the box $\square$ represents its attribution (the confined/deconfined sector, or ${\rm SU}(M)$-partially-deconfined phase, etc...).

One comment is that the feature of the correlation between K_i and θ_i is the effect of the residual symmetry after taking the static diagonal gauge, what we emphasized in the previous section. One may expect that the two-phase separation mean the two peaks for the distribution of K_i corresponding to the confined and deconfined sectors. Unlike the naive guess, the residual symmetry implies a single peak which satisfies equation (6.19) and (6.21) simultaneously.

[17] We studied the configurations with $M = 18, 30, 42$. The number of sampled data (θ_i, K_i) are $16416, 31488, 16557$ for the above values of M, respectively.

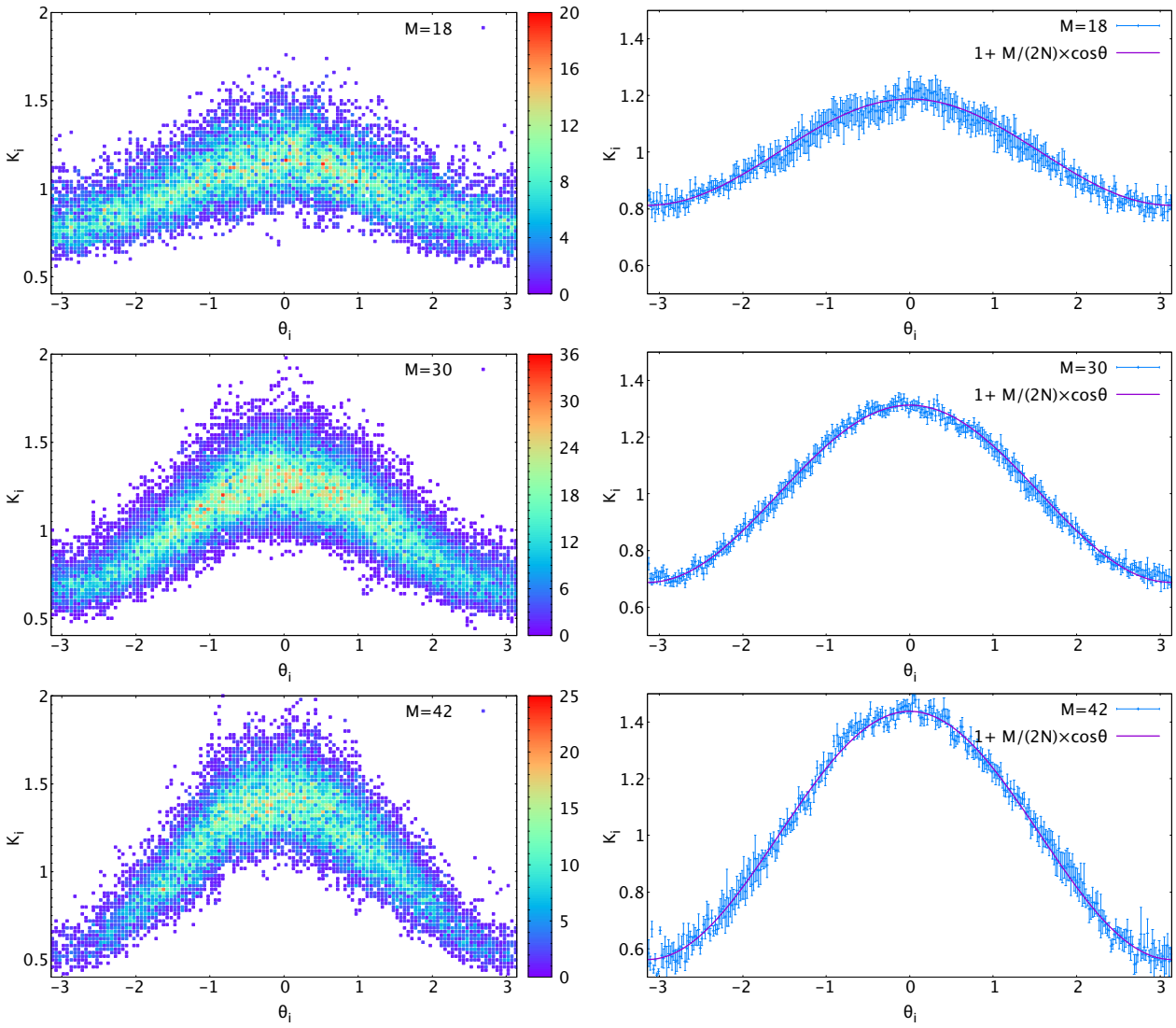

(a) 2D histogram

(b) Binned histogram

Figure 13: Correlation θ_i vs K_i, $N = 48, D = 2$, $L = 16$, at the critical temperature $T = T_c = \frac{1}{\ln 2}$. (a) The two-dimensional histograms of (θ_i, K_i). (b) The binned K_i by averaging within the bin $\Delta\theta = 0.02$. The magenta lines represent $1 + \frac{M}{2N}\cos\theta$. The error bars are estimated by jackknife analysis. These plots are taken from reference [17].

6.4 Case : Yang-Mills matrix model

So far, we mainly consider the two-phase coexistence in the theory without interaction. Including interactions among the degrees of freedom makes things more complicated, and one may doubt the presence of the intermediate phase coexisting occurs. To demonstrate partial deconfinement can take place even in the theory beyond the weak coupling regime, we study the Yang-Mills matrix model

$$S = N \int_0^\beta \mathrm{d}t \, \mathrm{Tr} \left[\frac{1}{2} (D_t X_I)^2 - \frac{1}{4} [X_I, X_J]^2 \right]. \tag{6.25}$$

The index I, J run 1 to D, and in this analysis, we take $D = 9$ where the model had been studied [16, 87, 95, 96][18] as known as bosonic BFSS model since it is the bosonic part of the Banks-Fischler-Shenker-Susskind matrix model [33, 34]. The circumference of the temporal circle β is related to temperature T by $\beta = T^{-1}$, and the covariant derivative is $D_t X_I = \partial_t X_I - \mathrm{i}[A_t, X_I]$, where A_t is the gauge field. In this model, a first order transition near $T = 0.885$ [16] exists with a hysteresis in a narrow range[19] [20] , as sketched in figure 14. We can read the hysteresis off from the two-peak signal of the Monte Carlo sampling for the observables. Below, we approximate the phase transition does not exhibit the hysteresis due to its mildness, and study the properties of the configurations at fixed temperature $T = 0.885$. At the temperature, we vary the value of P from 0 to $\frac{1}{2}$, along the green dotted line in figure 14, similar to the analysis for the Gaussian matrix model. We expect that the above treatment captures the physic of the partially-deconfined phase (orange dotted line).

At the fixed temperature in the transition region, we figure out numerically that the similar relations in the Gaussian matrix model (4.86), (4.89) and (4.90) holds for the Yang-Mills matrix model [16]; Namely, with an identification $2P = \frac{M}{N}$, we obtain [21]

$$\rho^{(\mathrm{P})}(\theta) = \left(1 - \frac{M}{N}\right) \cdot \frac{1}{2\pi} + \frac{M}{N} \cdot \frac{1}{2\pi} (1 + \cos\theta), \tag{6.26}$$

$$E = \left\langle -\frac{3N}{4\beta} \int \mathrm{d}t \ \mathrm{Tr} \, [X_I, X_J]^2 \right\rangle = (N^2 - M^2)\varepsilon_0 + M^2 \varepsilon_1, \qquad \varepsilon_0 \simeq 6.14, \quad \varepsilon_1 \simeq 6.60, \tag{6.27}$$

and

$$R \equiv \left\langle \frac{N}{\beta} \int \mathrm{d}t \ \mathrm{Tr} \, X_I^2 \right\rangle = (N^2 - M^2) r_0 + M^2 r_1. \qquad r_0 \simeq 2.20, \quad r_1 \simeq 2.29. \tag{6.28}$$

These relations strongly support partial deconfinement in this model. Furthermore, the explicit separation to the $\mathrm{SU}(M)$- and $\mathrm{SU}(N-M)$-sectors shown in figure 1 is demonstrated in the latest paper [17]. Again, unlike in the Gaussian model, the separation into two different sectors is highly nontrivial due to the interaction in this

[18] See also references [97–101] for the analysis of the classical dynamics of the Yang-Mills matrix model.

[19] According to the study [16], the two-state signal appears $0.884 \lesssim T \lesssim 0.886$ for $N = 64$, number of lattice sites $L = 24$.

[20] See also references [102, 103] for the phase structure.

[21] The numerical fits in reference [16] were performed in a slightly different way, that is, the power was not fixed to 2. The difference does not have any influence to the main results.

model. In this section, we show the separation is doable, at least, in the Yang-Mill matrix model which is beyond weak coupling. Analogous to the analysis of the Gaussian matrix model explained in section 6.3, we focus on the aspects of master fields of the lattice configurations in this model at the fixed temperature.

One remark is that, theoretically, there is not a clear and strong reasoning to forbid the nontrivial M-dependence to the physics in partial deconfinement. In the presence of interactions between the confined and deconfined sectors, the averaging in the confined and deconfined sectors can be influenced by M. Rather, it seems natural that the magnitude of the intersector interaction changes depending on the ratio of the coexistence M/N. To go straight, it does not affect our argument significantly whether the M-dependence exists or not, as we will discuss later again.

In this section, we use the static diagonal gauge, as we did in section 6.3, i.e., the gauge field is fixed to $A_t = \mathrm{diag}\left(\frac{\theta_1}{\beta}, \cdots, \frac{\theta_N}{\beta}\right)$. Unlike the Gaussian matrix model, we generate lattice configurations employing the "efficient" simulation introducing the source term restricting the value of the Polyakov loop to a specific range, as explained in section 6.1. In the range of the Polyakov loop we set on (6.1), applying this method does not change the physics from the previous research [16], and hence, we can reference its result and regard it same the results performed under the constraint.

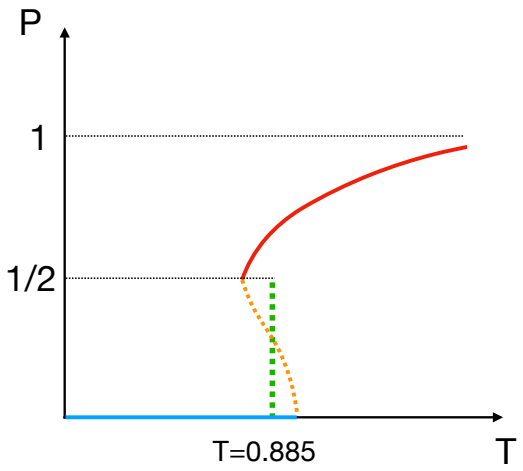

Figure 14: Sketch of the phase structure of the $D = 9$ Yang-Mills matrix model with respect to the Polyakov loop, which is taken from the paper [17]. The red and blue lines correspond to the completely-deconfined and confined phases, the minima of the free energy in the canonical ensemble. The orange dotted line corresponds to the partially-deconfined phase, maxima of the free energy. We emphasize that although this phase is not favored in the canonical ensemble, it is stable in the microcanonical ensemble. In the canonical ensemble, a first order transition occurs around $T = 0.885$ [16]. In reference [17], the properties of the configurations at fixed temperature $T = 0.885$ were studied as the master fields, varying the value of P (along the green line). As a comment for other observables, the previous research [16] had found the behaviors of E and R, equations (6.27) and (6.28).

6.4.1 Distributions of scalar degrees of freedom

Just as in the Gaussian matrix model, the relation equation (6.28) implies that partial deconfinement occurs and the separation of the distribution of $X_{I,ij}$ to $\rho^{(\mathrm{X})}_{\mathrm{con}}(x)$ and $\rho^{(\mathrm{X})}_{\mathrm{dec}}(x)$ can be seen by the same expression (6.8). The goal in this section is to demonstrate it.

Here, we are assuming that $\rho^{(\mathrm{X})}_{\mathrm{con}}(x)$ and $\rho^{(\mathrm{X})}_{\mathrm{dec}}(x)$ are independent of M as we did in the Gaussian matrix model. As we will see, it seems valid with a reasonable accuracy, although the small M-dependence may exist. In section 6.5, we will show a different analysis that does not assume M-independence with employing a different simulation.

We show the distributions $\rho^{(\mathrm{X})}_{\mathrm{con}}(x)$ and $\rho^{(\mathrm{X})}_{\mathrm{dec}}(x)$ in figure 15 by using equations (6.16) and (6.17). The same distributions can be obtained up to error bars by using several pairs (M, M'), and it shows that the confined and deconfined sectors behave in a difference manner. Moreover, the variances evaluated by the histograms $\rho^{(\mathrm{X})}_{\mathrm{con}}(x)$ and $\rho^{(\mathrm{X})}_{\mathrm{dec}}(x)$ in figure 15 are shown in table 2 in appendix D, which supports the consistency of our analysis. If $\rho^{(\mathrm{X})}_{\mathrm{con}}(x)$ and $\rho^{(\mathrm{X})}_{\mathrm{dec}}(x)$ do not depend of the size of the deconfined sector M, the variances must be related to r_0 and r_1 according to equations (6.28) and (6.8),

$$\sigma^2_{\mathrm{con}} \equiv \int \mathrm{d}x\, x^2 \rho^{(\mathrm{X})}_{\mathrm{con}}(x) = \frac{r_0}{d} \simeq \frac{2.20}{9} \simeq 0.244, \tag{6.29}$$

$$\sigma^2_{\mathrm{dec}} \equiv \int \mathrm{d}x\, x^2 \rho^{(\mathrm{X})}_{\mathrm{dec}}(x) = \frac{r_1}{d} \simeq \frac{2.29}{9} \simeq 0.254. \tag{6.30}$$

We can see a reasonable agreement with the values in table 2 in appendix D.

One may wonder that it only means a separation into M^2 and $N^2 - M^2$ degrees of freedom, not one into the $\mathrm{SU}(M)$- and $\mathrm{SU}(N-M)$-sectors. In addition to this, we ideally should not assume from the beginning that $\rho^{(\mathrm{X})}_{\mathrm{con}}(x)$ and $\rho^{(\mathrm{X})}_{\mathrm{dec}}(x)$ are independent of M. We will demonstrate the separation to such a $\mathrm{SU}(M)$- and $\mathrm{SU}(N-M)$-sectors more explicitly in section 6.5 by employing the constrained simulation .

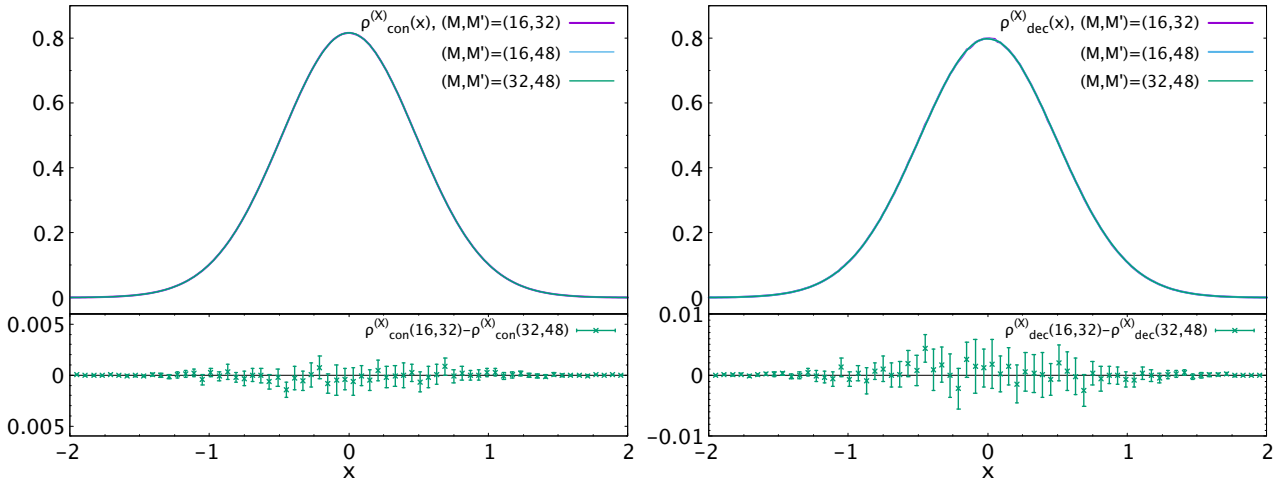

(a) $\rho^{(\mathrm{X})}_{\mathrm{con}}(x)$ (b) $\rho^{(\mathrm{X})}_{\mathrm{dec}}(x)$

Figure 15: Distributions $\rho^{(\mathrm{X})}_{\mathrm{con}}(x)$ and $\rho^{(\mathrm{X})}_{\mathrm{dec}}(x)$ in the "efficient" simulation of the Yang-Mills matrix model, $N = 64$, $L = 24$, and $T = 0.885$. The same distributions can be obtained within the error bars by using several combinations (M, M'). The error bars are estimated by jackknife analysis. These plots are taken from reference [17].

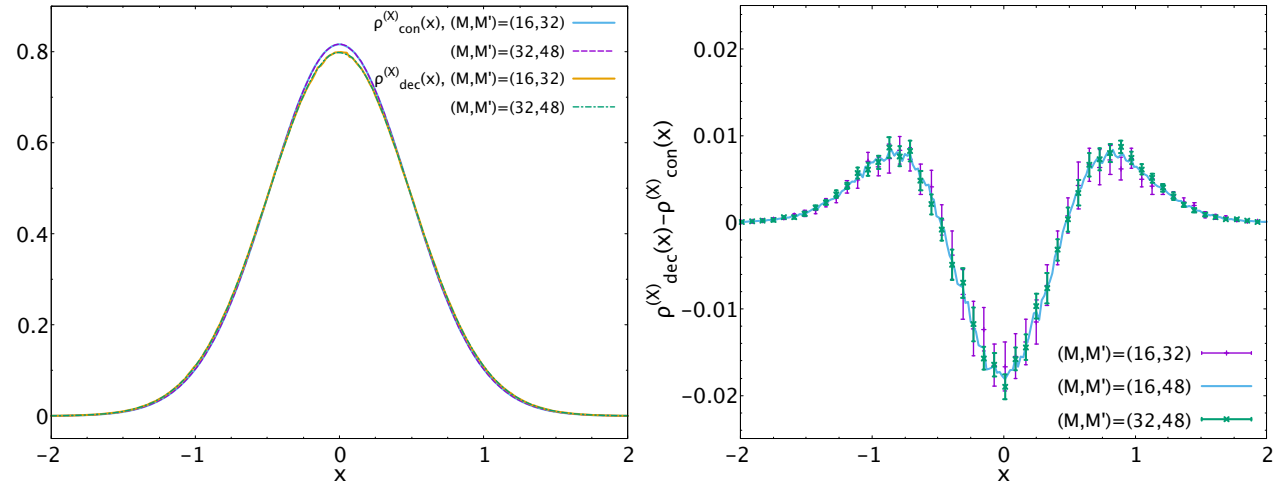

(a) Distributions (b) Difference

Figure 16: Comparison between $\rho^{(\mathrm{X})}_{\mathrm{dec}}(x)$ and $\rho^{(\mathrm{X})}_{\mathrm{con}}(x)$ shown in figure 15. (a) A tiny discrepancy can be seen between $\rho^{(\mathrm{X})}_{\mathrm{con}}(x)$ and $\rho^{(\mathrm{X})}_{\mathrm{dec}}(x)$. (b) The difference $\rho^{(\mathrm{X})}_{\mathrm{dec}}(x) - \rho^{(\mathrm{X})}_{\mathrm{con}}(x)$ is significantly larger than the error bars of $\rho^{(\mathrm{X})}_{\mathrm{dec}}(x)$ and $\rho^{(\mathrm{X})}_{\mathrm{con}}(x)$. The error bars are estimated by jackknife analysis. These plots are taken from reference [17].

6.4.2 Correlation between scalar and gauge degrees of freedom

As well as the Gaussian matrix model, we can study partial deconfinement in terms of the correlation between the $K_i \equiv \sum_{I,j} \frac{1}{\beta} \int \mathrm{d}t |X_{I,ij}|^2$ and θ_i in the Yang-Mills matrix model. At first, from the numerical fit (6.28),

$$\langle K_i \rangle_{\mathrm{con}} = r_0 = 9\sigma^2_{\mathrm{con}}, \qquad \langle K_i \rangle_{\mathrm{GWW},N} = r_1 = 9\sigma^2_{\mathrm{dec}}, \tag{6.31}$$

which is, by the way, unlike the case of the Gaussian matrix model, since we could compute the variances for that model analytically. Here again, we assume that the r_0 and r_1 obtained in equation (6.31) are the contributions from the confined and deconfined sectors (the blue area and red area in figure 1). In other words, the assumption means that the properties of the master fields does not depend on the value of M. Then,

$$\langle K_i \rangle_{\mathrm{dec}} = r_0 + \frac{M}{N} \cdot (r_1 - r_0), \tag{6.32}$$

is the natural form when θ_i corresponding to it is in the deconfined sector. The distribution of the Polyakov line phases in the confined and deconfined sectors are identical to those in the Gaussian matrix model, $\frac{1}{2\pi}$ and $\frac{1+\cos\theta}{2\pi}$. Hence, analogous to the form in equation (6.23) for the Gaussian matrix model, we assign an ansatz

$$K_i = r_0 + \frac{M}{N} \cdot 2(r_1 - r_0)\cos\theta_i, \tag{6.33}$$

for the correlation between K_i and θ_i in the Yang-Mills matrix model.

Figure 17 shows the correlation between θ_i and K_i obtained by numerical simulations. The values of r_0 and r_1 are obtained by using equation (6.33) as fit ansatz, which is consistent with the values of the variances in table 2 in appendix D.

Same as the result of the Gaussian matrix model, this result supports the occurrence of partial deconfinement for the scalar fields; with combining (6.33), the distribution of the Polyakov line phases $\rho^{(\mathrm{P})}(\theta)$ which shows the two-phase separation[22)] reproduces the expected values (6.31) and (6.32). It indicates that the separation of scalar degrees of freedom into two different sectors takes place in conjunction with the separation of the gauge degrees of freedom θ_i in a consistent way.

[22)] For the plot of the distribution $\rho^{(\mathrm{P})}(\theta)$, see also the figure 15 in reference [16].

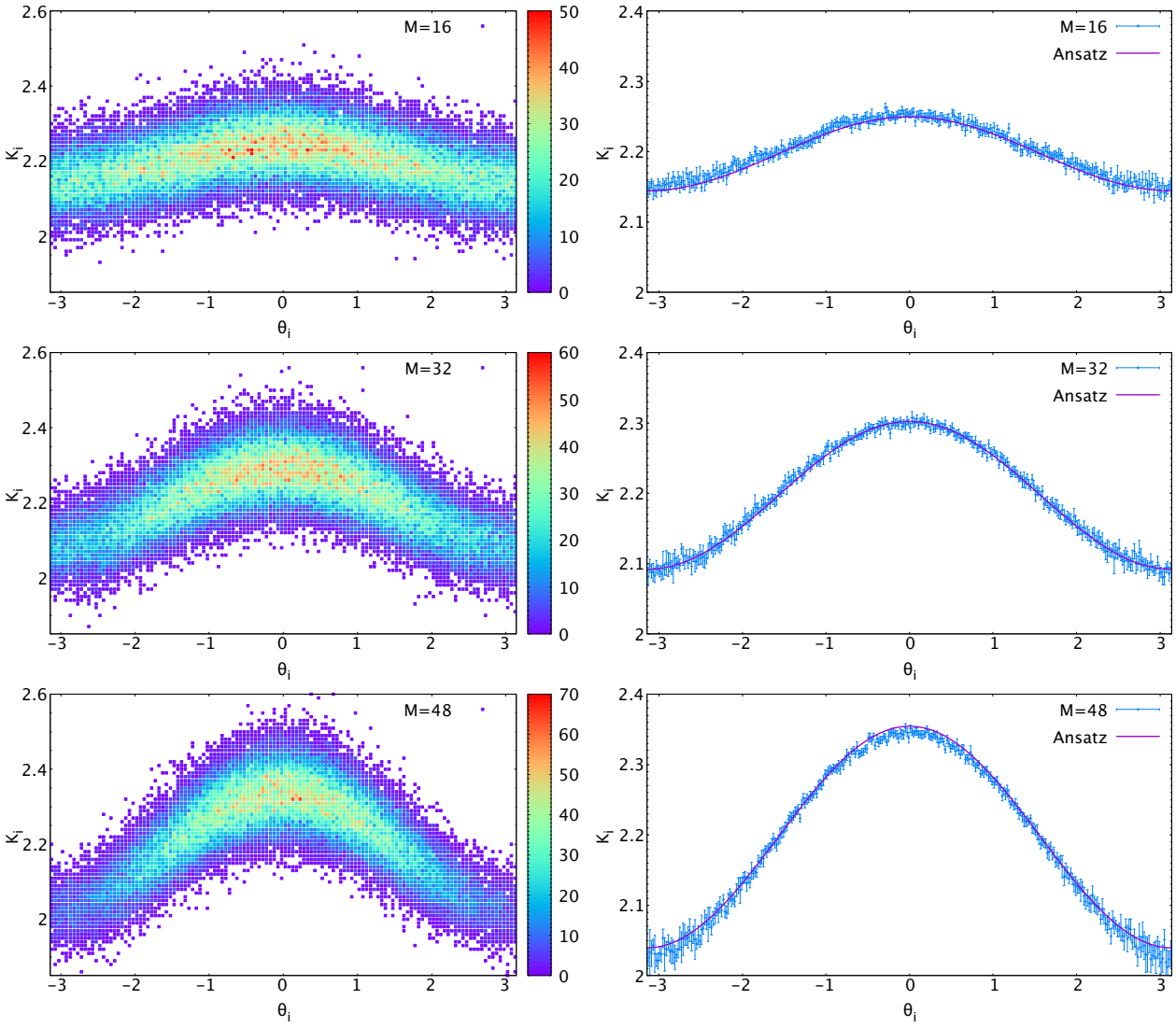

(a) 2D histogram

(b) Binned histogram

Figure 17: Correlation between θ_i vs K_i for the Yang-Mills matrix model with $N = 64$, $L = 64$, $T = 0.885$. The total number of data points for each M is $(N = 64) \times$ (# configurations) in table 2 placed in appendix D. The center symmetry is fixed sample by sample such that $P = |P|$. (a) The two-dimensional histograms of (θ_i, K_i). (b) The binned K_i by averaging within the bin $\Delta\theta = 0.02$. The magenta lines show fit results performed by equation (6.33), by using the best-fit values $r_0 = 2.197$ and $r_1 = 2.302$. The values obtained by the fits are consistent with the values of the variances in table 2 placed in appendix D. The error bars are estimated by jackknife analysis. These plots are taken from reference [17].

6.5 Case : Yang-Mills matrix model with constrained simulation

In this section, we perform another numerical analysis that the $M \times M$-block-structure like figure 1 is manifest. As explained in section 6.1, we call the method constrained simulation.

Again, we adopt the lattice regularization in the static diagonal gauge to Monte Carlo simulation. The center symmetry is fixed sample by sample such that $P = |P|$. Although the difference from the previous analysis is the source term we introduced, the way of numerical analysis we performed are slightly modified based on the form of separation. At first, we confirm as a consistency check that the thermodynamics of this model is undeformed under an introduction of the source term (6.3) in the next section. After that, we study the distributions of scalars and the correlation between the scalar and gauge degrees of freedom what we did in the previous section, in an essentially same but a bit different manner.

6.5.1 Consistency checks

At finite N, this constraint may change the theory slightly since the Polyakov loops in each sector $P_M = \frac{1}{2}$ and $P_{N-M} = 0$ are valid only when M and $N - M$ are sufficiently huge integers. For $N = 48, 64$ and 128, $\frac{M}{N} = 0.25, 0.50$ and 0.75, we can confirm the finite N effects are small.

On behalf of the numerical data, we show the consistency check for $N = 64$ configurations. In figure 18, we

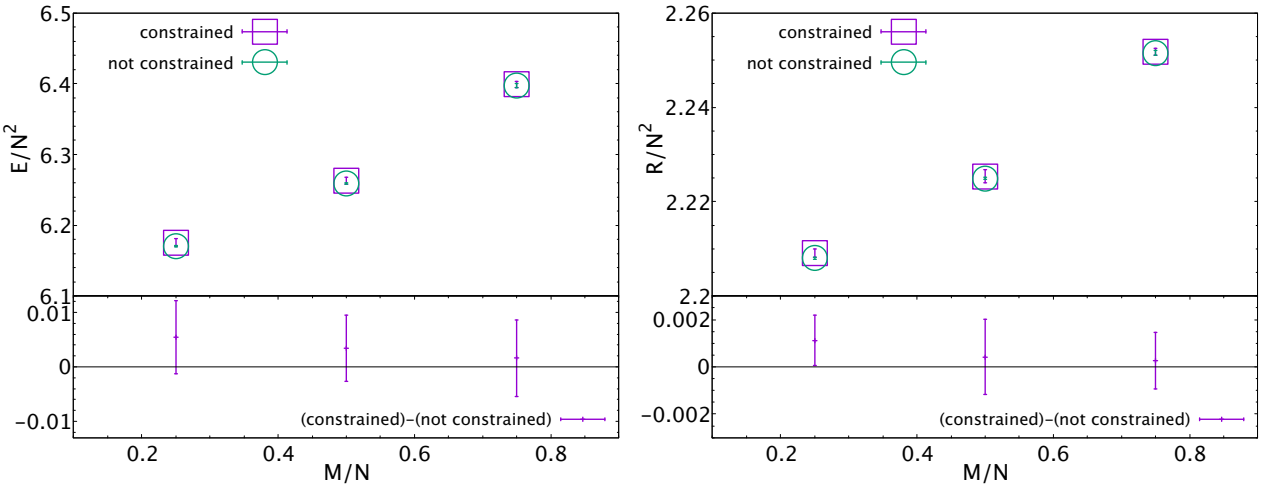

(a) E/N^2 (b) R/N^2

Figure 18: Comparison observables obtained by the simulations with and without the source term (6.3), for the Yang-Mills matrix model, $N = 64$, $L = 24$, and $T = 0.885$. The error bars are estimated by jackknife analysis. These plots are taken from reference [17].

compare the quantities E/N^2 and R/N^2 calculated the configurations with and without the constraint (6.3). It

shows good agreements between them up to error bars, which implies that the addition of the source term for constraint does not modify the thermodynamics of this model.

The distributions of the Polyakov line phases $\rho^{(\mathrm{P})}(\theta)$ for all θ (i.e. both in the confined and deconfined sectors) obtained from the constrained simulations at $T = 0.885$ are plotted in figure 19. It shows nice matchings with $\frac{1}{2\pi}\left(1 + \frac{M}{N}\cos\theta\right)$, which is the confirmed behavior theoretically and numerically in the partially-deconfined phases of the Yang-Mills matrix model. These observations reinforce the expectation we mentioned before that the source term in equation (6.3) does not modify the thermodynamic properties of the model.

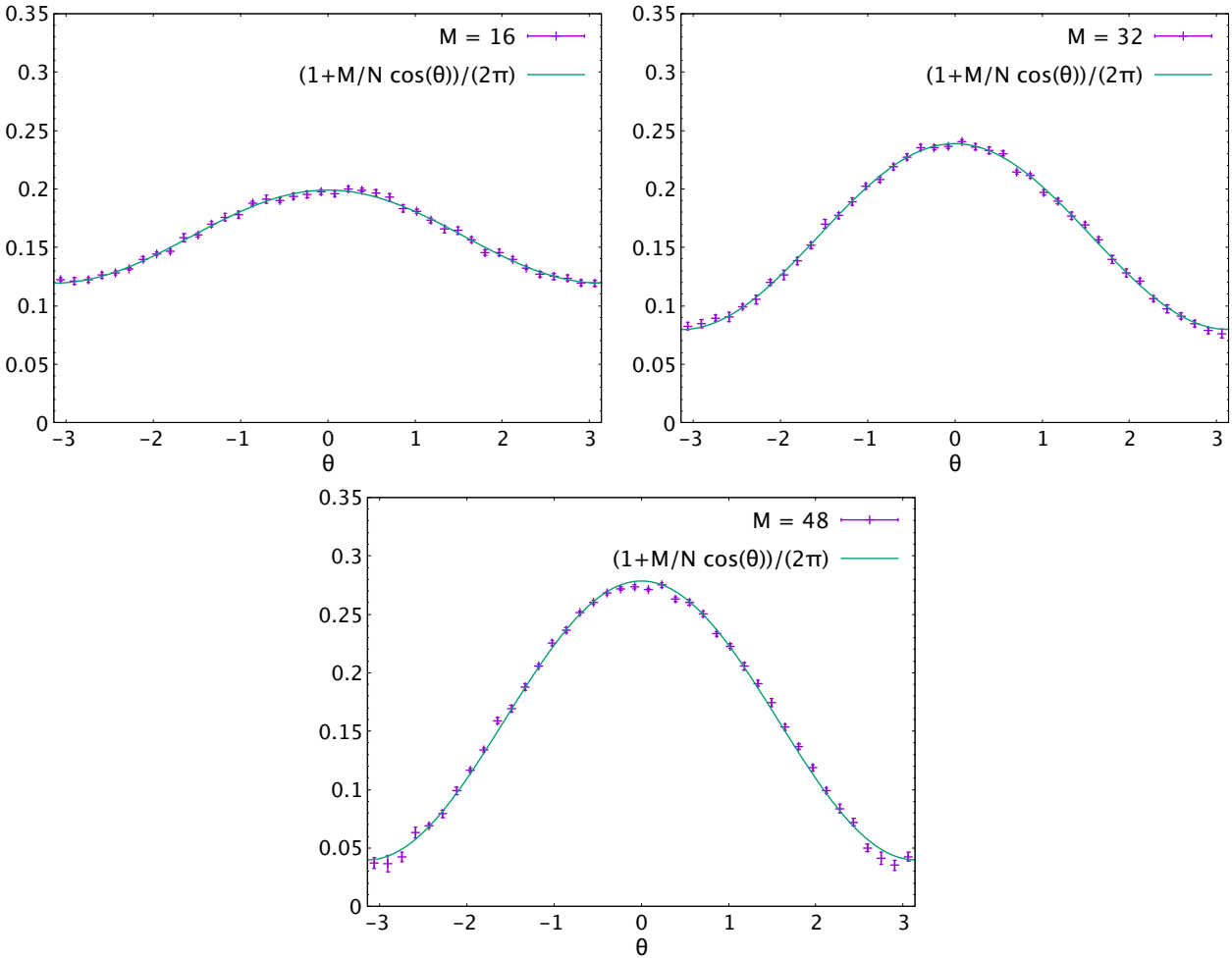

Figure 19: Distribution of the Polyakov line phases $\rho^{(\mathrm{P})}(\theta)$ obtained by the constrained simulations of the Yang-Mills matrix model, $N = 64$, $L = 24$, $M = 16, 32, 48$, and $T = 0.885$. The green lines represent $\frac{1}{2\pi}\left(1 + \frac{M}{N}\cos\theta\right)$. The error bars are estimated by jackknife analysis. These plots are taken from reference [17].

6.5.2 Distributions of scalar degrees of freedom

Let us firstly consider the distribution of the scalar degrees of freedom $\{X_{I,jk}\}$ again. In the previous analysis for the Yang-Mills matrix model discussed in section 6.4.1, the distribution $\rho^{(\mathrm{X})}_{\mathrm{con}}(x)$ and $\rho^{(\mathrm{X})}_{\mathrm{dec}}(x)$ are estimated by using equation (6.8) where we assumed that they do not depend on the size M. Here, we can estimate the distributions without assuming M-independence due to the explicit separation of the constraint; In the set of the independent scalars x, the distribution $\rho^{(\mathrm{X})}_{\mathrm{dec}}(x)$ and $\rho^{(\mathrm{X})}_{\mathrm{con}}(x)$ can be determined with $1 \leq j, k \leq M$ and from the rest, corresponding to the $M \times M$-upper-left block and the rest in matrix configuration, respectively.

The numerical results for $\rho^{(\mathrm{X})}_{\mathrm{con}}(x)$ and $\rho^{(\mathrm{X})}_{\mathrm{dec}}(x)$ are shown in figures 20 and 21. We can see an obvious discrepancy between $\rho^{(\mathrm{X})}_{\mathrm{con}}(x)$ and $\rho^{(\mathrm{X})}_{\mathrm{dec}}(x)$ from those. In addition, figure 22 shows the comparison of the distributions obtained from the constrained and "efficient" simulations. It displays a reasonable agreement, and hence, these independent results guarantee the validity of each other. These observations provide us with an explicit confirmation of the $M \times M$-block structure.

While we have not mentioned up to here, a small M-dependence can be seen in the plots of the constrained simulation and in comparison with the results without the constraint. When looking at the values of the variances in table 3 placed in appendix D in detail, one can see a similar dependence. We furthermore estimate the values of the off-diagonal blocks in the confined sector separately, shown in the same table. There, a similar M-dependence is visible. We will discuss this in section 6.6 which is a summary of this section. As we will explain there, our conclusions are not influenced so much even if such an M-dependence affects.

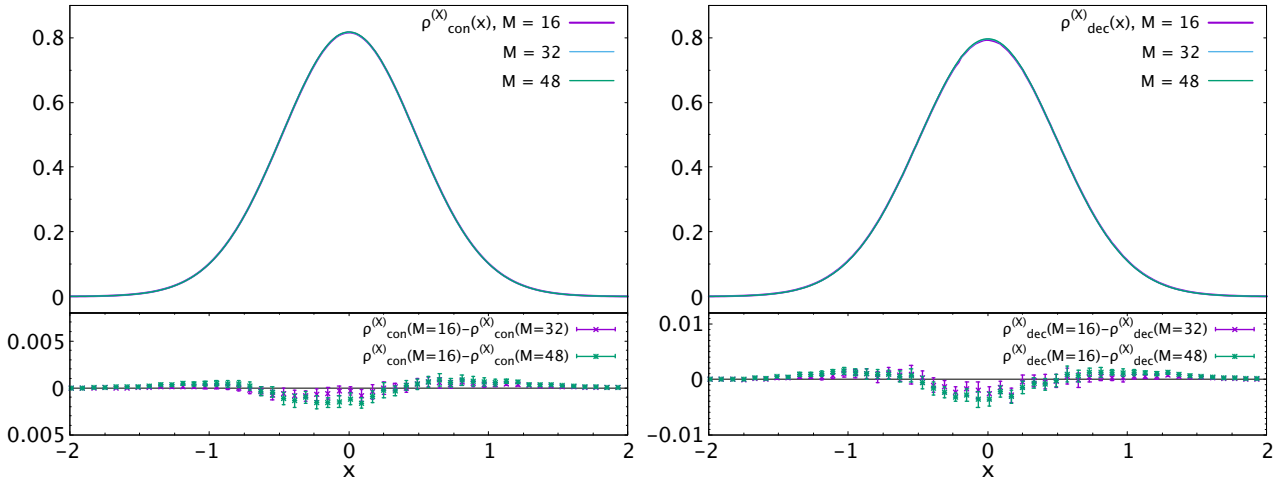

(a) $\rho^{(\mathrm{X})}_{\mathrm{con}}(x)$ (b) $\rho^{(\mathrm{X})}_{\mathrm{dec}}(x)$

Figure 20: Distributions $\rho^{(\mathrm{X})}_{\mathrm{con}}(x)$ and $\rho^{(\mathrm{X})}_{\mathrm{dec}}(x)$ obtained from different values of N and M in the constrained simulation of the Yang-Mills matrix model with $N = 64$, $L = 24$, $T = 0.885$. The error bars are estimated by jackknife analysis. These plots are taken from reference [17].

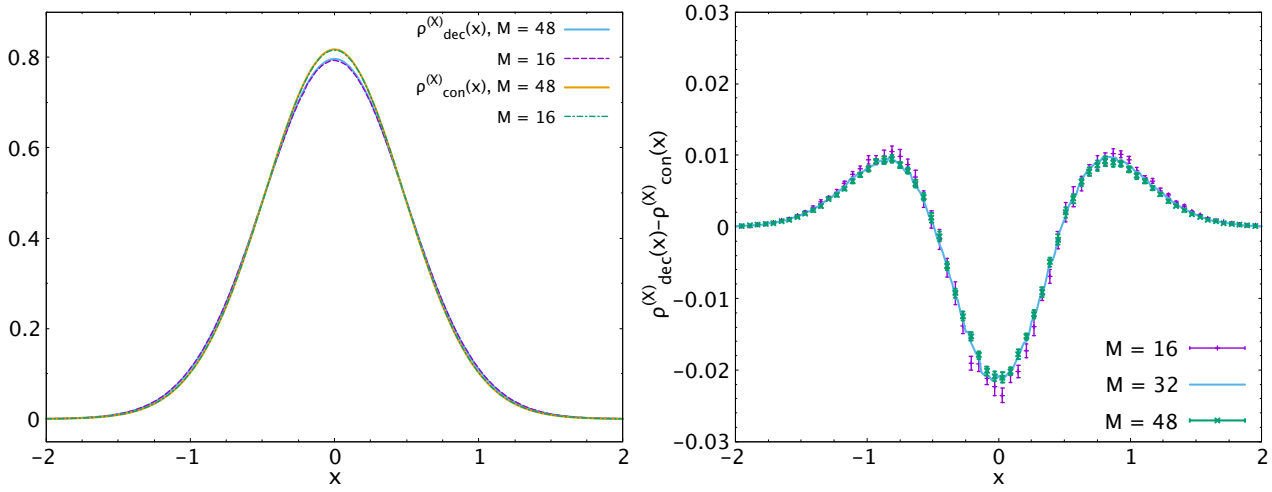

(a) Distributions (b) Difference

Figure 21: Comparison between $\rho^{(\mathrm{X})}_{\mathrm{con}}(x)$ and $\rho^{(\mathrm{X})}_{\mathrm{dec}}(x)$ showed in figure 20 for the constrained simulations of the Yang-Mills matrix model with $N = 64$, $L = 24$, $T = 0.885$. a) $\rho^{(\mathrm{X})}_{\mathrm{con}}(x)$ and $\rho^{(\mathrm{X})}_{\mathrm{dec}}(x)$. (b) The difference $\rho^{(\mathrm{X})}_{\mathrm{dec}}(x) - \rho^{(\mathrm{X})}_{\mathrm{con}}(x)$ is sufficiently larger than the error bars of the distributions. The error bars are estimated by jackknife analysis. These plots are taken from reference [17].

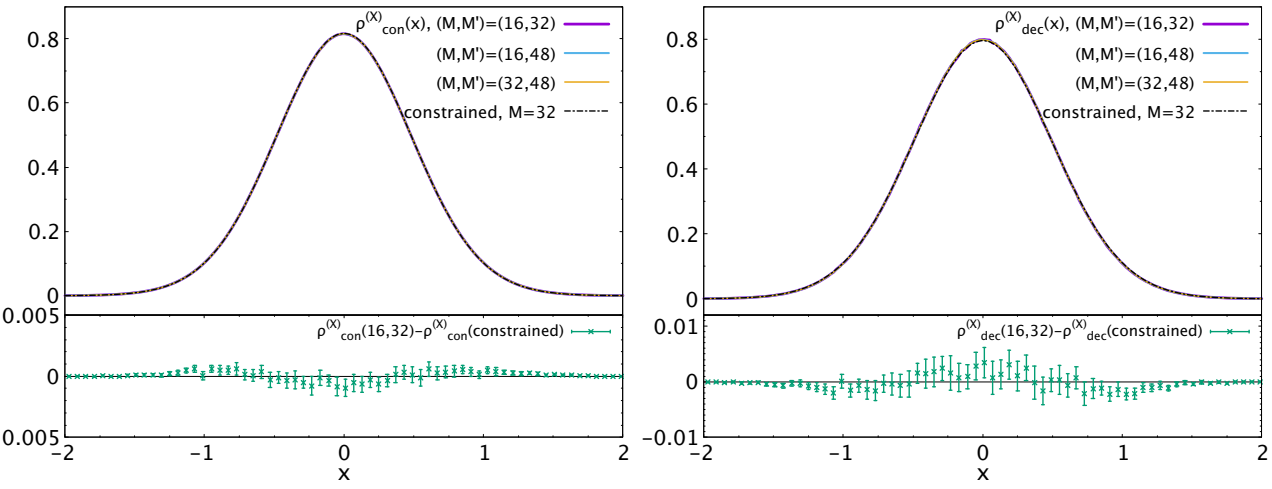

(a) $\rho^{(\mathrm{X})}_{\mathrm{con}}(x)$ (b) $\rho^{(\mathrm{X})}_{\mathrm{dec}}(x)$

Figure 22: Comparison with and without constraint for the Yang-Mills matrix model with $N = 64$, $L = 24$, and $T = 0.885$. The error bars are estimated by jackknife analysis. These plots are taken from reference [17].

6.5.3 Correlation between scalar and gauge degrees of freedom

In this section, let us again study the correlation between θ_i and K_i with the explicit separation. We discuss the cases with and without taking into account a possible M-dependence of $\rho^{(\mathrm{X})}_{\mathrm{con}}(x)$ and $\rho^{(\mathrm{X})}_{\mathrm{dec}}(x)$. Both cases describe the data at the same level of precision.

At first, we forget the M-dependence and assign the ansatz for the θ-dependence of K_i given by equation (6.33). The values of r_0 and r_1 are taken from the analysis we obtained figure 17. The results are shown with the magenta lines in figure 23. The figure is essentially the same as figure 17, except the addition of the source term (6.3) to the action of the model. Moreover in this case, due to the explicit separation using the constrained simulation, we can confirm equation (6.33) separately in each sector, which is shown in figure 24. It enables us to see the residual symmetry in the master field.

Next, we take the possible M-dependence into account. In the constrained simulation, the expectation values $\langle K_i \rangle_{\mathrm{con}}$ and $\langle K_i \rangle_{\mathrm{dec}}$ can be obtained directly as

$$\langle K_i \rangle_{\mathrm{dec}} = \left\langle \frac{1}{M} \sum_{i=1}^{M} K_i \right\rangle, \qquad \langle K_i \rangle_{\mathrm{con}} = \left\langle \frac{1}{N-M} \sum_{i=M+1}^{N} K_i \right\rangle. \tag{6.34}$$

These values relate to the variances in each sector via the quantity R in equation (6.28). They are listed in table 3 placed in appendix D, and hence

$$\langle K_i \rangle_{\mathrm{dec}} = \left(\frac{M}{N} \cdot \sigma^2_{\mathrm{dec}} + \left(1 - \frac{M}{N} \right) \cdot \sigma^2_{\text{con,off-diag}} \right) \times 9, \tag{6.35}$$

and

$$\langle K_i \rangle_{\mathrm{con}} = 9\sigma^2_{\mathrm{con}}. \tag{6.36}$$

Here, σ^2_{dec}, σ^2_{con} and $\sigma^2_{\text{con,off-diag}}$ are the variances of the distributions of x in the deconfined sector, in the confined sector, and the off-diagonal block in the confined sector, respectively. Using them, an ansatz can be obtained without imposing the M-independence of the distributions $\rho^{(\mathrm{X})}_{\mathrm{con}}(x)$ and $\rho^{(\mathrm{X})}_{\mathrm{dec}}(x)$;

$$K_i = \langle K_i \rangle_{\mathrm{con}} + 2(\langle K_i \rangle_{\mathrm{dec}} - \langle K_i \rangle_{\mathrm{con}}) \cos\theta_i, \tag{6.37}$$

analogous to the previous analyses in the Gaussian and Yang-Mills matrix models. The dotted-black lines in the right panels of figure 23 and figure 24 show the results of the analysis. Both ansatzs express the numerical data at the same level of precision, and the difference between the ansatzs with and without imposing the M-dependence (6.37) and (6.33) is too small to judge the quality of ansatz compared to the errors at this point.

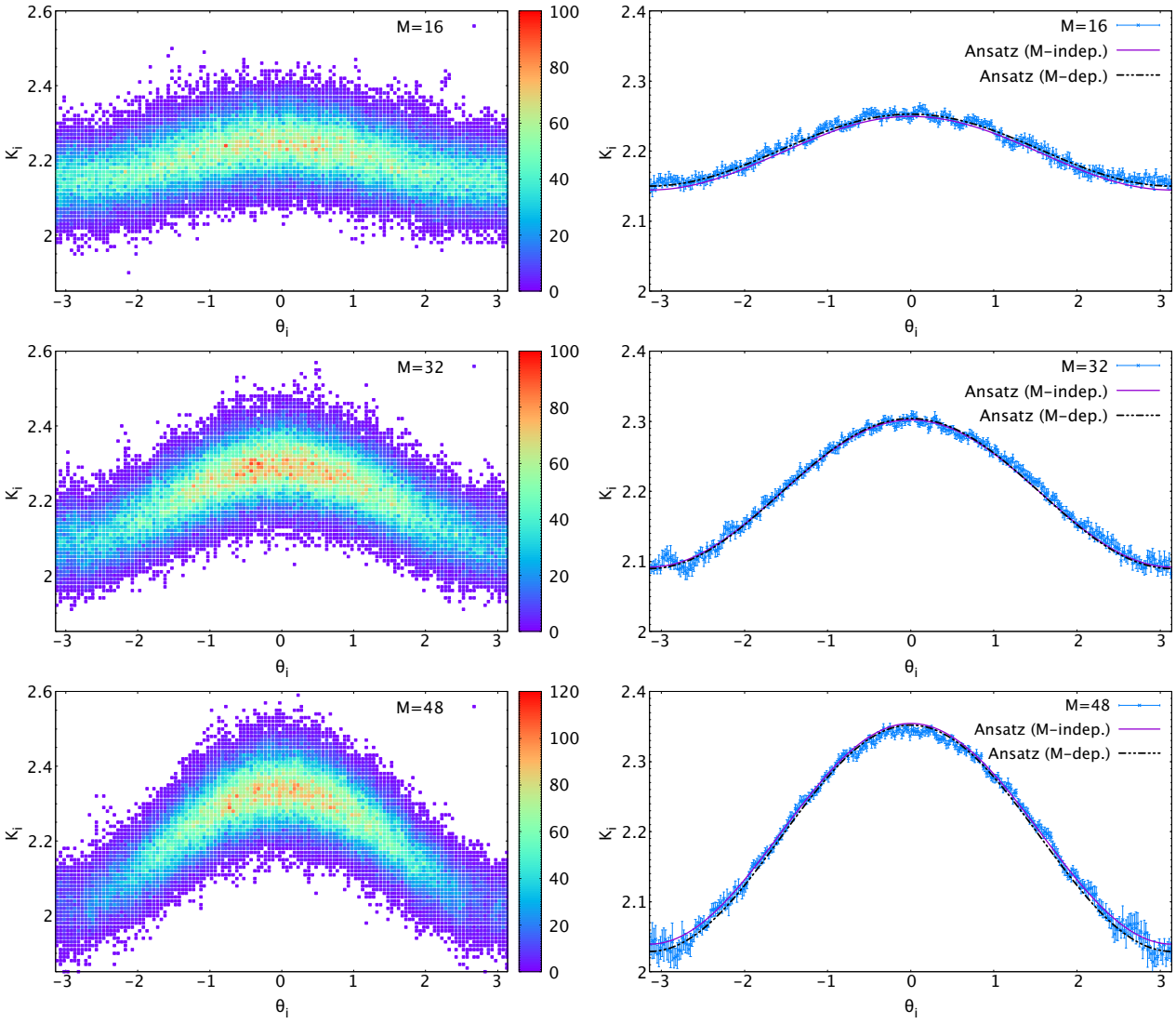

(a) 2D histogram

(b) Binned histogram

Figure 23: Correlation between θ_i vs K_i for the constrained simulation of the Yang-Mills matrix model with $N = 64$, $L = 24$, $M = 16, 32$ and 48 at $T = 0.885$. For each M, 1500 configurations are used (the total number of points is $(N = 64) \times 1500$). (a) The two-dimensional histograms of (θ_i, K_i). It shows the data points from the confined and deconfined sector together. (b) The binned K_i by averaging within the bin $\Delta\theta = 0.02$. The magenta lines represent equation (6.33), with r_0 and r_1 from figure 17. The black dotted lines represent equation (6.37), with variances from table 3 placed in appendix D. The error bars are estimated by jackknife analysis. These plots are taken from reference [17].

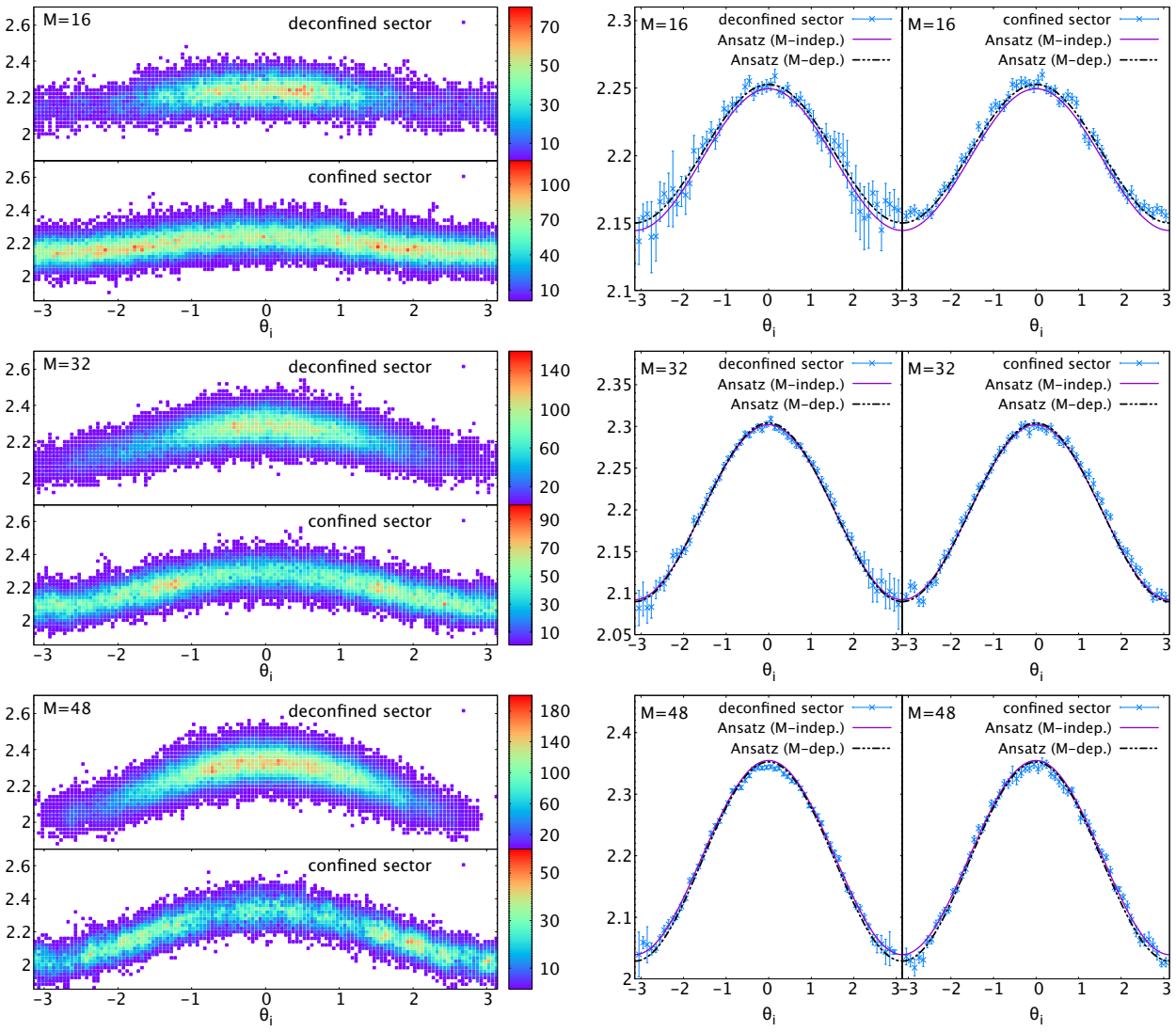

(a) 2D histogram

(b) Binned histogram

Figure 24: Correlation between θ_i vs K_i for the constrained simulation of the Yang-Mills matrix model with $N = 64$, $L = 24$, $M = 16$, 32, and 48 at $T = 0.885$. The confined and deconfined sectors are shown separately, and $\Delta\theta = 0.1$ is taken for (b). The total number of the data points are $M \times 1500$ and $(64 - M) \times 1500$ for the deconfined and confined sectors, respectively. These plots are taken from reference [17].

6.5.4 Energy increment coming from deconfined sector

Until here, performing the constrained simulation, we have seen the separation consistent with partial deconfinement via the properties of master field.

In fact, we can furthermore demonstrate the evidence of two-phase coexistence; using the insight of the weak coupling regime, the zero-point energy is the only contribution of the confined sector, and hence, the energy contribution from the deconfined sector is dominant in the partially-deconfined phase. It becomes a strong evidence to the occurrence of the two-phase coexistence even beyond the weak coupling regime if we can confirm the energy contribution comes only from the deconfined $M \times M$-block generated in the constrained simulation. The goal in this section is to reveal that.

Let us introduce the notation $X_{I\mathrm{dec}}$ and $X_{I\mathrm{con}}$ to denote the deconfined and confined sectors of the matrix field configuration X_I, respectively. By definition, $X_I = X_{I\mathrm{dec}} + X_{I\mathrm{con}}$. The energy E in equation (6.27) includes the contribution

$$E_{\mathrm{con}} \equiv \left\langle -\frac{3N}{4\beta} \int_0^\beta \mathrm{d}t \ \mathrm{Tr}[X_{I\mathrm{con}}, X_{J\mathrm{con}}]^2 \right\rangle , \tag{6.38}$$

which is only from the confined part, and the terms involving $X_{I\mathrm{dec}}$,

$$E_{\mathrm{dec}} \equiv E - E_{\mathrm{con}}. \tag{6.39}$$

We can expect that the contribution from the deconfined part and the interaction between confined and deconfined part is concentrated in the quantity E_{dec}. To check it, we construct the configurations as shown in figure 25, replaced $X_{I\mathrm{dec}}$ with the elements in the completely-confined phase. In other words, the $\mathrm{SU}(M)$-sector is refilled with the confined configuration by performing another type of constrained simulation. When we need generic configurations in the completely-confined phase, we generate the lattice configurations without tuning the Polyakov loops in each sector P_M and P_{N-M} zero, although the obtained P must be zero. In order for the comparison to perform the another constrained simulation, we introduce the new source term

$$\Delta S = \begin{cases} \frac{\gamma}{2} \left(|P_M| - \delta \right)^2 & (|P_M| > \delta) \\ \frac{\gamma}{2} \left(|P_{N-M}| - \delta \right)^2 & (|P_{N-M}| > \delta) \end{cases} \tag{6.40}$$

to the action of the model. Under this constraint, the counterparts of E_{con} and E_{dec} we need to compute are denoted by $E^{(0)}_{\mathrm{con}}$ and $E^{(0)}_{\mathrm{dec}}$.

As shown in figure 26, We observe that E_{con} and $E^{(0)}_{\mathrm{con}}$ are remarkably close. It leads, with a nice numerical accuracy, that the increments of the energy from the one in the completely-confined phase originates only from E_{dec}. Note that the tiny discrepancy can be seen in this analysis, which seems the M-dependence.

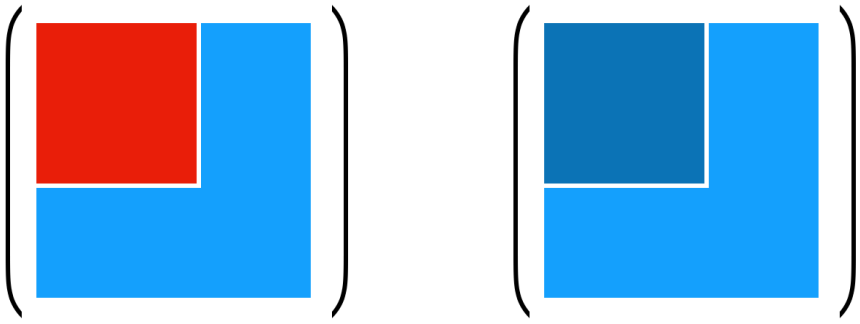

Figure 25: Schematic pictures for two different kinds of constrained simulations. [Left] Field configuration of partially-deconfined phase with the source term equation (6.3). [Right] Field configuration of completely-confined phase with the constraint term equation (6.40). This picture is taken from reference [17].

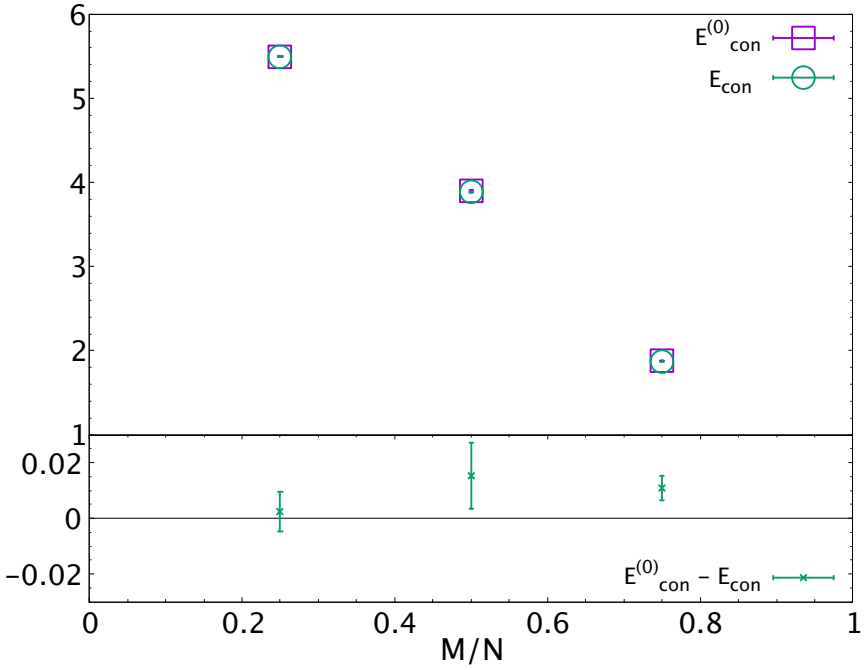

Figure 26: Energy contributions E_{con} and $E^{(0)}_{\mathrm{con}}$ for the constrained simulation of the Yang-Mills matrix model with $N = 64$, $M = 16$, 32, and 48, 24 lattice points. The error bars are estimated by jackknife analysis. This plot is taken from reference [17].

6.6 Summary of the numerical results

In this section, we present the summary of the simulation results and look back the connection to partial deconfinement.

We performed the lattice Monte Carlo simulations for the Gaussian matrix model in section 6.3 and the Yang-Mills matrix model in section 6.4 and section 6.5. As explained in section 6.1, the bosonic matrix field configurations are generated by the naive simulation in the Gaussian matrix model, and by the "efficient" or constrained simulation in the Yang-Mills matrix model.

In order to investigate the configurations as the aspect of master field, we mainly analyzed them in two approaches; focusing on the distribution of the independent scalar degrees of freedom $x \in \{X_{I,ij}\}$, $\rho^{(\mathrm{X})}(x)$, and the correlation between the scalar and gauge degrees of freedom. In the estimate of $\rho^{(\mathrm{X})}(x)$, we confirmed that the split of the distribution into two distinct functions $\rho^{(\mathrm{X})}_{\mathrm{con}}(x)$ and $\rho^{(\mathrm{X})}_{\mathrm{dec}}(x)$ can be done with an appropriate ratio of mixture determined by M in both bosonic matrix models. The separability gives an evidence of the two-phase coexistence in terms of the scalar field configuration, which can happen even beyond weak coupling. In the analysis of θ_j and K_j, we saw that the correlation between them which can be identified with the two-phase separation occurs consistently in the both sectors of fields. The identification can be derived analytically in the Gaussian matrix model. We observed the analogous correlation numerically in the Yang-Mills matrix model, and hence, the model at strong coupling is also following the partial deconfinement scenario. Moreover, the results show that the way of separation is not uniquely determined due to the residual permutation symmetry with respect to the Polyakov line phases θ_j.

In the Yang-Mills matrix model, we additionally performed the constrained simulation to find out the separation into the $\mathrm{SU}(M)$- and $\mathrm{SU}(N-M)$-sectors. Practically, we generated the configurations the upper-left $M \times M$ block that behaves in the Gross-Witten-Wadia point of the $\mathrm{SU}(M)$ theory (like figure 1) is manifest. In other words, we performed the simulation with a specific 'gauge-fixing' by introducing the source term ΔS. The reason to do so is to demonstrate the explicit separation associated with the phenomenon consistent with gauge symmetry breaking, not just the division of M^2 and $N^2 - M^2$ degrees of freedom. In addition, this procedure has an advantage that we can examine the feature of the confined and deconfined sectors individually and directly. The safety of the constrained simulation is confirmed by the several check, the matching of observables such as the distribution of the Polyakov line phase or the variances of scalars with the one of unconstrained simulations. Furthermore, we confirmed the energy contribution from the deconfined block dominates in the constrained simulation, which agrees with the nature of the deconfinement and the two-phase coexistence.

In the results of the Yang-Mills matrix models which is the interacting model, we observed the small discrepancies which may be understood as the nontrivial M-dependence. As mentioned in the main text before, there is no obvious theoretical reason that the distributions $\rho^{(\mathrm{X})}_{\mathrm{con}}(x)$ and $\rho^{(\mathrm{X})}_{\mathrm{dec}}(x)$ are completely independent of M, although we assumed that. Rather, it is natural that the interaction between the confined and deconfined sectors

affects the manner of separation depending on M.

The M-dependence must be more noticeable in the simulations with the constraint, if it appears, and actually, we can see the discrepancies depending on M in the several plots for both analysis. In table 3 placed in appendix D, almost the same dependence on $\frac{M}{N}$ is shown for the results of $N = 48$, 64, and 128, which implies this M-dependence is unlikely to be a finite-N artifact. It is possible that such an intricate M-dependence can be determined as a finite-lattice-size artifact or an effect coming from the smallness of M itself.

In the analysis established for the Gaussian matrix model, we have assumed that the distributions $\rho^{(\mathrm{X})}_{\mathrm{con}}(x)$ and $\rho^{(\mathrm{X})}_{\mathrm{dec}}(x)$ are independent of M. In constrained simulations, we confirmed the separation between two sectors even if taking into account a possible M-dependence. There, the difference between the confined and deconfined sectors turned out to be much larger than a possible M-dependence. Therefore, it does not contradict our conclusions, the occurrence of two-phase coexistence in the space of color degrees of freedom, even if the M-dependence we observed survives in the ideal setting.

7 Conclusion and outlook

In this thesis, we have presented the evidences of the two-phase coexisting phenomena in the space of the color degrees of freedom called *partial deconfinement* in the context of the deconfinement for the theory at finite temperature. It states that the partially-deconfined phase appears in the phase structure of the gauge theory as a thermal phase separated by the Hagedorn and Gross-Witten-Wadia transitions. Partial deconfinement has been originally conjectured to be the gauge theory counterpart of the black hole phase in dual gravity via the gauge/gravity duality. In the AdS/CFT correspondence of the four-dimensional $\mathcal{N} = 4$ super Yang-Mills theory, the small black hole phase with negative specific heat appears in the intermediate energy region in the dual type IIB supergravity in $\mathrm{AdS}_5 \times \mathrm{S}^5$, which is proposed to be the dual of the partially-deconfined phase. For several weakly-coupled large N gauge theories, the intermediate phase is tractable in an analytical manner using the Polyakov loops, and characterized by the number of gauge field degrees of freedom in the deconfined sector M, closely related to the rank of gauge group. For the $\mathrm{U}(N)$ or $\mathrm{SU}(N)$ gauge theory at large N, the coexisting can be interpreted as the spontaneous breaking of gauge symmetry to $\mathrm{SU}(M) \times \mathrm{SU}(N-M)$ and the Polyakov loops and the Polyakov line phases work as the order parameter of this symmetry breaking. Since it has been known that the deconfinement can exhibit even in the large N theory at zero coupling, and/or finite spatial volume (or without spatial directions!), the partial deconfinement scenario provides further understanding of their thermodynamics. We confirmed, by performing the lattice Monte Carlo simulations of the bosonic matrix models, that partial deconfinement can take place even beyond the weak coupling regime, as the coexistence of the confined and deconfined sectors.

One demanding future direction is the connection to the actual deconfinement transition in four-dimensional QCD with fundamental quarks at finite temperature and density with $N = 3$. The partially-deconfined phase exists in the large-N QCD, and its phase structure is quite similar to the one of real QCD, in which the deconfinement transition is thought to be rather the cross-over [104]. The Gross-Witten-Wadia transition between the partially- and completely-deconfined phase is characterized by the gap formation for the distribution function of the Polyakov line phases around $\theta = \pm\pi$ which becomes somehow singular at large N. The analogous 'transition' has to exist in more broad class of gauge theory, and real QCD is likely to this class. That $N = 3$ is considered to be large in an analytical [105] and numerical [106] senses, and the numerical simulations for the $\mathrm{SU}(N)$ pure Yang-Mills theory on lattice [107, 108], for the $(2+1)$-flavor QCD [109], and the theoretical observations regarding the Gross-Witten-Wadia transition [110, 111] provides the consistent results and discussions with the above transition ansatz. Interestingly, the analogous phenomenon to partial deconfinement has been argued in the context of the chiral symmetry breaking of QCD [112–117], and it is interesting to find out the relationship to partial deconfinement. Recently, a possibility not to refer to the large N limit in order to the split the partially-deconfined phase from the completely-confined and deconfined phases is pointed out [58]; the spontaneous breaking of global symmetry may be able to define the partially-deconfined phase in a consistent

manner with the original definition referring to the Gross-Witten-Wadia transition. Associated with the Elitzur's theorem [61], the well-known no-go theorem of gauge symmetry breaking, the spontaneous breaking of gauge symmetry accompanied with the breaking of global symmetry enables us easy to understand the concept of partial deconfinement. Of course, sticking on the large N theories and searching the application of the concept of two-phase separation is also meaningful approach. We have considered the thermal phase transition so far, and it is also possible to consider the setup with different boundary conditions like the periodic one. The studies focusing on the index which can be defined in $\mathcal{N} = 4$ super Yang-Mills theory on $\mathrm{S}^1 \times \mathrm{S}^3$ under that setup found the analogous phenomenon to the partially-deconfined phase [118–121]. The index is beneficial to investigate the gauge/gravity duality since it can be computed analytically even at strong coupling and agrees with the quantity observed in dual gravity [122]. Moreover, in the studies [123, 124], the first-order transitions in holography exhibit similar properties to partial deconfinement. In addition, the large-N models resembling the setting of QCD deserve to be examined analytically and numerically. Regarding that kind of model, any analogous study to the investigation of the bosonic matrix models in reference [17] is not employed yet. Further numerical analyses of the Gaussian matrix model with N_{f}-fundamental scalar fields would serve that purpose. We intend to perform that as a next step, including the improvement of the preliminary results for free sector [71].

To reveal partial deconfinement within the framework of the gauge/gravity duality is also a promising direction. Since it is an ongoing research and the full story is not yet clarified at the moment, we will mention in this outlook the possible scenarios including speculations. See the latest attempt to this topic [57], which finds a signal of the confined phase that may give a description of the M-theory. See also references [125–130, 96, 131] for the study of the deconfined phase done by several collaborations. As claimed in the proposal [33], block-diagonal configurations in the BFSS matrix model, which express the partially Higgsed situation, describe the multi-body state of D0-branes and strings in between. This interpretation leads to the multiple partially-deconfined sectors represented by multiple block configuration and the geometric picture of the partially-deconfined phase, which would give a natural expansion of the philosophy of BFSS, namely the emergent geometry from matrices, to the gauge/gravity duality. Note that the geometric picture of the matrix entries has had a puzzle [132] that seems not to be applicable in the gauge/gravity duality, and lately, an resolution was proposed [133] using notion of the wave packet in 'color space.' Note also that the scenario that the emergence of the bulk geometry is caused by the entanglement in holography [134, 135] would match the viewpoint [13, 136] since the color degrees of freedom in the confined sector can be entangled. This speculation may be related to the trendy topics regarding the holographic entanglement entropy [137–141] and the ideas proposed recently in references [142–145] proposing the bulk entanglement. Besides, it may connect to the tensor network representation of the bulk geometry [146] and the space of colors. In addition to above, it is intriguing to seek the relationship of partial deconfinement to other mechanisms of emergent geometry such as the ones in the Eguchi-Kawai model [147, 148] or the Ishibashi-Kawai-Kitazawa-Tsuchiya (IKKT) matrix model [149–152] since the eigenvalue distribution plays prominent roles there as well.

Regarding the lattice Monte Carlo simulation to examine the above speculations, it is numerically more stable in the BMN model [38] that is a mass deformed model of the BFSS matrix model with the parameter μ, due to the presence of the fuzzy-sphere vacua [153–155]. in that model with finite μ, a first-order transition at $T \sim \mu$ is expected [156]. At larger μ, since the transition temperature becomes higher and the lattice size needed for study of the transition becomes smaller, simulations near the transition temperature are less demanding. See the latest study of our collaboration [57], and also references [157–159] for previous attempts of the BMN matrix model. Not only the Monte Carlo simulation, it is also practically useful to employ the machine learning or quantum computations techniques towards the matrix model. There are various experimental studies utilizing machine learning [160, 161] and quantum computation [162–164] for the investigation of matrix models.

Acknowledgements

The author is supported by the JSPS KAKENHI Grant Number JP 21J13014. The numerical simulations were performed on ATHENE, the HPC cluster of the Regensburg University Compute Centre; the HPC cluster ARA of the University of Jena; the cluster machine named *Pochi* at the University of Tsukuba. Computing support for the works came also from the Lawrence Livermore National Laboratory (LLNL) Institutional Computing Grand Challenge program.

I am grateful to Prof. Goro Ishiki for generous and effortful supervision. I am also grateful to Dr. Masanori Hanada for extensive supports as a collaborator of numerous researches and an another supervisor. I appreciate the members of the Monte Carlo String/M-theory Collaboration (MCSMC), Jordan Cotler, Shinji Ejiri, Hidenori Fukaya, Masakiyo Kitazawa, Takeshi Morita, Shin Nakamura, Hidehiko Shimada, Shingo Takeuchi, and someone who refereed the paper [71] for helpful discussions, comments, and collaborations. I am thankful to all the members of the HET group at the University of Tsukuba, particularly Nobuyuki Ishibashi, Takeshi Yamazaki, Yuhma Asano, and Hiroshi Ohno for helpful discussions, comments, and exercises. I thank the football team, *FC Riron*, and its members for giving me a lot of opportunity of my fun and health recovery. I also thank Shinichiro Akiyama and Hiroshi Takeda for studying and working together from my early days in HET group at the university. I thank the members of the community belonging the HET students in the same year, *Abenomics*, particularly Yoshihiko Abe, Motoko Fujiwara, and Keigo Shimada. I am thankful to Yuji Higuchi, Akihiro Nagata, and Atsushi Yasuda for spending the wonderful and priceless days with me in the nanosatellite developing project at the university, *YUI project*, which lays the foundation of my carrier as a researcher. Finally, I could not have finished my graduate student without the financial and emotional supports from my family. I represent my greatest appreciation to my parents, Hisao and Mutsumi Watanabe, and my younger brothers, Michinari and Yoshitaka Watanabe.

Appendices

A Canonical ensemble vs microcanonical ensemble

In the microcanonical ensemble, thermodynamic states which maximaize the entropy $S(E)$ realize when some specific energy E restricted to a small range $[E, E+dE]$ is given. The entropy $S(E)$ relates to the density of states $\Omega(E)$ as $S(E) = \ln \Omega(E)$. The microcanonical temperature $T_{\rm MC}$ is obtained from the first law of thermodynamics as

$$\frac{1}{T_{\rm MC}} = \frac{{\rm d}S}{{\rm d}E} \,. \tag{A.1}$$

By using this relation, the specific heat is

$$\frac{{\rm d}E}{{\rm d}T_{\rm MC}} = -\frac{1}{T_{\rm MC}^2}\left(\frac{{\rm d}^2 S}{{\rm d}E^2}\right)^{-1}. \tag{A.2}$$

In the canonical ensemble, temperature $T = \frac{1}{\beta}$ is a controllable parameter. The Euclidean path integral governs the behaviors of thermodynamics in the canonical ensemble, and the partition function is given by

$$Z(T) = \int {\rm d}E\, \Omega(E) {\rm e}^{-\beta E} = \int {\rm d}E\, {\rm e}^{-F(E,T)/T} \,, \tag{A.3}$$

and the free energy F is defined by

$$F(E,T) = E - TS(E) \,. \tag{A.4}$$

Here, we assume for simplicity that the maximum of entropy is unique at each energy E. By taking the derivative of the free energy with the energy,

$$\frac{\partial F(E,T)}{\partial E} = 1 - T\frac{{\rm d}S(E)}{{\rm d}E} = 1 - \frac{T}{T_{\rm MC}(E)} \,. \tag{A.5}$$

Therefore, at the stationary point of the free energy, $T_{\rm MC}(E) = T$. Furthermore, the second derivative is

$$\frac{\partial^2 F(E,T)}{\partial E^2} = +\frac{T}{T_{\rm MC}^2}\left(\frac{{\rm d}E}{{\rm d}T_{\rm MC}}\right)^{-1}. \tag{A.6}$$

The result implies that positive (negative) specific heat in the microcanonical ensemble (A.2) corresponds to the minimized (maximized) free energy in the canonical ensemble.

A.1 The multiple maxima in the microcanonical ensemble

Let us further consider there are two local maxima of the entropy $S_1(E)$ and $S_2(E)$ associated with phase-1 and phase-2, as shown in the top row of figure 27. Suppose that $S_1(E) > S_2(E)$ at $E > E_{\rm c}$ and $S_1(E) < S_2(E)$

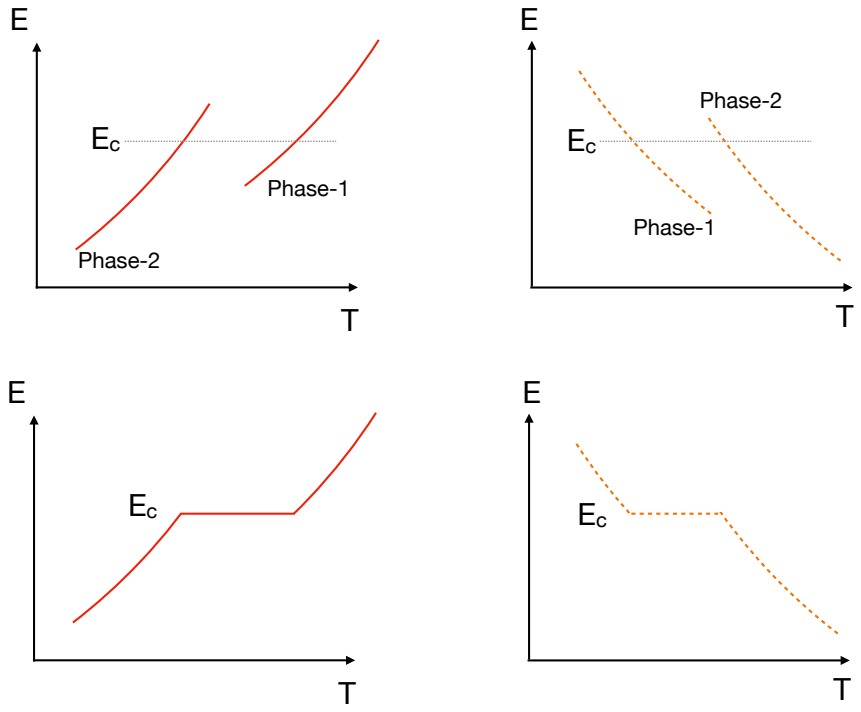

Figure 27: [Top] Coexistence of two local maxima of entropy $S_1(E)$ and $S_2(E)$ corresponding to phase-1 and phase-2 in the microcanonical ensemble. [Bottom] Free energy minimum and maximum are shown in the left and right panels, respectively. This picture is taken from reference [57].

at $E < E_c$, and hence, a first-order transition occurs at $E = E_c$. The entropy $S(E)$ in (A.3) becomes $S = \ln\left(e^{S_1} + e^{S_2}\right)$, which is well-approximated solely by S_1 and S_2 at $E > E_c$ and $E < E_c$, respectively. However, we have to take into account both phases when the energy E approaches sufficiently close to E_c,.

We have

$$\frac{\mathrm{d}S(E)}{\mathrm{d}E} = \frac{1}{\mathrm{e}^{S_1} + \mathrm{e}^{S_2}} \times \left(\frac{\mathrm{e}^{S_1}}{T_{\mathrm{MC},1}} + \frac{\mathrm{e}^{S_2}}{T_{\mathrm{MC},2}} \right) , \tag{A.7}$$

where $\frac{1}{T_{\mathrm{MC},i}} = \frac{\mathrm{d}S_i}{\mathrm{d}E}$ is the microcanonical temperature of phase-i ($i = 1, 2$). When E varies slightly from below E_c to above E_c, temperature moves from $T_{\mathrm{MC},2}$ to $T_{\mathrm{MC},1}$. Therefore, the phase diagram in the canonical ensemble becomes the bottom row of figure 27.

Suppose another maximum of the entropy $S_3(E)$ corresponding to phase-3 appears as shown in figure 28, and $S_3(E)$ is always smaller than at least $S_1(E)$ or $S_2(E)$. Even though, phase-3 does not affect the canonical phase diagram at all; see the bottom row of figure 28. Still, it is possible that phase-3 may be visible in the canonical simulation if other parameters than energy exist fortunately.

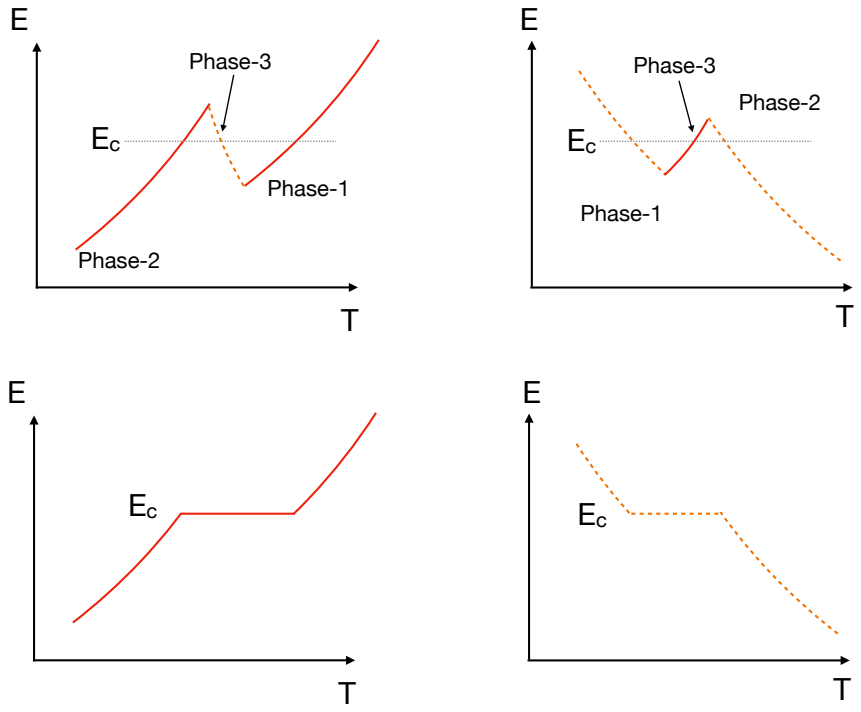

Figure 28: [Top] Coexistence of three local maxima of entropy $S_1(E), S_2(E)$, and $S_3(E)$ in the microcanonical ensemble. [Bottom] Corresponding phase diagram in the canonical ensemble. Free energy minimum and maximum are shown in the left and right panels, respectively. This picture is taken from reference [57].

B Ant trail and D-branes

A phenomenological model of the formation of an ant trail [165] has similar behaviors to the D-branes in string theory. This relative simple model gave us some lessons for the understanding of the D-branes forming the black hole and the concept of the partial deconfinement. Here we briefly review this model and its correspondence to the physics of D-branes and open strings in between [10, 14].

Consider a system with a colony of N ants and one source of food at somewhere. For later comparison with the large-N gauge theories, let N be a huge number. When some ants fortunately find the food source and bring them back to their nest, they leave a pheromone trail along the way between the food source and the nest. Then many ants begin to be attracted by the pheromone and join the trail to the food source and secrete the pheromone. The strength of the attraction relates to the total mount of secreted pheromones pN_{trail}, where N_{trail} is the number of the ants forming the ant-trail and p is the pheromone contribution from each ant. Therefore, more ants join the trail, and more pheromones are released, which in turn leads more and more ants joining it.

The situation of this mathematical model of the collective animal behavior is similar to the one of the system with many-body D-branes. Let M D-branes form a bound state, and one of the remaining M D-branes be close by. There are also open strings that can attach among the M different D-branes. At sufficiently high-temperature region, each open string mode are highly excited and can contribute more to the dynamics, which can capture the D-brane outside of the bound state. This implies that the system at a high temperature corresponds to the one with a large value of the pheromone parameter, and hence,

$$\begin{aligned} N_{\text{trail}} &\longleftrightarrow M, \\ p &\longleftrightarrow T. \end{aligned} \tag{B.1}$$

In reference [165], an "equation of states,"

$$\frac{\mathrm{d}N_{\text{trail}}}{\mathrm{d}t} = (\alpha + pN_{\text{trail}})(N - N_{\text{trail}}) - \frac{sN_{\text{trail}}}{s + N_{\text{trail}}}, \tag{B.2}$$

is introduced in order to describe the behavior of the ants. The parameter α is the probability that each ant find the food source eventually, and s controls the rate that ants leave the trail. By solving the equilibrium condition $\frac{\mathrm{d}N_{\text{trail}}}{\mathrm{d}t} = 0$, we can estimate the size of the stationary ant-trail. The parameters p, α, s that depend on the several internal and external factors of the biological system are fixed and N_{trail} has been calculated as the function of N in the original context. Here, we fix α, s, and N, and calculate N_{trail} as the function of p in order to compare with the physics of the black holes and its gauge theory counterpart. For this reason, an interesting 'large-N' limit is where $\alpha \sim N^{-1}, p \sim N^{-1}$, and $s \sim N^1$ [10, 14]. The solution of $\frac{\mathrm{d}N_{\text{trail}}}{\mathrm{d}t} = 0$, or namely the saddles are shown in figure 29, where $x \equiv \frac{N_{\text{trail}}}{N}$ and $\tilde{p} \equiv Np$, by varying $\tilde{s}$. We also fix $\alpha = \frac{1}{N}, \tilde{s} \equiv \frac{s}{N} = 0.1, 1.0, 5.0$, and $N = 10^5$ in the plot. The saddles appear where the inflow/outflow of the ants in the trail is balancing. Since we vary $\tilde{s}$ and see the response of N_{trail}, the treatment resembles to being in the canonical ensemble. Three pictures

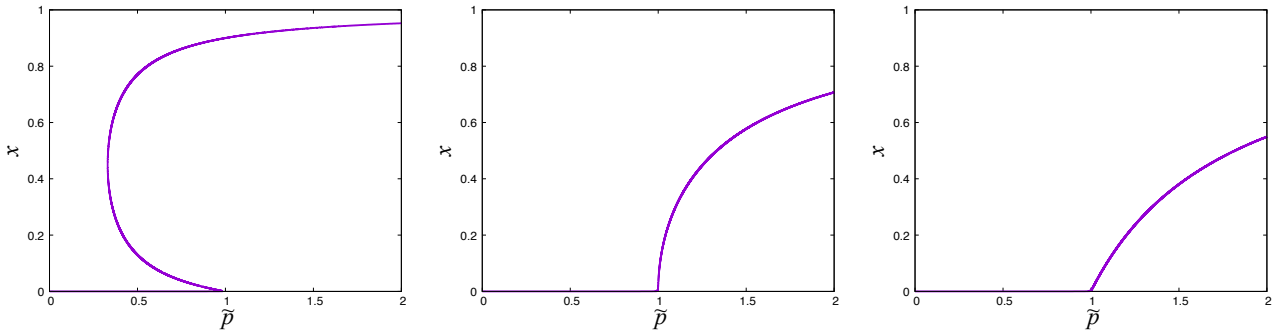

(a) $\tilde{s} = 0.1$ (b) $\tilde{s} = 1.0$ (c) $\tilde{s} = 5.0$

Figure 29: Plot x versus $\tilde{p}$ in the ant trail model (B.2).

in figure 29 resembles ones in figure 4, which brings the insight with respect to the phase structure of the large-N gauge theories at finite temperature.

C Functional determinants in matrix models

In this appendix, we overview how to perform the functional integral and obtain the effective potential in terms of the Polyakov loops u_n. It aims for the $(0+1)$-dimensional matrix models, but it can be generalized to the theory in higher dimensional spacetime. See references [9, 166] for more detail.

Let us consider the $\mathrm{U}(N)$ gauged bosonic matrix model (Gaussian matrix models with or without N_{f} fundamental scalar fields) in which the temporal direction is compactified to S^1. The circumference of it may be interpreted as the inverse temperature β. We take the static diagonal gauge $\partial_t A_t = 0$, or equivalently,

$$A_t = \frac{1}{\beta}\,\mathrm{diag}\,(\alpha_1, \cdots, \alpha_N), \tag{C.1}$$

where the α_j are the Polyakov line phases, independent on the time. Substituting the form of the gauge fixing into the covariant derivatives of the adjoint and fundamental scalar fields $D_t X = \partial_t X - \mathrm{i}[A_t, X]$, and $\tilde{D}_t\phi = \partial_t\phi - \mathrm{i}A_t\phi$, we can compute that

$$\frac{1}{2}\int \mathrm{d}t\ \mathrm{Tr}\left[X_I\left(-D_t^2 + \Delta^2\right)X_I\right] = \frac{\beta}{2}\sum_{n,i,j} X_{I,ij}^{(n)}\left(\frac{4\pi^2 n^2}{\beta^2} + \frac{4\pi n}{\beta}(\alpha_i - \alpha_j) + (\alpha_i - \alpha_j)^2 + \Delta^2\right)X_{I,ji}^{(-n)} \tag{C.2}$$

$$\frac{1}{2}\int \mathrm{d}t\ \phi_A\left(-\tilde{D}_t^2 + \Delta^2\right)\phi_A = \frac{\beta}{2}\sum_{n,i} \phi_{a,i}^{(n)}\left(\frac{4\pi^2 n^2}{\beta^2} + \frac{4\pi n}{\beta}\alpha_i + (\alpha_i)^2 + \Delta^2\right)\phi_{a,i}^{(-n)}, \tag{C.3}$$

where Δ is some parameter such as the thermal mass, and we use the Fourier modes

$$X_I(t) = \sum_{n=-\infty}^{\infty} X_I^{(n)} \mathrm{e}^{\frac{2\pi\mathrm{i}nt}{\beta}}, \tag{C.4a}$$

$$\phi_A(t) = \sum_{n=-\infty}^{\infty} \phi_A^{(n)} \mathrm{e}^{\frac{2\pi\mathrm{i}nt}{\beta}}. \tag{C.4b}$$

Here, the correspondence with respect to the Fourier modes

$$\partial_t \Leftrightarrow \frac{2\pi\mathrm{i}n}{\beta}, \tag{C.5}$$

may be useful. They actually bring the functional determinants for the adjoint and fundamental scalar fields when performing the path integral.

Using the formula

$$\sin(\pi z) = \pi z \prod_{n=1}^{\infty}\left(1 - \frac{z^2}{n^2}\right), \tag{C.6}$$

and we can rewrite (denoting the part depending on the Polyakov line phases as just α),

$$\prod_{n=-\infty}^{\infty}\left(\frac{4\pi^2 n^2}{\beta^2} + \frac{4\pi n}{\beta}\alpha + \alpha^2 + \Delta^2\right)$$

$$
\begin{aligned}
&= (\alpha^2+\Delta^2)\left[\prod_{m\neq 0}\frac{\beta}{2\pi m}\right]^{-2}\left[\prod_{n=1}^{\infty}\left(1-\frac{\beta^2(\alpha^2-\Delta^2)}{2\pi^2n^2}+\left(\frac{\beta^2}{4\pi^2n^2}\right)^2(\alpha^2+\Delta^2)^2\right)\right]\\
&= (\alpha^2+\Delta^2)\left[\prod_{m\neq 0}\frac{\beta}{2\pi m}\right]^{-2}\left[\prod_{n=1}^{\infty}\left(1-\frac{\beta^2(\alpha+\mathrm{i}\Delta)^2}{4\pi^2n^2}\right)\left(1-\frac{\beta^2(\alpha-\mathrm{i}\Delta)^2}{4\pi^2n^2}\right)\right]\\
&= \left[\prod_{m\neq 0}\frac{\beta}{2\pi m}\right]^{-2}\left(\frac{4}{\beta^2}\right)\sin\left[\frac{\beta(\alpha+\mathrm{i}\Delta)}{2}\right]\sin\left[\frac{\beta(\alpha-\mathrm{i}\Delta)}{2}\right]\\
&= \mathcal{N}\mathrm{e}^{\beta\Delta}\Big(1-\mathrm{e}^{-\beta\Delta+\mathrm{i}\beta\alpha}\Big)\Big(1-\mathrm{e}^{-\beta\Delta-\mathrm{i}\beta\alpha}\Big),
\end{aligned}
\tag{C.7}
$$

where

$$
\mathcal{N} = \frac{1}{\beta^2}\left[\prod_{m\neq 0}\frac{\beta}{2\pi m}\right]^{-2}, \tag{C.8}
$$

is the overall infinite constant. One can neglect it since it is independent of Δ and α and does not affect to physic, especially for the effective potential we want. Remember that the equivalence of $\ln\det(\cdot)$ and $\mathrm{Tr}\ln(\cdot)$ and the Taylor expansion of the logarithmic function

$$
\ln(1-x) = -\sum_{n=1}^{\infty}\frac{x^n}{n}, \tag{C.9}
$$

and then, the functional determinant in each field becomes

$$
\begin{aligned}
\frac{1}{2}\ln\det\big(-D_t^2+\Delta^2\big) &= \frac{1}{2}\ln\mathrm{e}^{\beta\Delta}+\frac{1}{2}\,\mathrm{Tr}\left\{\ln\Big(1-\mathrm{e}^{-\beta\Delta+\mathrm{i}\beta\alpha}\Big)+\ln\Big(1-\mathrm{e}^{-\beta\Delta-\mathrm{i}\beta\alpha}\Big)\right\}\\
&= \frac{\beta\Delta}{2}-\frac{1}{2N^2}\sum_{i,j}^{N}\sum_{n=1}^{\infty}\frac{1}{n}\Big\{\Big(\mathrm{e}^{-\beta\Delta}\ \mathrm{e}^{\mathrm{i}\beta\alpha_i}\ \mathrm{e}^{-\mathrm{i}\beta\alpha_j}\Big)^n+\Big(\mathrm{e}^{-\beta\Delta}\ \mathrm{e}^{-\mathrm{i}\beta\alpha_i}\ \mathrm{e}^{\mathrm{i}\beta\alpha_j}\Big)^n\Big\}\\
&= \frac{\beta\Delta}{2}-\sum_{n=1}^{\infty}\frac{x^{n\Delta}}{n}|u_n|^2,
\end{aligned}
\tag{C.10}
$$

and

$$
\begin{aligned}
\frac{1}{2}\ln\det\Big(-\tilde{D}_t^2+\Delta^2\Big) &= \frac{1}{2}\ln\mathrm{e}^{\beta\Delta}+\frac{1}{2}\,\mathrm{Tr}\left\{\ln\Big(1-\mathrm{e}^{-\beta\Delta+\mathrm{i}\beta\alpha}\Big)+\ln\Big(1-\mathrm{e}^{-\beta\Delta-\mathrm{i}\beta\alpha}\Big)\right\}\\
&= \frac{\beta\Delta}{2}-\frac{1}{N}\sum_{i,j}^{N}\sum_{n=1}^{\infty}\frac{1}{n}\Big\{\Big(\mathrm{e}^{-\beta\Delta}\ \mathrm{e}^{\mathrm{i}\beta\alpha_i}\Big)^n+\Big(\mathrm{e}^{-\beta\Delta}\ \mathrm{e}^{-\mathrm{i}\beta\alpha_i}\Big)^n\Big\}\\
&= \frac{\beta\Delta}{2}-\sum_{n=1}^{\infty}\frac{x^{n\Delta}}{n}(u_n+u_n^*).
\end{aligned}
\tag{C.11}
$$

Note that we should be careful about the trace $\mathrm{Tr}(\cdot)$ represents whether for the adjoint or fundamental representation.

The final form of the effective potential of the theory with both types of scalar fields is

$$\begin{aligned} V_{\text{eff}}(\beta) &= -\ln Z \\ &= \frac{dN^2}{2}\ln\det\left(-D_t^2+1\right) - \frac{N^2}{2}\ln\det\left(-D_t^2\right) + \frac{NN_{\text{f}}}{2}\ln\det\left(-\tilde{D}_t^2+1\right) \\ &= \frac{\beta N^2}{2}\left(D+\frac{N_{\text{f}}}{N}\right) + N^2\sum_{n=1}^{\infty}\frac{1}{n}\left\{(1-Dx^n)|u_n|^2 - \frac{N_{\text{f}}}{N}x^n(u_n+u_n^*)\right\}, \end{aligned} \tag{C.12}$$

as desired. As mentioned in the beginning of this appendix, we can refer to the computation of reference [9] for more generic theories.

D Data of simulations

In this appendix, we list several numerical data generated by the lattice Monte Carlo simulations for the matrix models. They are taken from the our research [17] for partial deconfinement beyond the weak coupling regime.

Gaussian matrix model

Table 1: Variances in the Gaussian matrix model. $D = 2, N = 32$ at the critical temperature $T = T_{\mathrm{c}} = \frac{1}{\ln D}$. The number of lattice sites is L. The total number of x is obtained by $\#x = (N^2 = 32^2) \times (D = 2) \times L \times$ (# configurations). These data are taken from reference [17].

L	(M, M')	Confined	Deconfined	# configs. of (M, M')
4	(16, 24)	0.50(3)	0.63(4)	(389, 801)
16	(16, 24)	0.50(4)	0.62(5)	(241, 408)
24	(16, 24)	0.50(3)	0.63(4)	(165, 287)
24	(16, 30)	0.50(2)	0.62(1)	(165, 289)
24	(24, 30)	0.50(4)	0.62(2)	(287, 289)

Yang-Mills matrix model ("efficient")

Table 2: Variances of $\rho_{\mathrm{con}}^{(\mathrm{X})}$ and $\rho_{\mathrm{dec}}^{(\mathrm{X})}$ in the "efficient" simulation of the Yang-Mills matrix model simulation, $N = 64$, $T = 0.885$, with 24 lattice sites. The total number of x is obtained by $\#x = (N^2 = 64^2) \times (D = 9) \times (L = 24) \times$ (# configurations). These data are taken from reference [17].

(M, M')	σ_{con}^2	σ_{dec}^2	# configs. of (M, M')
(16, 32)	0.2447(5)	0.254(3)	(854, 857)
(16, 48)	0.2447(4)	0.254(1)	(854, 814)
(32, 48)	0.2447(8)	0.254(1)	(857, 814)

As explained in section 6.4, if $\rho_{\mathrm{con}}^{(\mathrm{X})}(x)$ and $\rho_{\mathrm{dec}}^{(\mathrm{X})}(x)$ do not depend of the size of the deconfined sector M, the variances must relate to r_0 and r_1 in equations (6.28) and (6.8),

$$\sigma_{\mathrm{con}}^2 \equiv \int \mathrm{d}x\, x^2 \rho_{\mathrm{con}}^{(\mathrm{X})}(x) = \frac{r_0}{d} \simeq \frac{2.20}{9} \simeq 0.244, \tag{D.1a}$$

$$\sigma^2_{\mathrm{dec}} \equiv \int \mathrm{d}x\, x^2 \rho^{(\mathrm{X})}_{\mathrm{dec}}(x) = \frac{r_1}{d} \simeq \frac{2.29}{9} \simeq 0.254. \tag{D.1b}$$

The agreement with the values in table 2 seems reasonable.

Yang-Mills matrix model (constrained)

Table 3: Variances of $\rho^{(\mathrm{X})}_{\mathrm{con}}$ and $\rho^{(\mathrm{X})}_{\mathrm{dec}}$ in the constrained simulation of the Yang-Mills matrix model, $N = 48, 64$ and 128, $T = 0.885$, with 24 lattice sites. The last column is the variance of the distribution of the off-diagonal block of the confined sector. These data are taken from reference [17].

N	M	σ^2_{dec}	σ^2_{con}	$\sigma^2_{\mathrm{con,off\text{-}diag}}$	# configs.
48	12	0.2588(5)	0.2442(2)	0.2438(8)	1500
64	16	0.2581(2)	0.2446(1)	0.2439(3)	1500
128	32	0.2582(2)	0.2445(1)	0.2439(1)	500
48	24	0.2568(1)	0.2439(1)	0.2433(2)	1500
64	32	0.2567(1)	0.2441(1)	0.2434(2)	1500
128	64	0.2566(1)	0.2438(1)	0.2431(1)	500
48	36	0.2557(2)	0.2438(3)	0.2433(5)	1500
64	48	0.2555(1)	0.2434(1)	0.2430(2)	1500
128	96	0.2556(1)	0.2433(1)	0.2428(1)	500

E Details of lattice simulations

E.1 Yang-Mills matrix model

In the numerical analysis [17], we utilize the following lattice action, introduced an one-dimensional lattice with L sites, and the static diagonal gauge is taken;

$$S_{\rm YMMM} = S_{\rm bosonic} + S_{\rm FP}, \tag{E.1}$$

where

$$S_{\rm bosonic} = \frac{N}{2a}\sum_{t=1}^{L}\sum_{I=1}^{9}{\rm Tr}\left(UX_I(t+a)U^\dagger - X_I(t)\right)^2 - \frac{Na}{4}\sum_{t=1}^{L}\sum_{I,J}{\rm Tr}\left[X_I(t), X_J(t)\right]^2, \tag{E.2}$$

and

$$S_{\rm FP} = -\sum_{i<j} 2\ln\left|\sin\left(\frac{\theta_i-\theta_j}{2}\right)\right|. \tag{E.3}$$

There are $D=9$, $N\times N$ hermitian matrices X_I in the adjoint representation of ${\rm U}(N)$ gauge group at each lattice point. The link variable is

$$U = {\rm diag}\left(e^{i\theta_1/L}, \cdots, e^{i\theta_N/L}\right), \tag{E.4}$$

which is independent on time t. The Polyakov line phases θ_j lie on between $\pm\pi$. Note that, depending on the analysis, we added ΔS for the "efficient" and constrained simulations. The above is the lattice action with a naive lattice discretization, and we can also reduce the discretization errors by using the tree-level improved action, which is actually used for the study of the D0-brane matrix model [131, 167, 16]. The lattice simulation with the gauge-fixing is similarly to the study of the D0-brane matrix model in references [168, 125, 129]. For more details about the lattice setup, see section 2. 2 of reference [167] and a useful document [169]. We have used the Hybrid Monte Carlo algorithm [170].

E.2 Gaussian matrix model

With respect to the lattice action of the Gaussian matrix model ($N_{\rm f}=0$), we have just replaced the potential term of the Yang-Mills matrix model with

$$S_{\rm pot} = \frac{aN}{2}\sum_{t=1}^{L}\sum_{I=1}^{D}{\rm Tr}X_I(t)^2, \tag{E.5}$$

where D is set to 2 in our analysis.

For the Gaussian matrix model with $N_{\rm f}$-fundamental scalar fields, we have added the following terms to the original Gaussian matrix model;

$$S_{\rm fund} = N\sum_{t=1}^{L}\sum_{A=1}^{N_{\rm f}}\left[\frac{2}{a}\left\{|\phi_A(t)|^2 - \sum_{i=1}^{N}{\rm Re}\left(\phi_{A,i}(t+a)U_{ii}\phi^*_{A,i}(t)\right)\right\} + a|\phi_A(t)|^2\right]. \tag{E.6}$$

There are $N_{\rm f}$ complex vector fields in the fundamental representation of $\mathrm{U}(N)$ gauge group at each lattice point. When we introduce interactions, we just add the lattice discretized interaction terms in principle.

E.3 Case : Gaussian matrix model with fundamental scalars

As explained in section 4.3.3, introducing the matter fields in the fundamental representation modifies the phase structure of the model drastically. The intermediate phase between the 'Hagedorn' and Gross-Witten-Wadia transitions becomes thermodynamically stable in this case, unlike the original Gaussian matrix model which exhibits the first order phase transition at the critical temperature. Hence, it is more suitable to demonstrate the concept of partial deconfinement and study the features of it. The following analysis and numerical result are based on the study in progress [71].

Our strategy has been to define the distribution function of independent degrees of freedom for the matter fields as well as the gauge field. Here again, following the belief, we study the distribution with respect to the scalars in fundamental representation, $\sqrt{2N}\phi_{A,j}$. We denote them as the variable φ and its distribution as $\rho^{(\phi)}(\varphi)$ analogous to the one for the adjoint field $\rho^{(\mathrm{X})}(x)$. According to the faith of partial deconfinement, we set an ansatz

$$\rho^{(\phi)}(\varphi; M) = \left(1 - \frac{M}{N}\right)\rho^{(\phi)}_{\rm con}(\varphi) + \frac{M}{N}\rho^{(\phi)}_{\rm dec}(\varphi). \tag{E.7}$$

In this case, the size of deconfined sector M is related to the temperature T as we can see in the phase structure 6, which is different from the case without the fundamental scalars.

To introduce the distribution functions in this model, we begin with the action (4.98), which includes the $N_{\rm f}$-fundamental scalar fields ϕ_A. Analogous to the Gaussian matrix model with $N_{\rm f} = 0$, let us estimate the energy contributions from each type of the scalar fields. From the virial theorem, we can obtain

$$E^{(\mathrm{X})} \equiv \frac{N}{\beta}\int \mathrm{d}t \sum_I \mathrm{Tr}\, X_I^2, \qquad E^{(\phi)} \equiv \frac{N}{\beta}\int \mathrm{d}t \sum_A |\phi_A|^2. \tag{E.8}$$

The expectation values of these quantities in the path integral formalism connect to the expectation values obtained by the distribution functions;

$$\left\langle E^{(\mathrm{X})} \right\rangle = DN^2 \left\langle x^2 \right\rangle = D(N^2 - M^2)\left\langle x^2 \right\rangle_{\rm con} + DM^2 \left\langle x^2 \right\rangle_{\rm dec}, \tag{E.9}$$

$$\left\langle E^{(\phi)} \right\rangle = NN_{\rm f} \left\langle \varphi^2 \right\rangle = N_{\rm f}(N - M)\left\langle \varphi^2 \right\rangle_{\rm con} + N_{\rm f}M \left\langle \varphi^2 \right\rangle_{\rm dec}, \tag{E.10}$$

where

$$\left\langle x^2 \right\rangle = \int \mathrm{d}x\ x^2 \rho^{(\mathrm{X})}(x), \qquad \left\langle \varphi^2 \right\rangle = \int \mathrm{d}\varphi\ \varphi^2 \rho^{(\phi)}(\varphi). \tag{E.11}$$

The energy contributions can be computed analytically at each temperature T by equations (4.107) and (4.108), and hence, we can compute the variances of the distribution for the adjoint and fundamental scalars as well. We utilize those values for a consistency check of the analysis.

For the lattice Monte Carlo simulations of this model, we perform the constrained simulation from the beginning. Then, we confirm its consistency with the original thermodynamics of the model which is tractable in an analytic manner. The distributions of the Polyakov line phases in the confined and deconfined sector $\rho^{(\mathrm{P})}_{\mathrm{con}}(\theta)$ and $\rho^{(\mathrm{P})}_{\mathrm{dec}}(\theta)$ are shown in figure 30. We can see the matching of the numerical results with the analytic form of the phase distributions $\rho^{(\mathrm{P})}(\theta)$ and $\rho^{(\mathrm{P})}_{\mathrm{dec}}(\theta; T_{\mathrm{GWW}}(M))$ obtained in equations (4.102) and (4.105), shown in the figure. Although we cannot state quantitatively about the discrepancy due to the absence of the numerical errors at this point, we can expect improvements for the simulation with larger N and more statistics since this constraint is justified in the large N limit, or at least, sufficiently large but finite integer N.

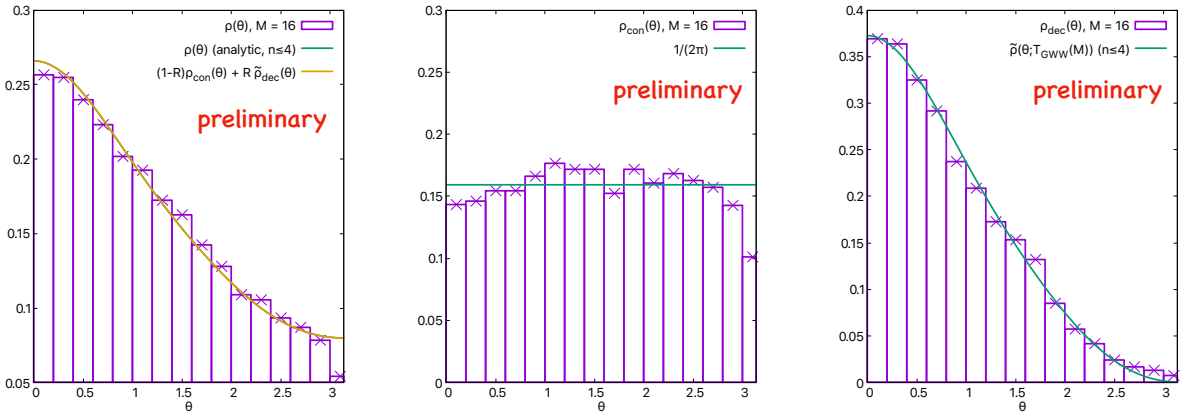

Figure 30: **[Preliminary]** Distribution of the Polyakov line phases $\rho^{(\mathrm{P})}(\theta; T)$, $\rho^{(\mathrm{P})}_{\mathrm{con}}(\theta)$, and $\rho^{(\mathrm{P})}_{\mathrm{dec}}(\theta; T_{\mathrm{GWW}}(M))$ from the constrained simulations of the Gaussian matrix model with N_{f} fundamental scalar fields, $D = 2$, $N = 32$, the number of lattice sites $L = 8$, $M = 16$, $R = \frac{M}{N} = 0.5$. The center symmetry is fixed sample by sample such that $P = |P|$.

The preliminary results of the distribution functions for scalars in the confined and deconfined sectors are shown in figures 31 and 32. They show reasonable agreements with the several M at $N = 32$, and significant difference with the confined and deconfined sectors. We comment that, as a consistency check, we can see the trend of matching for the variances and some thermodynamic quantities with the theoretical prediction. We also notice the discrepancies, especially around $\theta = \pi$ (and also $-\pi$). It is expected to come from the finite-N effect that affects the attractive/repulsive forces among the Polyakov line phases, and therefore, the configurations around there is hardly generated.

In order to confirm above observations more rigidly, more lattice Monte Carlo simulations with larger N is needed. The goal is to determine the phase structure ab initio and demonstrate the two-phase coexistence in the intermediate phase of the interacting model with fundamental scalar fields. Therefore, this analysis has an aspect to establish the methodology for aiming the further simulations of the model with interaction.

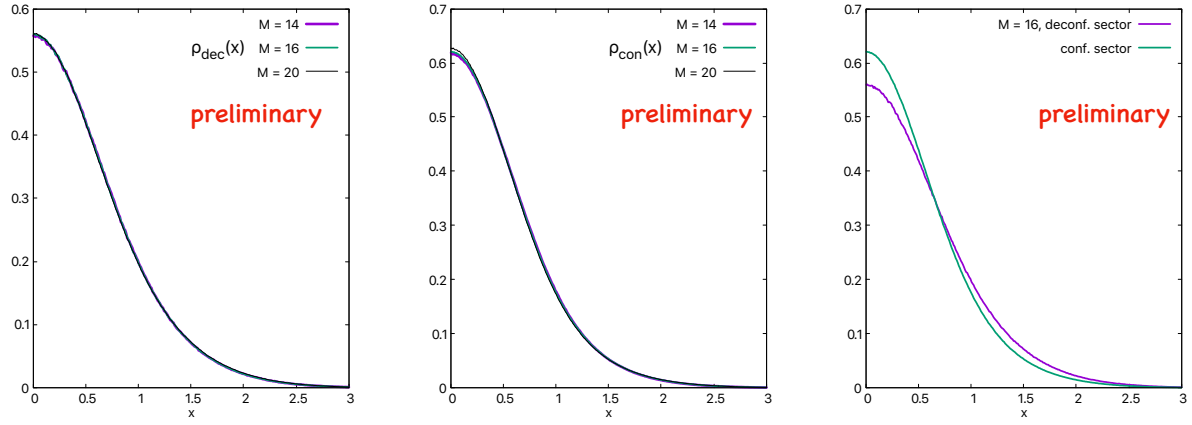

Figure 31: **[Preliminary]** Distributions $\rho^{(\mathrm{X})}_{\mathrm{dec}}(x)$ and $\rho^{(\mathrm{X})}_{\mathrm{con}}(x)$ from the constrained simulation of the Gaussian Matrix model with N_{f} fundamental scalar fields, $D = 2$, $N = 32$, $N_{\mathrm{f}} = 8$, the number of lattice sites $L = 8$, for several M which is equivalently temperatures. We use the symmetry that the phase distribution is even function due to the fixing of the center symmetry ambiguity.

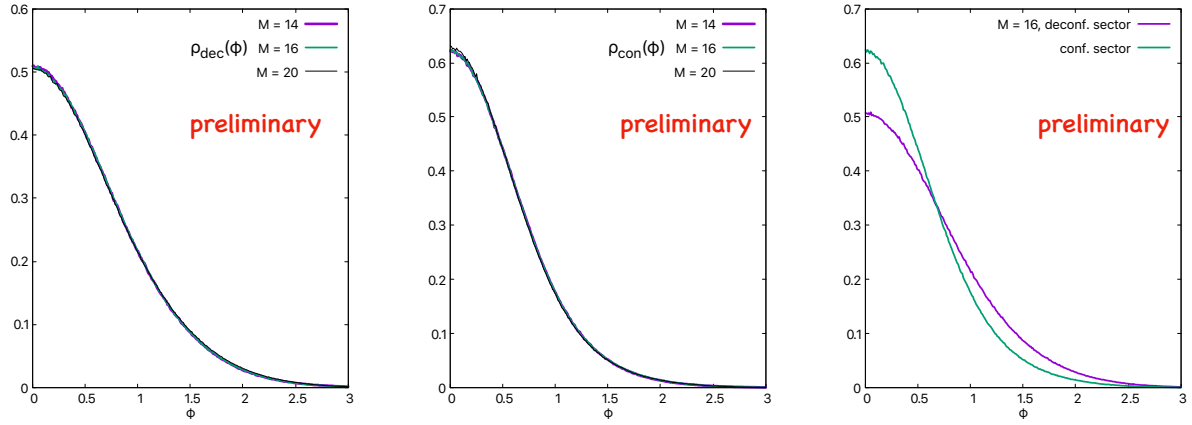

Figure 32: **[Preliminary]** Distributions $\rho^{(\phi)}_{\mathrm{dec}}(\varphi)$ and $\rho^{(\phi)}_{\mathrm{con}}(\varphi)$ from the constrained simulations of the Gaussian Matrix model with N_{f} fundamental scalar fields, $D = 2$, $N = 32$, $N_{\mathrm{f}} = 8$, the number of lattice sites $L = 8$, for several M which is equivalently temperatures. We use the symmetry that the phase distribution is even function due to the fixing of the center symmetry ambiguity.

E.3.1 A technical remark for constrained simulations

If the adjacent Polyakov line phases θ_p, θ_q become closer or coincide at somewhere, the Faddeev-Popov term associated with the gauge fixing $S_{\rm FP}$ (E.3) becomes extremely large. That gives an infinitely strong repulsive force, which leaves the ordering of θ unchanged in the Monte Carlo simulation. Although, due to the S_N permutation symmetry, it is not the problem in the original model, without the source term ΔS, it actually is if ΔS is introduced to the action. We can understand it from that the configurations for θ may freeze at the initial condition; if we impose the initial condition $\theta_1 < \theta_2 < \cdots < \theta_N$, for example, the distribution we desire — $\frac{1+\cos\theta}{2\pi}$ for $\theta_1, \cdots, \theta_M$ and $\frac{1}{2\pi}$ for $\theta_{M+1}, \cdots, \theta_N$ — cannot be realized by the constrained simulation.

To avoid this problem, we carried out the following method; at each step of the Monte Carlo simulation, the random permutations for p-th and q-th row/column of the field configuration ($1 \leq p \leq M$ and $M+1 \leq q \leq N$) were performed. After each the permutation, we test it by the Metropolis test not to violate any condition in the Markov Chain Monte Carlo. The fact that this procedure works well indicates the non-uniqueness of the separation into two distinct sectors, which appears in the Gaussian matrix model as the residual symmetry. Since we assign a very huge coefficient of the source term γ, the permutation is accepted only when $\theta_p \simeq \theta_q$, which corresponds to the residual permutation symmetry.

F More on $\rho^{(\mathrm{X})}$ in Yang-Mills matrix model

In this appendix, we mention the observations to the distribution $\rho^{(\mathrm{X})}(x)$ in the Yang-Mills matrix model for future reference.

We compare the distributions $\rho^{(\mathrm{X})}_{\mathrm{con}}(x)$ and $\rho^{(\mathrm{X})}_{\mathrm{dec}}(x)$ with the Gaussian distributions with the variances in equations (6.29) and (6.30). Figure 33 shows the results, which displays that $\rho^{(\mathrm{X})}_{\mathrm{con}}(x)$ and $\rho^{(\mathrm{X})}_{\mathrm{dec}}(x)$ are close but not matching to the Gaussian distributions. The discrepancy may come from a finite-N or finite-lattice-spacing effect. We also compare the distribution $\rho^{(\mathrm{X})}_{\mathrm{con}}$ in the transition region with $\rho^{(\mathrm{X})}(x)$ at a low temperature, that is, in the completely-confined phase. The left panel of figure 34 shows the results of the comparison, which displays the small temperature dependence.

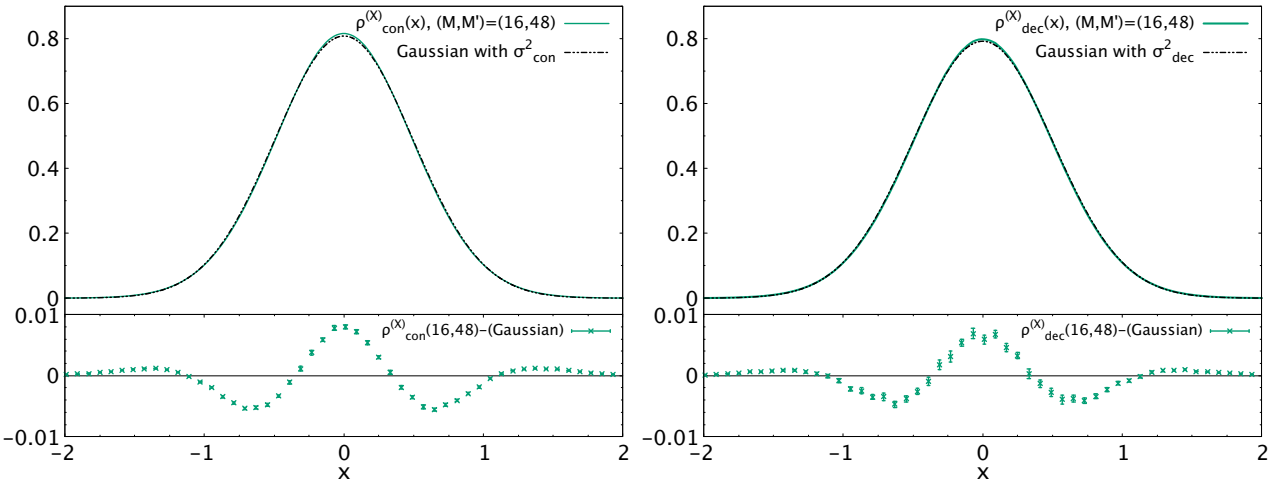

(a) $\rho^{(\mathrm{X})}_{\mathrm{con}}(x)$ (b) $\rho^{(\mathrm{X})}_{\mathrm{dec}}(x)$

Figure 33: Comparison between $\rho^{(\mathrm{X})}_{\mathrm{con}}(x)$ and $\rho^{(\mathrm{X})}_{\mathrm{dec}}(x)$ of the Yang-Mills matrix model and the Gaussian distributions. The histograms of $\rho^{(\mathrm{X})}_{\mathrm{con}}(x)$ and $\rho^{(\mathrm{X})}_{\mathrm{dec}}(x)$ are same as ones in figure 15. The variances of the Gaussian distributions are $\sigma^2_{\mathrm{con}} = 0.244$ and $\sigma^2_{\mathrm{dec}} = 0.254$. The error bars are estimated by jackknife analysis. These plots are taken from reference [17].

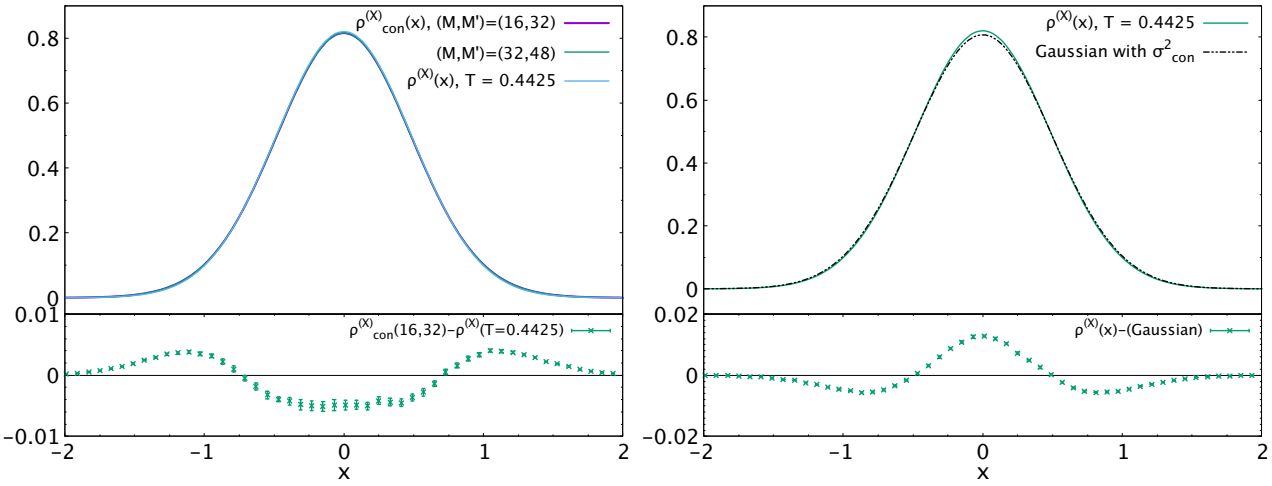

(a) $\rho^{(\mathrm{X})}(x)$ and $\rho^{(\mathrm{X})}_{\mathrm{con}}(x)$ (b) With the Gaussian distribution

Figure 34: (a) Comparison between $\rho^{(\mathrm{X})}(x)$ at a low temperature ($T = 0.4425 \approx 0.5 \cdot T_c$) and the distribution $\rho^{(\mathrm{X})}_{\mathrm{con}}(x)$ at $T = 0.885$. The histogram $\rho^{(\mathrm{X})}(x)$ is plotted by 500 configurations, and $\rho^{(\mathrm{X})}_{\mathrm{con}}(x)$ is same as one in figure 15. (b) Comparison $\rho^{(\mathrm{X})}(x)$ at $T = 0.4425$ with the Gaussian distribution. The variance is $\sigma^2_{\mathrm{con}} = 0.244$. The error bars are estimated by jackknife analysis. These plots are taken from reference [17].

References

[1] E. Witten, *String theory dynamics in various dimensions*, Nucl. Phys. B **443** (1995) 85–126 [arXiv:hep-th/9503124].

[2] G. 't Hooft, *Dimensional reduction in quantum gravity*, Conf. Proc. C **930308** (1993) 284–296 [arXiv:gr-qc/9310026].

[3] L. Susskind, *The World as a hologram*, J. Math. Phys. **36** (1995) 6377–6396 [arXiv:hep-th/9409089].

[4] J. M. Maldacena, *The Large N limit of superconformal field theories and supergravity*, Int. J. Theor. Phys. **38** (1999) 1113–1133 [arXiv:hep-th/9711200 [hep-th]]. [Adv. Theor. Math. Phys.2,231(1998)].

[5] S. S. Gubser, I. R. Klebanov, and A. M. Polyakov, *Gauge theory correlators from noncritical string theory*, Phys. Lett. B **428** (1998) 105–114 [arXiv:hep-th/9802109].

[6] E. Witten, *Anti-de Sitter space and holography*, Adv. Theor. Math. Phys. **2** (1998) 253–291 [arXiv:hep-th/9802150].

[7] S. W. Hawking and D. N. Page, *Thermodynamics of Black Holes in anti-De Sitter Space*, Commun. Math. Phys. **87** (1983) 577.

[8] O. Aharony, S. S. Gubser, J. M. Maldacena, H. Ooguri, and Y. Oz, *Large N field theories, string theory and gravity*, Phys. Rept. **323** (2000) 183–386 [arXiv:hep-th/9905111 [hep-th]].

[9] O. Aharony, J. Marsano, S. Minwalla, K. Papadodimas, and M. Van Raamsdonk, *The Hagedorn - deconfinement phase transition in weakly coupled large N gauge theories*, Adv. Theor. Math. Phys. **8** (2004) 603–696 [arXiv:hep-th/0310285 [hep-th]]. [,161(2003)].

[10] M. Hanada, G. Ishiki, and H. Watanabe, *Partial Deconfinement*, JHEP **03** (2019) 145 [arXiv:1812.05494 [hep-th]].

[11] M. Hanada and J. Maltz, *A proposal of the gauge theory description of the small Schwarzschild black hole in $AdS_5 \times S^5$*, JHEP **02** (2017) 012 [arXiv:1608.03276 [hep-th]].

[12] D. Berenstein, *Submatrix deconfinement and small black holes in AdS*, JHEP **09** (2018) 054 [arXiv:1806.05729 [hep-th]].

[13] M. Hanada, A. Jevicki, C. Peng, and N. Wintergerst, *Anatomy of Deconfinement*, JHEP **12** (2019) 167 [arXiv:1909.09118 [hep-th]].

[14] M. Hanada and B. Robinson, *Partial-Symmetry-Breaking Phase Transitions*, Phys. Rev. D **102** no. 9, (2020) 096013 [arXiv:1911.06223 [hep-th]].

[15] M. Hanada, H. Shimada, and N. Wintergerst, *Color confinement and Bose-Einstein condensation*, JHEP **08** (2021) 039 [arXiv:2001.10459 [hep-th]].

[16] G. Bergner, N. Bodendorfer, M. Hanada, E. Rinaldi, A. Schäfer, and P. Vranas, *Thermal phase transition in Yang-Mills matrix model*, JHEP **01** (2020) 053 [arXiv:1909.04592 [hep-th]].

[17] H. Watanabe, G. Bergner, N. Bodendorfer, S. Shiba Funai, M. Hanada, E. Rinaldi, A. Schäfer, and P. Vranas, *Partial deconfinement at strong coupling on the lattice*, JHEP **02** (2021) 004 [arXiv:2005.04103 [hep-th]].

[18] B. Sundborg, *The Hagedorn transition, deconfinement and N=4 SYM theory*, Nucl. Phys. **B573** (2000) 349–363 [arXiv:hep-th/9908001 [hep-th]].

[19] D. J. Gross and E. Witten, *Possible Third Order Phase Transition in the Large N Lattice Gauge Theory*, Phys. Rev. **D21** (1980) 446–453.

[20] S. R. Wadia, *A Study of U(N) Lattice Gauge Theory in 2-dimensions*, arXiv:1212.2906 [hep-th].

[21] E. Berkowitz, M. Hanada, and J. Maltz, *A microscopic description of black hole evaporation via holography*, Int. J. Mod. Phys. D **25** no. 12, (2016) 1644002 [arXiv:1603.03055 [hep-th]].

[22] A. V. Ramallo, *Introduction to the AdS/CFT correspondence*, Springer Proc. Phys. **161** (2015) 411–474 [arXiv:1310.4319 [hep-th]].

[23] I. R. Klebanov, *TASI lectures: Introduction to the AdS / CFT correspondence*, in Theoretical Advanced Study Institute in Elementary Particle Physics (TASI 99): Strings, Branes, and Gravity, pp. 615–650. 9, 2000. arXiv:hep-th/0009139.

[24] D. Bigatti and L. Susskind, *TASI lectures on the holographic principle*, in Theoretical Advanced Study Institute in Elementary Particle Physics (TASI 99): Strings, Branes, and Gravity, pp. 883–933. 8, 1999. arXiv:hep-th/0002044.

[25] J. L. Petersen, *Introduction to the Maldacena conjecture on AdS / CFT*, Int. J. Mod. Phys. A **14** (1999) 3597–3672 [arXiv:hep-th/9902131].

[26] K. Becker, M. Becker, and J. H. Schwarz, *String Theory and M-Theory: A Modern Introduction*. Cambridge University Press, 2006.

[27] M. Natsuume, *AdS/CFT Duality User Guide*, vol. 903. 2015. arXiv:1409.3575 [hep-th].

[28] B. Zwiebach, *A First Course in String Theory*. Cambridge University Press, 2009.

[29] B. Ydri, *Matrix Models of String Theory*. IOP Publishing, 2018.

[30] J. D. Bekenstein, *Black holes and entropy*, Phys. Rev. **D7** (1973) 2333–2346.

[31] S. W. Hawking, *Particle Creation by Black Holes*, Commun. Math. Phys. **43** (1975) 199–220. [,167(1975)].

[32] N. Itzhaki, J. M. Maldacena, J. Sonnenschein, and S. Yankielowicz, *Supergravity and the large N limit of theories with sixteen supercharges*, Phys. Rev. **D58** (1998) 046004 [arXiv:hep-th/9802042 [hep-th]].

[33] T. Banks, W. Fischler, S. H. Shenker, and L. Susskind, *M theory as a matrix model: A Conjecture*, Phys. Rev. **D55** (1997) 5112–5128 [arXiv:hep-th/9610043 [hep-th]]. [,435(1996)].

[34] B. de Wit, J. Hoppe, and H. Nicolai, *On the Quantum Mechanics of Supermembranes*, Nucl. Phys. **B305** (1988) 545. [,73(1988)].

[35] E. Bergshoeff, E. Sezgin, and P. K. Townsend, *Supermembranes and Eleven-Dimensional Supergravity*, Phys. Lett. B **189** (1987) 75–78.

[36] N. Seiberg, *Why is the matrix model correct?*, Phys. Rev. Lett. **79** (1997) 3577–3580 [arXiv:hep-th/9710009].

[37] W. Taylor, *The M(atrix) model of M theory*, NATO Sci. Ser. C **556** (2000) 91–178 [arXiv:hep-th/0002016].

[38] D. E. Berenstein, J. M. Maldacena, and H. S. Nastase, *Strings in flat space and pp waves from N=4 superYang-Mills*, JHEP **04** (2002) 013 [arXiv:hep-th/0202021 [hep-th]].

[39] R. Gregory and R. Laflamme, *Black strings and p-branes are unstable*, Phys. Rev. Lett. **70** (1993) 2837–2840 [arXiv:hep-th/9301052 [hep-th]].

[40] O. J. C. Dias, J. E. Santos, and B. Way, *Lumpy $AdS_5 \times S^5$ black holes and black belts*, JHEP **04** (2015) 060 [arXiv:1501.06574 [hep-th]].

[41] O. J. C. Dias, J. E. Santos, and B. Way, *Localised $AdS_5 \times S^5$ Black Holes*, Phys. Rev. Lett. **117** no. 15, (2016) 151101 [arXiv:1605.04911 [hep-th]].

[42] L. G. Yaffe, *Large N phase transitions and the fate of small Schwarzschild-AdS black holes*, Phys. Rev. D **97** no. 2, (2018) 026010 [arXiv:1710.06455 [hep-th]].

[43] Y. Hyakutake, *Boosted Quantum Black Hole and Black String in M-theory, and Quantum Correction to Gregory-Laflamme Instability*, JHEP **09** (2015) 067 [arXiv:1503.05083 [gr-qc]].

[44] T. Harmark and N. A. Obers, *Phase structure of black holes and strings on cylinders*, Nucl. Phys. B **684** (2004) 183–208 [arXiv:hep-th/0309230].

[45] B. Kol, *The Phase transition between caged black holes and black strings: A Review*, Phys. Rept. **422** (2006) 119–165 [arXiv:hep-th/0411240].

[46] G. T. Horowitz and T. Wiseman, *General black holes in Kaluza–Klein theory*, pp. 69–98. 2012. arXiv:1107.5563 [gr-qc].

[47] M. Kalisch, *Numerical construction and critical behavior of Kaluza-Klein black holes*, other thesis, Jena U., 2, 2018.

[48] J. L. Hovdebo and R. C. Myers, *Black rings, boosted strings and Gregory-Laflamme*, Phys. Rev. D **73** (2006) 084013 [arXiv:hep-th/0601079].

[49] T. Banks, W. Fischler, I. R. Klebanov, and L. Susskind, *Schwarzschild black holes from matrix theory*, Phys. Rev. Lett. **80** (1998) 226–229 [arXiv:hep-th/9709091].

[50] T. Banks, W. Fischler, I. R. Klebanov, and L. Susskind, *Schwarzschild black holes in matrix theory. 2.*, JHEP **01** (1998) 008 [arXiv:hep-th/9711005].

[51] T. Banks, W. Fischler, and I. R. Klebanov, *Evaporation of Schwarzschild black holes in matrix theory*, Phys. Lett. B **423** (1998) 54–58 [arXiv:hep-th/9712236].

[52] G. T. Horowitz and E. J. Martinec, *Comments on black holes in matrix theory*, Phys. Rev. D **57** (1998) 4935–4941 [arXiv:hep-th/9710217].

[53] G. T. Horowitz, *Comments on black holes in string theory*, Class. Quant. Grav. **17** (2000) 1107–1116 [arXiv:hep-th/9910082].

[54] E. Witten, *Bound states of strings and p-branes*, Nucl. Phys. **B460** (1996) 335–350 [arXiv:hep-th/9510135 [hep-th]].

[55] E. Witten, *Anti-de Sitter space, thermal phase transition, and confinement in gauge theories*, Adv. Theor. Math. Phys. **2** (1998) 505–532 [arXiv:hep-th/9803131 [hep-th]]. [,89(1998)].

[56] O. Aharony, O. Bergman, D. L. Jafferis, and J. Maldacena, *N=6 superconformal Chern-Simons-matter theories, M2-branes and their gravity duals*, JHEP **10** (2008) 091 [arXiv:0806.1218 [hep-th]].

[57] **MCSMC** Collaboration, G. Bergner, N. Bodendorfer, M. Hanada, S. Pateloudis, E. Rinaldi, A. Schäfer, P. Vranas, and H. Watanabe, *Confinement/deconfinement transition in the D0-brane matrix model – A signature of M-theory?*, arXiv:2110.01312 [hep-th].

[58] M. Hanada, J. Holden, M. Knaggs, and A. O'Bannon, *Global Symmetries and Partial Confinement*, arXiv:2112.11398 [hep-th].

[59] E. Brezin, C. Itzykson, G. Parisi, and J. B. Zuber, *Planar Diagrams*, Commun. Math. Phys. **59** (1978) 35.

[60] M. C. Ogilvie, P. N. Meisinger, and J. C. Myers, *Exploring Partially Confined Phases*, PoS **LATTICE2007** (2007) 213 [arXiv:0710.0649 [hep-lat]].

[61] S. Elitzur, *Impossibility of spontaneously breaking local symmetries*, Phys. Rev. D **12** (Dec, 1975) 3978–3982. https://link.aps.org/doi/10.1103/PhysRevD.12.3978.

[62] K. Rajagopal and F. Wilczek, *The Condensed matter physics of QCD*, pp. 2061–2151. 11, 2000. arXiv:hep-ph/0011333.

[63] H. J. Schnitzer, *Confinement/deconfinement transition of large N gauge theories with N(f) fundamentals: N(f)/N finite*, Nucl. Phys. B **695** (2004) 267–282 [arXiv:hep-th/0402219].

[64] R. Hagedorn, *Statistical thermodynamics of strong interactions at high-energies*, Nuovo Cim. Suppl. **3** (1965) 147–186.

[65] J. Jurkiewicz and K. Zalewski, *Vacuum Structure of the U(N $\to$ Infinity) Gauge Theory on a Two-dimensional Lattice for a Broad Class of Variant Actions*, Nucl. Phys. B **220** (1983) 167–184.

[66] O. Aharony, J. Marsano, S. Minwalla, K. Papadodimas, and M. Van Raamsdonk, *A First order deconfinement transition in large N Yang-Mills theory on a small S**3*, Phys. Rev. D **71** (2005) 125018 [arXiv:hep-th/0502149].

[67] O. Aharony, J. Marsano, and M. Van Raamsdonk, *Two loop partition function for large N pure Yang-Mills theory on a small S**3*, Phys. Rev. D **74** (2006) 105012 [arXiv:hep-th/0608156].

[68] O. Aharony, J. Marsano, S. Minwalla, K. Papadodimas, M. Van Raamsdonk, and T. Wiseman, *The Phase structure of low dimensional large N gauge theories on Tori*, JHEP **01** (2006) 140 [arXiv:hep-th/0508077].

[69] T. J. Hollowood and J. C. Myers, *Deconfinement transitions of large N QCD with chemical potential at weak and strong coupling*, JHEP **10** (2012) 067 [arXiv:1207.4605 [hep-th]].

[70] H. J. Schnitzer, *Confinement/deconfinement transition of large N gauge theories in perturbation theory with N(f) fundamentals: N(f)/N finite*, arXiv:hep-th/0612099.

[71] H. Watanabe, *in progress,*.

[72] C. Vafa and E. Witten, *Restrictions on Symmetry Breaking in Vector-Like Gauge Theories*, Nucl. Phys. B **234** (1984) 173–188.

[73] S. H. Shenker and X. Yin, *Vector Models in the Singlet Sector at Finite Temperature*, arXiv:1109.3519 [hep-th].

[74] M. A. Vasiliev, *Consistent equation for interacting gauge fields of all spins in (3+1)-dimensions*, Phys. Lett. B **243** (1990) 378–382.

[75] M. A. Vasiliev, *More on equations of motion for interacting massless fields of all spins in (3+1)-dimensions*, Phys. Lett. B **285** (1992) 225–234.

[76] M. A. Vasiliev, *Higher spin gauge theories in four-dimensions, three-dimensions, and two-dimensions*, Int. J. Mod. Phys. D **5** (1996) 763–797 [arXiv:hep-th/9611024].

[77] I. R. Klebanov and A. M. Polyakov, *AdS dual of the critical O(N) vector model*, Phys. Lett. B **550** (2002) 213–219 [arXiv:hep-th/0210114].

[78] S. Giombi and X. Yin, *Higher Spin Gauge Theory and Holography: The Three-Point Functions*, JHEP **09** (2010) 115 [arXiv:0912.3462 [hep-th]].

[79] S. Giombi and X. Yin, *Higher Spins in AdS and Twistorial Holography*, JHEP **04** (2011) 086 [arXiv:1004.3736 [hep-th]].

[80] J. Maldacena and A. Zhiboedov, *Constraining Conformal Field Theories with A Higher Spin Symmetry*, J. Phys. A **46** (2013) 214011 [arXiv:1112.1016 [hep-th]].

[81] J. Maldacena and A. Zhiboedov, *Constraining conformal field theories with a slightly broken higher spin symmetry*, Class. Quant. Grav. **30** (2013) 104003 [arXiv:1204.3882 [hep-th]].

[82] Y. Hikida, *Conformal Field Theory (*共形場理論入門　基礎からホログラフィへの道*)*. Kodansha Sientific, 2020.

[83] A. Einstein, *Quantentheorie des einatomigen idealen gases*, S-B Preuss. Akad. Berlin (1924) 261.

[84] F. London, *The λ-Phenomenon of Liquid Helium and the Bose-Einstein Degeneracy*, Nature **141** (Apr, 1938) 643–644.

[85] R. P. Feynman, *Atomic theory of the λ transition in helium*, Phys. Rev. **91** (1953) 1291.

[86] O. Penrose and L. Onsager, *Bose-einstein condensation and liquid helium*, Phys. Rev. **104** (1956) 576–584.

[87] O. Aharony, J. Marsano, S. Minwalla, and T. Wiseman, *Black hole-black string phase transitions in thermal 1+1 dimensional supersymmetric Yang-Mills theory on a circle*, Class. Quant. Grav. **21** (2004) 5169–5192 [arXiv:hep-th/0406210].

[88] D. Gaiotto, A. Kapustin, Z. Komargodski, and N. Seiberg, *Theta, Time Reversal, and Temperature*, JHEP **05** (2017) 091 [arXiv:1703.00501 [hep-th]].

[89] S. Chen, K. Fukushima, H. Nishimura, and Y. Tanizaki, *Deconfinement and $\mathcal{CP}$ breaking at $\theta = \pi$ in Yang-Mills theories and a novel phase for SU(2)*, Phys. Rev. D **102** no. 3, (2020) 034020 [arXiv:2006.01487 [hep-th]].

[90] S. Coleman, *Aspects of Symmetry: Selected Erice Lectures*. Cambridge University Press, 1985.

[91] E. Witten, *The 1/n expansion in atomic and particle physics*, in Recent developments in gauge theories, pp. 403–419. Springer, 1980.

[92] Y. Makeenko, *Large N gauge theories*, NATO Sci. Ser. C **556** (2000) 285–354 [arXiv:hep-th/0001047].

[93] R. Gopakumar and D. J. Gross, *Mastering the master field*, Nucl. Phys. **B451** (1995) 379–415 [arXiv:hep-th/9411021 [hep-th]].

[94] B. Lucini, M. Teper, and U. Wenger, *The High temperature phase transition in SU(N) gauge theories*, JHEP **01** (2004) 061 [arXiv:hep-lat/0307017].

[95] N. Kawahara, J. Nishimura, and S. Takeuchi, *Phase structure of matrix quantum mechanics at finite temperature*, JHEP **10** (2007) 097 [arXiv:0706.3517 [hep-th]].

[96] V. G. Filev and D. O'Connor, *The BFSS model on the lattice*, JHEP **05** (2016) 167 [arXiv:1506.01366 [hep-th]].

[97] C. Asplund, D. Berenstein, and D. Trancanelli, *Evidence for fast thermalization in the plane-wave matrix model*, Phys. Rev. Lett. **107** (2011) 171602 [arXiv:1104.5469 [hep-th]].

[98] C. T. Asplund, D. Berenstein, and E. Dzienkowski, *Large N classical dynamics of holographic matrix models*, Phys. Rev. **D87** no. 8, (2013) 084044 [arXiv:1211.3425 [hep-th]].

[99] S. Aoki, M. Hanada, and N. Iizuka, *Quantum Black Hole Formation in the BFSS Matrix Model*, JHEP **07** (2015) 029 [arXiv:1503.05562 [hep-th]].

[100] G. Gur-Ari, M. Hanada, and S. H. Shenker, *Chaos in Classical D0-Brane Mechanics*, JHEP **02** (2016) 091 [arXiv:1512.00019 [hep-th]].

[101] F. Aprile and F. Sanfilippo, *Quasi-Normal Modes from Non-Commutative Matrix Dynamics*, JHEP **09** (2017) 048 [arXiv:1611.00786 [hep-th]].

[102] T. Azuma, T. Morita, and S. Takeuchi, *Hagedorn Instability in Dimensionally Reduced Large-N Gauge Theories as Gregory-Laflamme and Rayleigh-Plateau Instabilities*, Phys. Rev. Lett. **113** (2014) 091603 [arXiv:1403.7764 [hep-th]].

[103] T. Morita and H. Yoshida, *Critical Dimension and Negative Specific Heat in One-dimensional Large-N Reduced Models*, Phys. Rev. D **101** no. 10, (2020) 106010 [arXiv:2001.02109 [hep-th]].

[104] Y. Aoki, G. Endrodi, Z. Fodor, S. Katz, and K. Szabo, *The Order of the quantum chromodynamics transition predicted by the standard model of particle physics*, Nature **443** (2006) 675–678 [arXiv:hep-lat/0611014].

[105] E. Witten, *Baryons in the 1/n Expansion*, Nucl. Phys. B **160** (1979) 57–115.

[106] B. Lucini and M. Panero, *SU(N) gauge theories at large N*, Phys. Rept. **526** (2013) 93–163 [arXiv:1210.4997 [hep-th]].

[107] S. Gupta, K. Huebner, and O. Kaczmarek, *Renormalized Polyakov loops in many representations*, Phys. Rev. D **77** (2008) 034503 [arXiv:0711.2251 [hep-lat]].

[108] A. Mykkanen, M. Panero, and K. Rummukainen, *Casimir scaling and renormalization of Polyakov loops in large-N gauge theories*, JHEP **05** (2012) 069 [arXiv:1202.2762 [hep-lat]].

[109] A. Bazavov and P. Petreczky, *Polyakov loop in 2+1 flavor QCD*, Phys. Rev. D **87** no. 9, (2013) 094505 [arXiv:1301.3943 [hep-lat]].

[110] A. Dumitru, J. Lenaghan, and R. D. Pisarski, *Deconfinement in matrix models about the Gross-Witten point*, Phys. Rev. D **71** (2005) 074004 [arXiv:hep-ph/0410294].

[111] H. Nishimura, R. D. Pisarski, and V. V. Skokov, *Finite-temperature phase transitions of third and higher order in gauge theories at large N*, Phys. Rev. D **97** no. 3, (2018) 036014 [arXiv:1712.04465 [hep-th]].

[112] C. Rohrhofer, Y. Aoki, G. Cossu, H. Fukaya, C. Gattringer, L. Y. Glozman, S. Hashimoto, C. B. Lang, and S. Prelovsek, *Symmetries of spatial meson correlators in high temperature QCD*, Phys. Rev. D **100** no. 1, (2019) 014502 [arXiv:1902.03191 [hep-lat]].

[113] M. Denissenya, L. Y. Glozman, and C. B. Lang, *Symmetries of mesons after unbreaking of chiral symmetry and their string interpretation*, Phys. Rev. D **89** no. 7, (2014) 077502 [arXiv:1402.1887 [hep-lat]].

[114] E. Shuryak, *Comments on "Three regimes of QCD" by L.Glozman*, arXiv:1909.04209 [hep-ph].

[115] L. Y. Glozman, *Reply to E. Shuryak's Comments on "Three regimes of QCD"*, arXiv:1909.06656 [hep-ph].

[116] L. Y. Glozman, *Fluctuations of conserved charges, chiral-spin symmetry, and deconfinement in an $SU(2)_{color}$ subgroup of $SU(3)_{color}$ above T_c*, Phys. Rev. D **102** no. 1, (2020) 014509 [arXiv:2005.10538 [hep-ph]].

[117] L. Y. Glozman and C. B. Lang, *A finite box as a tool to distinguish free quarks from confinement at high temperatures*, Eur. Phys. J. A **57** no. 6, (2021) 182 [arXiv:2007.10942 [hep-lat]].

[118] S. Choi, J. Kim, S. Kim, and J. Nahmgoong, *Comments on deconfinement in AdS/CFT*, arXiv:1811.08646 [hep-th].

[119] S. Choi, S. Jeong, and S. Kim, *The Yang-Mills duals of small AdS black holes*, arXiv:2103.01401 [hep-th].

[120] S. Choi, S. Jeong, S. Kim, and E. Lee, *Exact QFT duals of AdS black holes*, arXiv:2111.10720 [hep-th].

[121] A. Arabi Ardehali, J. Hong, and J. T. Liu, *Asymptotic growth of the 4d $\mathcal{N} = 4$ index and partially deconfined phases*, JHEP **07** (2020) 073 [arXiv:1912.04169 [hep-th]].

[122] C. Copetti, A. Grassi, Z. Komargodski, and L. Tizzano, *Delayed Deconfinement and the Hawking-Page Transition*, arXiv:2008.04950 [hep-th].

[123] A. F. Faedo, D. Mateos, D. Pravos, and J. G. Subils, *Mass Gap without Confinement*, JHEP **06** (2017) 153 [arXiv:1702.05988 [hep-th]].

[124] D. Elander, A. F. Faedo, D. Mateos, and J. G. Subils, *Phase transitions in a three-dimensional analogue of Klebanov-Strassler*, arXiv:2002.08279 [hep-th].

[125] K. N. Anagnostopoulos, M. Hanada, J. Nishimura, and S. Takeuchi, *Monte Carlo studies of supersymmetric matrix quantum mechanics with sixteen supercharges at finite temperature*, Phys. Rev. Lett. **100** (2008) 021601 [arXiv:0707.4454 [hep-th]].

[126] S. Catterall and T. Wiseman, *Black hole thermodynamics from simulations of lattice Yang-Mills theory*, Phys. Rev. **D78** (2008) 041502 [arXiv:0803.4273 [hep-th]].

[127] M. Hanada, A. Miwa, J. Nishimura, and S. Takeuchi, *Schwarzschild radius from Monte Carlo calculation of the Wilson loop in supersymmetric matrix quantum mechanics*, Phys. Rev. Lett. **102** (2009) 181602 [arXiv:0811.2081 [hep-th]].

[128] S. Catterall and T. Wiseman, *Extracting black hole physics from the lattice*, JHEP **04** (2010) 077 [arXiv:0909.4947 [hep-th]].

[129] M. Hanada, Y. Hyakutake, G. Ishiki, and J. Nishimura, *Holographic description of quantum black hole on a computer*, Science **344** (2014) 882–885 [arXiv:1311.5607 [hep-th]].

[130] D. Kadoh and S. Kamata, *Gauge/gravity duality and lattice simulations of one dimensional SYM with sixteen supercharges*, arXiv:1503.08499 [hep-lat].

[131] E. Berkowitz, E. Rinaldi, M. Hanada, G. Ishiki, S. Shimasaki, and P. Vranas, *Precision lattice test of the gauge/gravity duality at large-N*, Phys. Rev. **D94** no. 9, (2016) 094501 [arXiv:1606.04951 [hep-lat]].

[132] J. Polchinski, *M theory and the light cone*, Prog. Theor. Phys. Suppl. **134** (1999) 158–170 [arXiv:hep-th/9903165].

[133] M. Hanada, *Bulk geometry in gauge/gravity duality and color degrees of freedom*, Phys. Rev. D **103** no. 10, (2021) 106007 [arXiv:2102.08982 [hep-th]].

[134] J. M. Maldacena, *Eternal black holes in anti-de Sitter*, JHEP **04** (2003) 021 [arXiv:hep-th/0106112].

[135] M. Van Raamsdonk, *Building up spacetime with quantum entanglement*, Gen. Rel. Grav. **42** (2010) 2323–2329 [arXiv:1005.3035 [hep-th]].

[136] F. Alet, M. Hanada, A. Jevicki, and C. Peng, *Entanglement and Confinement in Coupled Quantum Systems*, arXiv:2001.03158 [hep-th].

[137] S. Ryu and T. Takayanagi, *Holographic derivation of entanglement entropy from AdS/CFT*, Phys. Rev. Lett. **96** (2006) 181602 [arXiv:hep-th/0603001].

[138] V. E. Hubeny, M. Rangamani, and T. Takayanagi, *A Covariant holographic entanglement entropy proposal*, JHEP **07** (2007) 062 [arXiv:0705.0016 [hep-th]].

[139] T. Faulkner, A. Lewkowycz, and J. Maldacena, *Quantum corrections to holographic entanglement entropy*, JHEP **11** (2013) 074 [arXiv:1307.2892 [hep-th]].

[140] D. L. Jafferis, A. Lewkowycz, J. Maldacena, and S. J. Suh, *Relative entropy equals bulk relative entropy*, JHEP **06** (2016) 004 [arXiv:1512.06431 [hep-th]].

[141] N. Engelhardt and A. C. Wall, *Quantum Extremal Surfaces: Holographic Entanglement Entropy beyond the Classical Regime*, JHEP **01** (2015) 073 [arXiv:1408.3203 [hep-th]].

[142] S. R. Das, A. Kaushal, G. Mandal, and S. P. Trivedi, *Bulk Entanglement Entropy and Matrices*, J. Phys. A **53** no. 44, (2020) 444002 [arXiv:2004.00613 [hep-th]].

[143] S. R. Das, A. Kaushal, S. Liu, G. Mandal, and S. P. Trivedi, *Gauge invariant target space entanglement in D-brane holography*, JHEP **04** (2021) 225 [arXiv:2011.13857 [hep-th]].

[144] E. A. Mazenc and D. Ranard, *Target Space Entanglement Entropy*, arXiv:1910.07449 [hep-th].

[145] T. Anous, J. L. Karczmarek, E. Mintun, M. Van Raamsdonk, and B. Way, *Areas and entropies in BFSS/gravity duality*, SciPost Phys. **8** no. 4, (2020) 057 [arXiv:1911.11145 [hep-th]].

[146] B. Swingle, *Entanglement Renormalization and Holography*, Phys. Rev. D **86** (2012) 065007 [arXiv:0905.1317 [cond-mat.str-el]].

[147] T. Eguchi and H. Kawai, *Reduction of Dynamical Degrees of Freedom in the Large N Gauge Theory*, Phys. Rev. Lett. **48** (1982) 1063.

[148] P. Kovtun, M. Unsal, and L. G. Yaffe, *Volume independence in large N(c) QCD-like gauge theories*, JHEP **06** (2007) 019 [arXiv:hep-th/0702021].

[149] N. Ishibashi, H. Kawai, Y. Kitazawa, and A. Tsuchiya, *A Large N reduced model as superstring*, Nucl. Phys. B **498** (1997) 467–491 [arXiv:hep-th/9612115].

[150] H. Aoki, S. Iso, H. Kawai, Y. Kitazawa, and T. Tada, *Space-time structures from IIB matrix model*, Prog. Theor. Phys. **99** (1998) 713–746 [arXiv:hep-th/9802085].

[151] J. Nishimura and F. Sugino, *Dynamical generation of four-dimensional space-time in the IIB matrix model*, JHEP **05** (2002) 001 [arXiv:hep-th/0111102].

[152] S.-W. Kim, J. Nishimura, and A. Tsuchiya, *Late time behaviors of the expanding universe in the IIB matrix model*, JHEP **10** (2012) 147 [arXiv:1208.0711 [hep-th]].

[153] Y. Lozano, C. Nunez, and S. Zacarias, *BMN Vacua, Superstars and Non-Abelian T-duality*, JHEP **09** (2017) 008 [arXiv:1703.00417 [hep-th]].

[154] J. Madore, *The fuzzy sphere*, Classical and Quantum Gravity **9** no. 1, (1992) 69–87.

[155] R. C. Myers, *Dielectric branes*, JHEP **12** (1999) 022 [arXiv:hep-th/9910053].

[156] M. S. Costa, L. Greenspan, J. Penedones, and J. Santos, *Thermodynamics of the BMN matrix model at strong coupling*, JHEP **03** (2015) 069 [arXiv:1411.5541 [hep-th]].

[157] S. Catterall and G. van Anders, *First Results from Lattice Simulation of the PWMM*, JHEP **09** (2010) 088 [arXiv:1003.4952 [hep-th]].

[158] Y. Asano, V. G. Filev, S. Kováčik, and D. O'Connor, *The non-perturbative phase diagram of the BMN matrix model*, JHEP **07** (2018) 152 [arXiv:1805.05314 [hep-th]].

[159] D. Schaich, R. G. Jha, and A. Joseph, *Thermal phase structure of a supersymmetric matrix model*, PoS **LATTICE2019** (2020) 069 [arXiv:2003.01298 [hep-lat]].

[160] X. Han and S. A. Hartnoll, *Deep Quantum Geometry of Matrices*, Phys. Rev. X **10** no. 1, (2020) 011069 [arXiv:1906.08781 [hep-th]].

[161] E. Rinaldi, X. Han, M. Hassan, Y. Feng, F. Nori, M. McGuigan, and M. Hanada, *Matrix Model simulations using Quantum Computing, Deep Learning, and Lattice Monte Carlo*, arXiv:2108.02942 [quant-ph].

[162] H. Gharibyan, M. Hanada, M. Honda, and J. Liu, *Toward simulating Superstring/M-theory on a quantum computer*, JHEP **07** (2021) 140 [arXiv:2011.06573 [hep-th]].

[163] A. J. Buser, H. Gharibyan, M. Hanada, M. Honda, and J. Liu, *Quantum simulation of gauge theory via orbifold lattice*, JHEP **09** (2021) 034 [arXiv:2011.06576 [hep-th]].

[164] C. Culver and D. Schaich, *Quantum computing for lattice supersymmetry*, in 38th International Symposium on Lattice Field Theory. 12, 2021. arXiv:2112.07651 [hep-lat].

[165] M. Beekman, D. J. T. Sumpter, and F. L. W. Ratnieks, *Phase transition between disordered and ordered foraging in pharaoh's ants*, Proceedings of the National Academy of Sciences **98** no. 17, (2001) 9703–9706 [http://www.pnas.org/content/98/17/9703.full.pdf]. http://www.pnas.org/content/98/17/9703.

[166] G. Mandal, M. Mahato, and T. Morita, *Phases of one dimensional large N gauge theory in a 1/D expansion*, JHEP **02** (2010) 034 [arXiv:0910.4526 [hep-th]].

[167] E. Berkowitz, M. Hanada, E. Rinaldi, and P. Vranas, *Gauged And Ungauged: A Nonperturbative Test*, JHEP **06** (2018) 124 [arXiv:1802.02985 [hep-th]].

[168] M. Hanada, J. Nishimura, and S. Takeuchi, *Non-lattice simulation for supersymmetric gauge theories in one dimension*, Phys. Rev. Lett. **99** (2007) 161602 [arXiv:0706.1647 [hep-lat]].

[169] M. Hanada, *A Users' Manual of Monte Carlo Code for the Matrix Model of M-theory*. https://sites.google.com/site/hanadamasanori/home/mmmm.

[170] S. Duane, A. D. Kennedy, B. J. Pendleton, and D. Roweth, *Hybrid Monte Carlo*, Phys. Lett. **B195** (1987) 216–222.